Report No.
UCB/SEMM-2024/03

Structural Engineering
Mechanics and Materials

Laboratory Tests, Analytical Modeling, and Design Model Development for Column-Foundation Connections with Headed Anchors

By

Benjamin L. Worsfold[1], Daniel Gaspar-Rodriguez[2], Dara Karać[3], John F. Silva[4], and Jack P. Moehle[5]

[1]Department of Civil, Environmental, and Geo-Engineering
University of Minnesota

[2]Degenkolb Engineers
Oakland, California

[3]Simpson Gumpertz & Heger Inc.
Los Angeles, California

[4]Hilti North America
San Rafael, California

[5]Department of Civil and Environmental Engineering
University of California, Berkeley

September 2024

Department of Civil and Environmental Engineering
University of California, Berkeley

ABSTRACT

In collaboration with practicing structural engineers and experts in anchoring to concrete, the authors undertook a research project to explore the requirements for anchoring columns to reinforced concrete foundations. In early discussions it was realized that, while there were design procedures that were in use in different design offices, the design procedures differed from office to office and few of the methods had been verified by laboratory testing. Based on this knowledge, a series of laboratory tests was designed and carried out to develop benchmark data on the following types of column-foundation problems:

- Interior footings supporting columns in direct tension and anchored by multiple anchor bolts, either with or without additional footing transverse reinforcement to increase strength and deformation capacity.
- Interior footings supporting column in direct bending and anchored by multiple anchor bolts, either with or without additional footing transverse reinforcement to increase strength and deformation capacity.

The laboratory tests were supplemented by nonlinear finite element studies using the software ATENA, both to calibrate the model material parameters and to extrapolate results from the laboratory tests to geometries that were not tested in the laboratory. Together, the laboratory and numerical studies were used to derive a design method to calculate the strength of connections in either direct tension, direct moment transfer, or combinations of the two, with or without additional transverse reinforcement intended to increase strength and deformation capacity. The authors subsequently worked with ACI Committee 318 Structural Concrete Building Code of the American Concrete Institute to develop design provisions that were approved and adopted in ACI 318-25 Building Code Requirements for Structural Concrete and Commentary.

ACKNOWLEDGMENTS

The authors would like to thank the following individuals for their invaluable insight and for graciously investing their time and energy into this project. Their involvement made this work possible and greatly improved the quality of the research results.

Rafael Sabelli, Managing Director and Director of Seismic Design, Walter P Moore, San Francisco, CA.

James Malley, Senior Principal, Degenkolb Engineers, San Francisco, CA.

Roberto Piccinin, Group Manager Code Development and Research, HILTI, Schaan, Liechtenstein.

The authors would also like to thank the sponsors of this project:

HILTI.

American Institute of Steel Construction.

ACI Foundation, Concrete Research Council.

Concrete Reinforcing Steel Institute.

Ron Klemencic, Chairman and C.E.O., Magnusson Klemencic Associates, Seattle, WA.

Clark Construction, San Francisco, CA.

CONCO, Concord, CA.

Alamillo Rebar, Benicia, CA.

Central Concrete Supply Co., San Jose, CA

Level 10 Construction, San Francisco, CA.

Cascade Steel Rolling Mills, Inc.

Precision Rebar & Accessories Inc.

PJ's Rebar Inc., Fremont, CA.

The authors would also like to thank the managers and staff of the Structural Engineering Laboratory at UC Berkeley for their support and problem-solving abilities during the design, construction, and testing phases of the project.

The work described herein was carried out by Benjamin L. Worsfold, Daniel Gaspar, and Dara Karać in partial fulfillment of graduate degree requirements in Structural Engineering, Mechanics, and Materials of the Department of Civil and Environmental Engineering, University of California, Berkeley, under the direction of Professor Jack P. Moehle. Authorship is noted in the individual chapters.

CONTENTS

CHAPTER 1 - COMPARATIVE STUDY OF PUNCHING SHEAR AND CONCRETE BREAKOUT[1]

by Daniel Gaspar Rodriguez and Jack P. Moehle

ABSTRACT

A laboratory research program was undertaken to compare the failure mechanisms and strengths of concrete foundation slabs subjected to punching shear and concrete breakout loadings. Four nominally identical reinforced concrete slabs were constructed and tested in a laboratory. One of the slabs was loaded in compression through a bearing surface to produce punching shear failure. The other three slabs were loaded in tension through eight anchor bolts arranged around a square perimeter to produce a similarly sized breakout failure. Variations in bearing area and local reinforcement detailing were introduced in the breakout tests to explore their effect on strength. One additional specimen was cast with a single anchor bolt to gather data on basic breakout strength. The test results indicate that punching shear and anchor breakout developed similar failure modes. Punching shear resulted in the largest strength with the largest failure surface. Ultimate load capacities normalized by the square root of the concrete compressive strength and by an effective failure area showed that the nominal failure stresses were nearly equal for the different test cases. The addition of slab deformed reinforcement in the vicinity of the anchor bearing head and oriented perpendicular to the direction of the anchor bolts resulted in a modest increase of the breakout ultimate capacity and of the residual strength.

Keywords: Footings, punching shear; concrete breakout; anchor group; headed anchor.

INTRODUCTION

The design of connections between steel columns and reinforced concrete foundations is of interest for structural engineers. For exterior columns in steel braced frames, the connections can be subjected to tensile or compressive forces depending on the direction of lateral loading resisted by the braced frame. The connection forces can be large enough to cause either punching shear failure in compression or

[1] Originally published as part of *ACI Structural Journal*, V. 118, No. 2, March 2021, DOI: 10.14359/51729345.

breakout failure in tension. The present paper presents laboratory test data and analyses to help understand the strengths of such connections.

Two-way punching shear failures and tension breakout failures both involve the development of truncated pyramidal failure surfaces. The similarity of the failure surfaces might suggest that the strengths of the two failure modes would be similar when the sizes of the failure surfaces are similar. The ACI 318-19 structural concrete building code, however, presents different methods for calculating punching shear and concrete breakout strengths that can result in markedly different design strengths, especially for thicker slabs. The different calculation methods and resulting strengths have raised a question among practicing engineers regarding the applicability and accuracy of the two methods.

To study this question, four nominally identical reinforced concrete slabs were constructed and tested in a laboratory. One of the slabs was loaded in compression through a bearing surface to produce punching shear failure. The other three slabs were loaded in tension through eight anchor bolts arranged around a square perimeter to produce a similarly sized breakout failure. Variations in bearing area and local reinforcement detailing were introduced in the breakout tests to explore their effect on strength. One additional specimen was cast with a single anchor bolt to gather data on basic breakout strength. Failure modes and strengths are compared to evaluate the effectiveness of the ACI 318-19 design methods for two-way punching shear and concrete breakout.

RESEARCH SIGNIFICANCE

The ACI 318 Building Code has different nominal strength calculation methods for base plate-to-foundation connections loaded in compression through the base plate versus those loaded in tension through anchor bolts, even though the failure mechanisms have similar appearance. The present research compares measured and calculated strengths for compression and tension cases. The effects of different anchor bolt detailing on tensile strengths are also presented. The results of the present study can help designers responsible for design of similar connections and may result in modifications to the ACI 318 building code.

EXPERIMENTAL PROGRAM

The test program comprised four base plate-to-footing tests and one supplementary single-anchor test. The specimen ID names P01, B01, B02, B03, and S01 are used to label these test specimens. Specimen P01 had a base plate loaded in compression to produce a punching failure. Specimens B01, B02, and B03 had base plates loaded in tension that were anchored to the footing concrete through eight anchor bolts to

produce breakout failure. Specimen S01 had a single anchor bolt loaded in tension to produce breakout failure. The specimens were constructed in two successive phases. Specimens P01 and B01 were cast from a single batch of concrete in Phase 1. Specimens B02, B03, and S01 were cast from a single batch of concrete in Phase 2.

TEST SPECIMENS

All specimens are considered half-scale models of full-size spread footings and were built as square slabs with 76 by 76 in. (1930x1930mm) plan dimensions and 9 in. (228mm) thickness. Rather than being uniformly supported on soil, the slabs were set and tested on line supports, arranged in an octagonal pattern and positioned such that moment and shear stress fields in the slabs near the connection would closely approximate those of a soil-supported footing subjected to compression loading (Gaspar, 2018).

Figure 1 shows elevation and plan views for the punching and 8-anchor-bolt breakout tests. For load application, a high-strength steel rod connects a steel base plate assembly to a hydraulic jack, which bears directly on the laboratory strong floor. To avoid significant strut action within the slab between the points of load application and the line supports, the shear span aspect ratio was set at $a/d = 3$, where a = distance from edge of base plate to nearest point of support and d = distance from extreme compression fiber to centroid of flexural tension reinforcement in the slab.

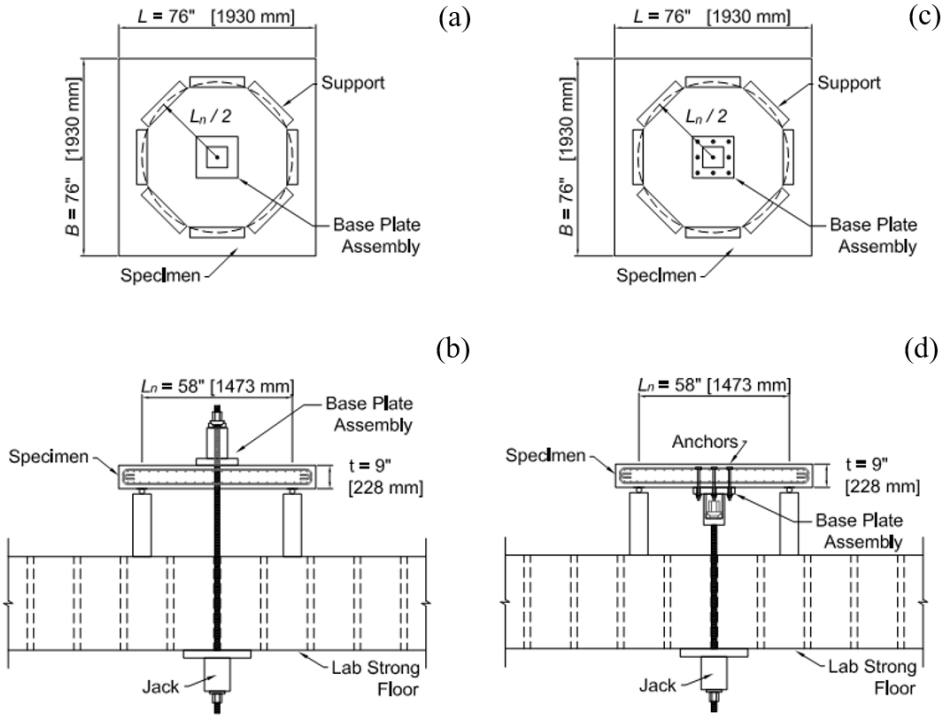

Figure 1 - Specimen dimensions and test setup configuration schematics: Punching shear test setup, (a) plan view and (b) elevation; Concrete breakout test setup, (c) plan view and (d) elevation.

The steel base plate assembly consisted of an 8-in. x 8-in. (203 mm x 203mm) box column welded to a 2-in. (50-mm) thick steel plate with plan dimensions of 16 in. (406 mm) and with stiffeners as shown in Figure 2. Holes for anchor bolts were positioned halfway between the face of the box column and the edge of the base plate. To promote uniform initial contact between the base plate and the concrete slab, the base plate was grouted to the concrete slab. To minimize accidental eccentricity, the high-strength steel rod passing through the center of the base plate assembly applied load through a semi-spherical bearing. The base plate assembly was designed to transfer the loading to the footing or the anchors (depending on the test) while remaining elastic and undergoing negligible axial deformations.

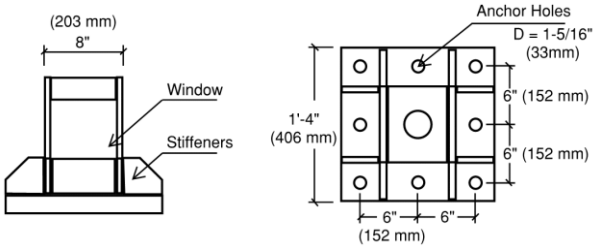

(a) (b)

Figure 2 – Base plate assembly. (a) elevation and (b) plan view

The concrete slab was reinforced top and bottom with nominal No. 4 bars spaced at s = 3-1/2 in. (89 mm) in both orthogonal directions resulting in a flexural reinforcement ratio A_s/sd = 0.80%, where A_s is the nominal cross-sectional area of a single No. 4 bar and d = 7 in. (178 mm) was taken as the average effective depth to the two layers of orthogonal bars. The reinforcement was sized to barely yield in the vicinity of the base plate for loads approaching the nominal punching shear strength, with reinforcement considered as Grade 60. For the test, however, Grade 100 reinforcement was used instead of Grade 60 reinforcement to ensure that large post-yield flexural tensile strains did not occur in the event that the actual load-carrying capacity was underestimated.

Dimensions of all specimens are shown in Figure 3. For specimens B01, B02, and B03, eight ¾-in. (19-mm) diameter anchor bolts were designed to be capable of resisting the expected group breakout load assuming a typical F1554 Gr55 steel. For the tests, however, F1554 Gr105 steel was used to ensure

linear-elastic behavior in case the breakout load was underestimated. For breakout specimen B01, the embedded end of the anchor bolts had heavy hex nuts with a bearing surface at h_{ef} = 7 in. (178 mm) below the concrete surface and nominal bearing area A_b = 0.91 in.^{2} (587 mm^2) per bolt, which was intended to be sufficient to avoid pull-out failure. Specimen B02 anchor heads were composed of two heavy hex nuts clamping a square bearing plate with ½ x 2-¼ x 2-¼ in. (13 x 57 x 57 mm) dimensions that provided A_b = 4.62 in.^{2} (2980 mm^2) with h_{ef} = 7 in. (178 mm), taken from the concrete surface to the bearing surface of the washer plate. Specimen B03 had the same type of bearing heads as B02 with the addition of reinforcement trim bars in both main orthogonal directions, extending a tension development length from each anchor bolt as shown in Figure 4. Trim bars were constructed using the same type of steel as the main longitudinal bars. Finally, specimen S01 had the same type of bearing head as B01 but had only a single anchor bolt at the column center.

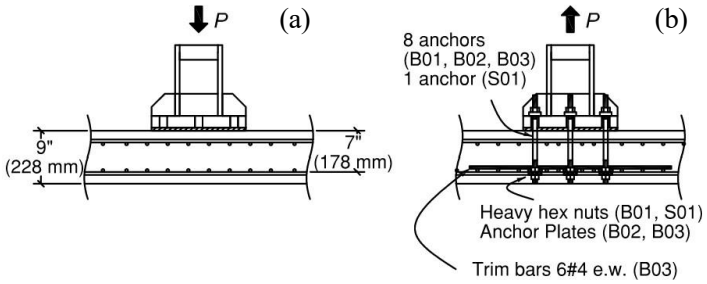

Figure 3 –Specimens reinforcement, base plate, and anchor bolt detailing. (a) Punching shear specimen P01; (b) Breakout specimens B01, B02, B03 and S01.

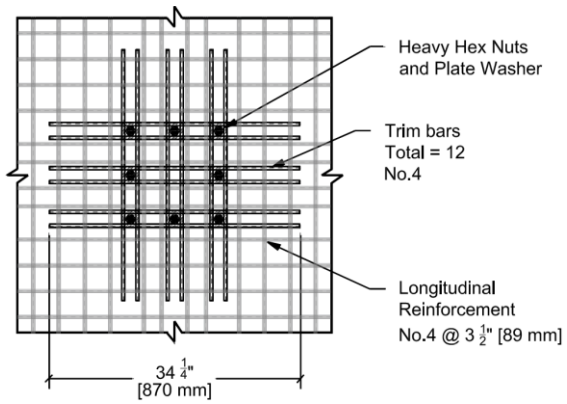

Figure 4 – Specimen B03; plan view of trim bars.

Materials

Commercial ready-mixed concrete with maximum coarse aggregate size of 3/8 in. (10 mm) ("pea gravel") was used in all footings. Targeted concrete compressive strength was 4000 psi (27.6 MPa). Cement was compliant with ASTM C150 TYPE II and specified ratio of water/cementitious materials (W/C) was 0.58. Measured concrete slump values were around 8 to 9 in. (203-228 mm) for both concrete casting phases.

Concrete mechanical properties determined from testing were f'_c (compressive strength), f_t (tensile strength), E_c (modulus of elasticity), and G_f (fracture energy). The first three index properties were determined from ASTM standard tests of 6-in. x 12-in. (152-mm x 305-mm) concrete cylinders cast simultaneously and stored with the test specimens. Table 1 presents mean measured results. Fracture energy beams where cast during phase 2 only and were tested at 41 days in accordance with RILEM procedure FMC 2 for fracture energy determination (RILEM TC, 1994). Measured fracture energy was 0.46 lb/in. (80 N/m).

ASTM A1035 Grade 100, or "MMFX", reinforcing steel was used in all specimens. Measured material properties were yield stress f_y = 134 ksi (923 N/mm^2), yield strain ε_y = 0.006, and maximum tensile stress f_u = 170 ksi (1170 N/mm^2).

Table 1 – Concrete mean mechanical properties

Specimen ID	Test Type	Phase	Concrete age during test [days]	Concrete compressive strength f'_c, psi (MPa)	Concrete tensile strength f_t, psi (MPa)	Concrete modulus of elasticity E_c, ksi (GPa)
P01	Punching shear	1	22	3820 (26.3)	345 (2.4)	3,220 (22.2)
B01	Concrete breakout	1	27	4170 (28.7)	367 (2.5)	3,330 (22.9)
B02	Concrete breakout	2	31	4920 (33.9)	471 (3.2)	3,230 (22.2)
B03	Concrete breakout	2	35	5140 (35.4)	438 (3.0)	3,120 (21.5)
S01	Single anchor	2	41	5230 (36.0)	417 (2.9)	3,270 (22.6)

*All properties in the table correspond to the test dates indicated.

Test setup

The selected boundary conditions were discrete support lines arranged in an octagonal plan configuration approximating a circular support with diameter L_n = 58 in. (1473 mm). Specimen dimensions and setup configuration are sketched in Figure 1.

The linear discrete supports composing the octagonal base were fabricated using wide flange sections with welded web stiffeners to avoid local buckling and ensure sufficiently stiff boundary conditions. A plain round steel bar was placed on top of each flanged member to provide moment release. Each test slab had steel bearing plates embedded in the concrete at the location of the round rods, resulting in a steel-on-steel support. Additionally, greased thin steel shims were slid in between the rollers and the bearing plates to ensure unrestrained lateral displacement and to fill any minor gaps between bearing plates and round bars.

The concentric point load was applied to a specimen through a high-strength prestressing rod tensioned by a hydraulic jack installed under the laboratory strong floor, as shown in Figure 1. The applied load was transferred directly to the slab through the steel base plate assembly shown in Figure 2. Figure 5 shows a photograph of the test setup for specimen P01. For the breakout specimens the high strength rod applies load directly to the base plate assembly underneath the slab. The load is then carried by the cast-in anchors to the top of the member and transferred to the slab and supports by bearing on the different anchor head details.

Figure 5– Punching shear specimen (P01) test setup.

Instrumentation

Applied force was measured using a set of load cells in line with the hydraulic jack. Vertical displacements of the slabs were measured at the top surface of the concrete or, in the case of the punching shear test, the top of the base plate assembly. For the concrete breakout tests for Phase 2, wire-pods were placed under the slab to measure vertical displacements directly on the column base plate. Electrical resistance strain gauges were attached to selected slab reinforcement for specimens P01, B01, B02, and B03 and to selected anchor bars for specimens B01, B02, and B03.

Testing procedure

Load was applied monotonically at a constant loading rate of 15 kips (67 kN) per minute until failure, with brief pauses for cracking inspections and preliminary test data checks. Loading continued after apparent failure to observe post-failure behavior.

TEST RESULTS – PUNCHING AND 8-BOLT BREAKOUT TESTS

Load – displacement response

Figure 6 shows measured relationships between applied load and resulting displacement for the punching shear test P01 and the three breakout tests using eight anchor bolts (B01, B02, and B03). All specimens were loaded monotonically until reaching maximum load, and then load application continued until residual strength stabilized. The load-displacement relationships show a reduction in stiffness at loads around 50 kips (222 kN), believed to be a result of flexural cracking in the slabs. Ultimate failure at maximum applied loads was in the form of a punching shear failure for P01 and breakout cone failure for B01, B02 and B03. Ultimate load capacities were 175, 99, 118, and 137 kips (778, 440, 525, 609 kN) for P01, B01, B02, and B03, respectively. These ultimate load measurements neglect self-weight, which accounts for around 1% of the total shear on the critical section. Self-weight estimates include the mobilized concrete cone, the hydraulic jack and all the steel components and measurement instruments supported by the specimen.

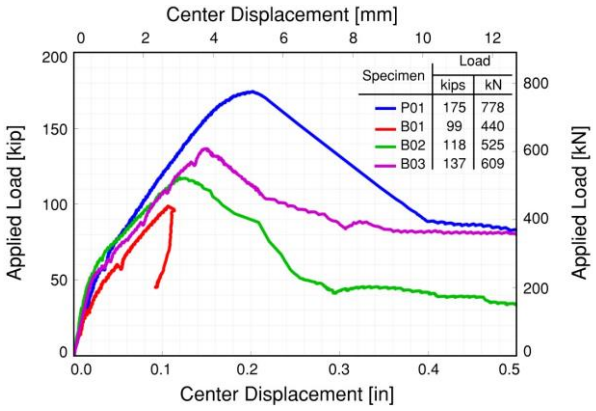

Figure 6 – Applied load - Center displacement

After punching or breakout failure, the resistance decreased with increasing vertical displacement of the failure cone, eventually stabilizing at a residual strength apparently associated with catenary action of flexural reinforcement crossing the failure surface. Ratios of residual strengths to ultimate strengths were approximately 0.45, 0.35, 0.35, and 0.58 for specimens P01, B01, B02, and B03, respectively. For specimens P01, B02, and B03, center displacement was measured with respect to the center of the concrete cone, such that the load-deformation response of the failure cone after failure can be seen directly in Figure 6. For specimen B01, center displacement was measured at the center of the slab on the opposite side of the failure cone. The slab rebounded after failure, leading to a reduction in the recorded displacement after failure as shown in Figure 6.

Figure 7 plots the displaced shapes measured along the centerline of each test specimen at the top surface of the slab just before failure.

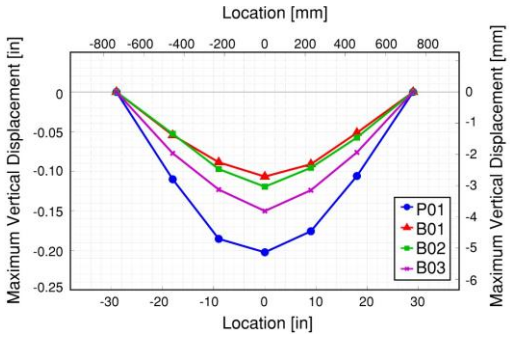

Figure 7 – Vertical displacement profiles measured along the centerline of each test specimen at the top surface of the slab just before failure.

Longitudinal steel strains

Strains in slab longitudinal reinforcement increased progressively with increasing applied load. Figure 8 plots the distribution of longitudinal reinforcement strain along the centerline of each test specimen just before reaching ultimate load capacity. The maximum strains near the center of the slab approach 0.002, which is close to the yield strain of Grade 60 reinforcement, but is well within the elastic range of response for the Grade 100 steel used in the test specimens.

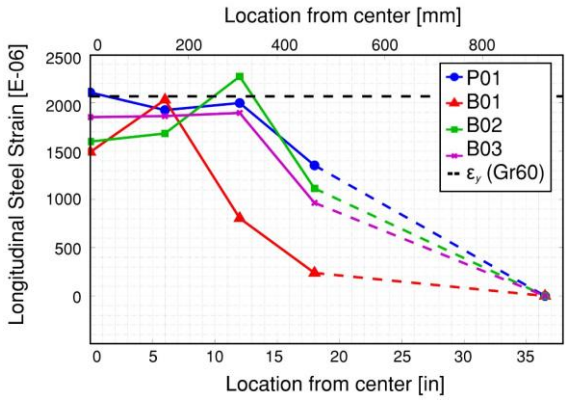

Figure 8 – Longitudinal steel strain distribution at maximum load.

Anchor and trim bar strains

Figure 9 plots the measured relationships between applied load and strains in individual anchor bolts. The three functioning strain gauges of specimen B01 show progressively increasing strain with increasing load, although gauge A3 lagged behind the other two gauges for higher load levels. It is possible that this reflected some eccentricity in the application of the load, malfunction of the strain gauge, or slippage of anchor bolt A3 relative to the other bolts. For specimens B02 and B03, the gauges indicated nearly identical force resisted by each of the four instrumented anchor bolts.

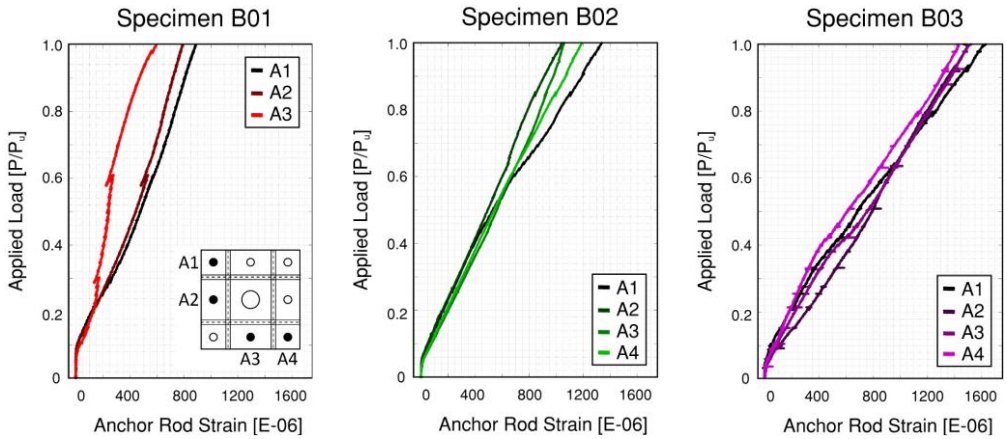

Figure 9 – Anchor rod strains

Figure 10 shows the measured strain on the added trim bars in specimen B03 as a function of applied load P normalized by ultimate load capacity P_u. Strain gages were located close to the anchor heads. The strains indicated compression (negative values) for loads up to around half the ultimate load capacity, which is consistent with anticipated flexure-induced compression in the uncracked slab. Strain gradients reverted from negative to positive for higher loads, indicating that the trim bars began acting as tensile reinforcement. At around the same load level, cracking was observed on the concrete slab surface and softening was apparent in the load-displacement relationship, suggesting that flexural cracks may have extended beyond the depth of the trim bars.

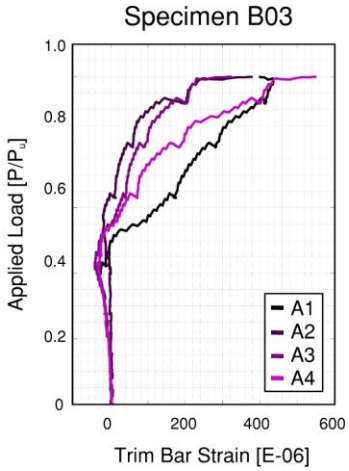

Figure 10 – Steel strains on trim bars

Failure surfaces

Punching and breakout failures were generally identifiable during testing by an abrupt noise accompanied by a modest increase in displacement and reduction in applied load. By tapping on the concrete surface it was apparent that a solid cone of concrete extended from near the top surface of the slab and angled outward toward the bottom surface. Where the failure surface engaged the bottom mat of slab reinforcement, the failure surface flattened to follow the reinforcement as it was split from the bottom of the slab.

After each test, the specimen was taken apart carefully so that the shape of the main failure surface could be characterized. Note that loose concrete might include some pieces that were part of the original failure cone but that were broken loose during the test or during demolition. Not including the portion of the failure surface that flattened near its intersection with the bottom reinforcement mat, the average inclination angles for the critical shear cracks were approximately 37°, 43°, 41°, and 33° relative to horizontal for specimens P01, B01, B02, and B03. Given the highly irregular failure surfaces, these reported angles are unavoidably subjective and imprecise. The reported angles are within the range commonly observed for punching shear and breakout failures (ASCE 426, 1974; Eligehausen et al., 2006). Figure 11 shows typical cross sections of the failure cone surfaces. It can be observed that the largest concrete cone corresponds to punching shear specimen P01, followed in order by breakout specimens B03, B02, and B01, which has an apparent correlation with the observed ultimate load capacity.

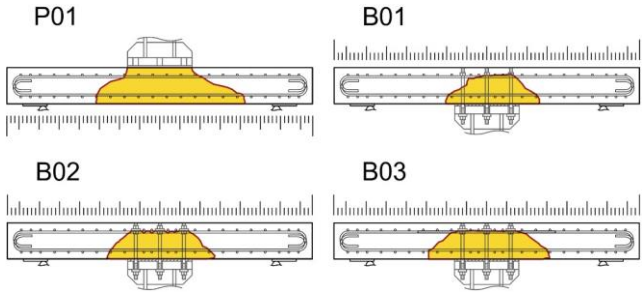

Figure 11 – Specimen failure surface, typical cross sections.

TEST RESULTS – SINGLE-BOLT BREAKOUT TEST

Test specimens B01, B02, and B03 each have eight anchor bolts, leading to a group breakout failure involving all eight anchor bolts. It was also of interest to obtain benchmark data from a test specimen (designated S01) using a single anchor bolt. For this test the base plate assembly was modified to pull a

single anchor bolt in concentric tension (Figure 3). The anchor bolt, heavy hex nut, and anchorage depth were nominally identical to those of specimen B01.

Test specimen S01 experienced breakout failure when the applied load reached 41 kips (182 kN), which is about 40% of specimen B01 ultimate load capacity. Slab flexural cracking was not apparent. Slab reinforcement tensile strains were not measured, but based on the results from specimen B01 they are estimated to have reached maximum values around 0.0003. Considering the anchor bolt nominal cross-sectional area of 0.44 in.^{2} (284 mm^2), the bolt stress at failure was approximately 93 ksi (640 MPa), which is less than the nominal yield value of F1554 Gr105 steel.

Figure 12 shows the measured relationships between applied load and displacements (relative to a fixed reference frame) of three points on the test specimen. The curve designated "Slab" refers to the displacement of the surface of the slab on the side opposite the base plate assembly. The curve designated "Bolt Head" refers to displacement at the free (unloaded) end of the anchor bolt at the point where it terminated within the slab. The curve designated "Base Plate" refers to the displacement measured on the base plate. The difference between Bolt Head displacement and Slab displacement corresponds to slip of the free end of the anchor bolt relative to the adjacent surface of the slab. The relatively large slip for loads near the failure load may be an indicator of concrete crushing beneath the heavy hex nut due to high bearing stress. With a nominal bearing area of A_b = 0.91 in.^{2} (587 mm^2), the bearing pressure at ultimate load P_u was approximately P_u/A_b = 45 ksi (310 MPa) = $8.6f'_c$. The difference between Base Plate displacement and the Bolt Head displacement is mainly due to elongation of the anchor bolt and deformation of the base plate assembly.

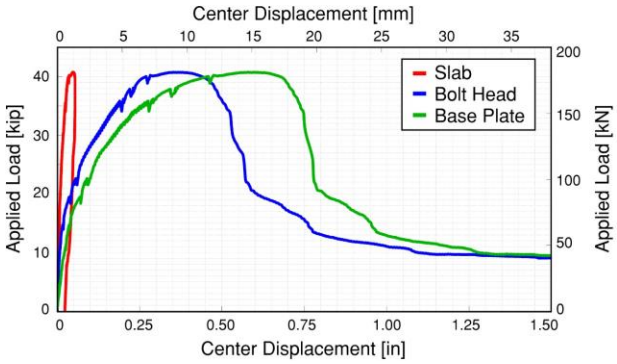

Figure 12 – Specimen S01. Applied load - center displacement plot. Measurements taken from position transducers for the slab and the anchor head; and wire-pods for the base plate.

ASSESSMENT OF EXPERIMENTAL RESULTS

Comparison with code prediction equations

Punching shear

ACI 318-19 defines nominal two-way shear strength (or punching shear strength) as the product of a concrete shear stress capacity and an area defined by an effective depth d and critical perimeter b_o. For columns supported on steel base plates, perimeter b_o is defined at $d/2$ from lines located halfway between the face of the column and the edge of the base plate. In the present study, however, the base plate was overdesigned to reduce bending deformations and to avoid plate yielding. Consequently, in the present study, the authors defined the critical perimeter b_o at $d/2$ from the edge of the base plate instead. This critical section assumption is supported by the observation that the upper surface of the failure cone in specimen P01 follows the outline of the base plate [Figure 11 (a)].

ACI 318-19 prescribes the nominal punching shear strength as the smallest value from equations (1), (2), and (3).

$$V_c = 4\lambda_s\lambda\sqrt{f_c'}b_o d, \text{psi}\ \left[0.33\lambda_s\lambda\sqrt{f_c'}b_o d, \text{MPa}\right] \quad (1)$$

$$V_c = \left(2+\frac{4}{\beta}\right)\lambda_s\lambda\sqrt{f_c'}b_o d, \text{psi}\ \left[\frac{1}{12}\left(2+\frac{4}{\beta}\right)\lambda_s\lambda\sqrt{f_c'}b_o d, \text{MPa}\right] \quad (2)$$

$$V_c = \left(\frac{\alpha_s d}{b_o}+2\right)\lambda_s\lambda\sqrt{f_c'}b_o d, \text{psi}\ \left[\frac{1}{12}\left(\frac{\alpha_s d}{b_o}+2\right)\lambda_s\lambda\sqrt{f_c'}b_o d, \text{MPa}\right] \quad (3)$$

where f_c' = specified compressive strength of concrete; β = ratio of long side to short side dimensions of the column (=1.0); λ_s = factor used to modify shear strength based on the effects of member depth (= 1.0); λ = modification factor to reflect the reduced mechanical properties of lightweight concrete (= 1.0); and α_s is an empirical constant (= 40 for interior columns). Using these equations, except using f_c' = measured compressive strength rather than specified compressive strength, the nominal punching shear strength of specimen P01 is calculated to be 159 kips (708 kN). The laboratory measured strength is 175 kips (778 kN), which is 1.10 times the calculated value.

Ospina and Hawkins (2017) have shown that the ACI 318-19 punching shear equations are conservative for slabs with effective depth less than 10 in. (250 mm). They report five tests with effective depth in the range from 7 to 8 in. (175-200 mm), with ratios of measured to calculated strengths ranging from 1.17 to 1.58, compared with 1.10 for the present test.

Single anchor concrete breakout

The ACI 318-19 equation for basic concrete breakout strength of a single anchor in cracked concrete is

$$N_b = k_c \lambda_a \sqrt{f_c'} h_{ef}^{1.5} \quad (4)$$

where k_c = 24, psi (10, MPa); λ_a = modification factor to reflect the reduced mechanical properties of lightweight concrete (= 1.0); and h_{ef} = effective embedment depth of anchor. For anchors located in a region where analysis indicates no cracking at service loads, the basic breakout strength can be increased by factor $\psi_{c,N}$ = 1.25. Where cracking is indicated, $\psi_{c,N}$ = 1.0. During the test on single-anchor specimen S01, the applied load was near but not quite to the load required to cause flexural cracking.

The ACI 318-19 provisions for anchoring to concrete are intended to represent nominal strength at a 5 percent fractile statistical level. To convert to a 50 percent fractile, the factor fmean can be used, defined by

$$f_{mean} = \frac{1}{(1 - k_{st} \cdot COV)} = \frac{1}{(1 - (1.65) \cdot (0.15))} = 1.333 \quad (5)$$

where k_{st} is a statistical parameter associated with a 5% probability of non-exceedance with a confidence of 90% (Hahn & Meeker, 1991). For an infinite data population, the value of k_{st} is 1.65. The value of the COV (coefficient of variation) for anchor design is generally assumed to be 15% (Fuchs, et al. 1995) whereby concrete tensile strength is assumed to have a minimum COV of 10% (ACI 318-19, §R22.2.2.2), (Eligehausen et al., 2006, pp. 71-75) and the remaining 5% can be assigned to (epistemic) modeling uncertainty.

Combining these effects, the 50 percent fractile breakout strength can be formulated as

$$N_{b,m} = k_c f_{mean} \psi_{c,N} \lambda_a \sqrt{f_c'} h_{ef}^{1.5} \quad (6)$$

where the product $k_c f_{mean} \psi_{c,N} \lambda_a$ = 32, psi (13.3, MPa) for cracked concrete and 40, psi (16.7, MPa) for uncracked concrete. Using the measured concrete compressive strength, this results in nominal strength of 42.9 kips (191 kN) for cracked concrete and 53.6 kips (238 kN) for uncracked concrete, which are 1.05 and 1.31 times the measured strength of 41 kips (182 kN) for specimen S01. It is plausible that the superposition of tensile stresses due to breakout and due to flexural tension combined to produce in a net reduction in the breakout strength, which may explain why the estimate obtained assuming cracked concrete is closer to the test value than the estimate obtained assuming uncracked concrete. Alternatively, these results might also be an outcome of the relatively low fracture energy obtained for this concrete. The available data are insufficient to conclude whether one or more of these effects were influential.

Group anchor concrete breakout

The ACI 318-19 equation for concrete breakout strength of a group of anchors located away from edges and subjected to concentric tension can be expressed as

$$N_{cbg} = \frac{A_{Nc}}{A_{Nco}} \psi_{c,N} N_b \quad (7)$$

where A_{Nc} = projected concrete failure area of the group of anchors, taking the base of the rectilinear geometrical figure that results from projecting the failure surface outward $1.5h_{ef}$ from a line passing through a row of adjacent anchors; and A_{Nco} is the projected concrete failure area of a single anchor with an edge distance equal or greater than $1.5h_{ef}$. Where an additional plate or washer is added at the head of the anchor, it is permitted to project the concrete failure area from an effective perimeter of the added plate washers located a distance equal to the plate thickness beyond the head. In the present study, for specimen B01 which has no added anchor plates, two values of the ratio $\frac{A_{Nc}}{A_{Nco}}$ are calculated, one at the bolt centerline as specified in ACI 318-19 and another at an effective perimeter defined by the outer edge of the heavy hex nut.

Following the procedures applied for single anchors, the 50 percent fractile breakout strength for the group of anchors can be formulated as

$$N_{bg,m} = k_c f_{mean} \psi_{c,N} \lambda_a \frac{A_{Nc}}{A_{Nco}} \sqrt{f_c'} h_{ef}^{1.5} \quad (6)$$

where the product $k_c f_{mean} \psi_{c,N} \lambda_a$ is as previously defined for single anchors.

Table 2 compares measured and calculated breakout strengths for the different assumptions of $\frac{A_{Nc}}{A_{Nco}}$ and different assumptions of whether the concrete region is uncracked or cracked. The best correlations are obtained measuring $\frac{A_{Nc}}{A_{Nco}}$ to the outer effective perimeter of the hex nuts or the added plate and assuming the concrete region is cracked. According to ACI 318-19, anchorage strength should be calculated assuming the concrete is cracked unless the anchor is "located in a region of a concrete member where analysis indicates no cracking at service load levels." In the present tests, the anchor load itself is the service load for the slab, and calculations indicate that load is sufficient to crack the concrete. Consequently, the authors interpret the Code as requiring the assumption of cracked concrete in this case. Alternative interpretations of the Code intent could be justified. For specimen B03, the added trim bars apparently added strength compared with specimen B02, but this effect is not considered in ACI 318-19.

Table 2 – Comparison of measured and calculated group breakout strengths

Specimen ID	Test P_u kip (kN)	Group Factor A_{nc} / A_{nco}	Concrete condition	50% fractile $N_{u,m}$ kip (kN)	$N_{u,m}$ / P_u
B01	99 (440)	2.47 (bolt centerline)	uncracked	118 (525)	1.19
			cracked	95 (422)	0.95
		2.66 (edge of hex nut)	uncracked	127 (565)	1.29
			cracked	102 (454)	1.03
B02	118 (525)	2.82 (effective perimeter)	uncracked	147 (654)	1.24
			cracked	117 (520)	0.99
B03	137 (609)	2.82 (effective perimeter)	uncracked	150 (667)	1.09
			cracked	120 (534)	0.87

Comparison between punching shear and anchor breakout strengths

Considering that the punching shear test and the breakout tests result in similarly shaped failure cones, it is of interest to compare the nominal shear stresses at failure for each test. For this purpose, the measured failure loads are normalized by the measured value of $\sqrt{f'_c}$ and by an effective concrete area defined by the product of an effective depth *d'* and a nominal perimeter b_o. For the punching shear specimen P01, the effective depth is the effective depth of the slab, that is, *d'* = 7 in. (178 mm), whereas for the breakout specimens, the effective depth is the effective depth of the slab minus the cover to the bearing surface of the head, that is, *d'* = 7 in. – 2 in. = 5 in. (127 mm). For the punching shear specimen P01, b_o is defined by straight lines a distance *d'*/2 away from the edge of the base plate. For breakout specimen B01, b_o is defined by straight lines a distance *d'*/2 away from the outer edge of the heavy hex nuts. For breakout specimens B02 and B03, b_o is defined by straight lines a distance *d'*/2 away from the effective perimeter of the added plate washers located a distance equal to the plate thickness beyond the hex nuts. Table 3 summarizes the relevant parameters used in the comparison.

Column (7) of Table 3 compares the relative stress capacities, that is, the ratios of the normalized stress in column (6) divided by the normalized stress for specimen P01. It is apparent that, when normalized by compressive strengths and nominal failure surfaces, the relative strengths are fairly constant among the four main test specimens. The one outlier is specimen B03, which had the added trim bars that are not considered in the normalization. It could be argued that the trim bars effectively increased the anchor head bearing area, thereby mobilizing more concrete and reaching a higher ultimate load.

The single anchor specimen test results are not included in Table 3 because of differences in head bearing stresses, slab service level stresses, and shape of the failure surface. A parallel calculation,

however, results in a ratio of 1.29 in column 7 of Table 3.

Table 3 – Punching shear vs. concrete breakout comparison

Specimen (1)	P_u, kip (kN) (2)	f_c', psi (MPa) (3)	d', in. (mm) (4)	b_o, in. (mm) (5)	$\frac{P_u}{b_o d' \sqrt{f_c'}}$, psi (MPa) (6)	Relative stress capacities (7)
P01	175 (778)	3820 (26.3)	7 (178)	92.0 (2340)	4.40 (0.367)	1.00
B01	99 (440)	4170 (28.7)	5 (127)	73.0 (1854)	4.20 (0.350)	0.95
B02	118 (525)	4920 (33.9)	5 (127)	77.0 (1956)	4.37 (0.364)	0.99
B03	137 (609)	5140 (35.4)	5 (127)	77.0 (1956)	4.96 (0.414)	1.13

SUMMARY AND CONCLUSIONS

A laboratory test program compared the failure mechanisms and strengths of concrete foundation slabs subjected to punching shear and to concrete breakout loadings. The slabs were designed to be representative of typical isolated footing elements supporting steel columns at one-half of full scale. One of the slabs was loaded through a base plate assembly to observe punching shear failure. Four other slabs were tested for breakout failure. One of these used the same base plate assembly as was used for the punching test, but in this case it supported eight cast-in anchor bolts with heavy hex nuts acting as anchor heads for loading in tension until breakout failure. In another breakout test, plate washers were added to increase the bearing area and in yet another breakout test with plate washers the slab had supplemental reinforcement. A final breakout test had a single anchor bolt with heavy hex nut.

Measured strengths were compared with nominal strengths of the ACI 318-19 building code. It was recognized that the ACI 318-19 equations for nominal breakout strength are calibrated to be at the 5 percent fractile statistical level. A factor was applied to adjust the breakout strength equations to a 50 percent fractile, which is the basis to determine nominal punching shear strength in ACI 318-19.

Experimental results indicate that:

1. The punching shear loading case resulted in the largest strength. Among the breakout tests with eight anchor bolts, the lowest strength occurred for the case with heavy hex nuts without plate washers, with strength equal to 57% of the punching shear strength. The breakout test with plate washers produced intermediate strength at 67% of the punching shear strength, while adding trim bars further increased strength to 78% of the punching shear strength.

2. The punching shear test specimen failed at a load 1.10 times the ACI 318-19 nominal two-way punching shear strength, which is in the range expected based punching tests of slabs of similar thickness.
3. For the breakout tests with eight anchor bolts, the measured strengths for specimens with heavy hex nuts and with plate washers were 95% and 99%, respectively, of the nominal breakout strengths (adjusted to the mean) calculated using ACI 318-19 nominal breakout strength equations for anchors in cracked concrete. The measured strengths fell well short of the ACI 318-19 nominal breakout strengths (adjusted to the mean) for anchors in uncracked concrete. It is plausible that the expressions for cracked concrete are more applicable because the anchor loads produced service stresses that cracked the slab concrete. However, other parameters such as relatively low fracture energy or inaccuracies in the model for group behavior may explain the relatively lower test results. Further study is required.
4. Added slab deformed reinforcement in the vicinity of the bearing head increased the breakout ultimate strength by 15% compared with the breakout strength without the added reinforcement. Residual strength was also increased from 0.35 P_u to 0.58 P_u as a result of including this additional reinforcement. It could be argued that the trim bars effectively increased the anchor head bearing area, thereby mobilizing more concrete and reaching a higher ultimate load. Further study is required.
5. Punching failure and breakout failure produced similarly shaped failure surfaces. However, the breakout failure surface area was smaller than the punching shear failure surface area because the anchor heads were embedded within the slab, thereby reducing the effective depth. When normalized by the square root of the concrete compressive strength and by an effective failure area, the normalized nominal failure stresses were similar for the different test cases.

ACKNOWLEDGMENTS

The work presented in this paper was partially funded by the HILTI Corporation and the ACI Foundation. Roberto Piccinin and John Silva from Hilti provided extensive and valuable discussion to envision and develop the test program. Ron Klemencic from Magnusson Klemencic Associates, Clark Construction, CONCO, Alamillo rebar, Central Concrete Supply Co., CRSI, and Precision Rebar & Accessories Inc. provided generous donations of labor and materials. James Malley from Degenkolb, and Rafael Sabelli from Walter P. Moore provided valuable data and advice.

NOTATION

a = distance from edge of base plate to nearest point of support

A_b = Anchor head nominal bearing area

A_{Nc} = projected concrete failure area of the group of anchors

A_{Nco} = projected concrete failure area of a single anchor with an edge distance equal or greater than $1.5h_{ef}$

A_s = nominal cross-sectional area of a single flexural reinforcing bar

b_o = perimeter of critical section for two-way shear in slabs and footings

COV = coefficient of variation for anchorage capacity

d = distance from extreme compression fiber to centroid of flexural tension reinforcement in the slab

d' = for the breakout specimens, it is the effective depth of the slab d minus the cover to the bearing surface of the head

E_c = modulus of elasticity of concrete

f'_c = compressive strength of concrete

f_{mean} = factor to convert 5 percent to 50 percent fractile capacity estimates for anchorage.

f_t = tensile strength of concrete

f_u = maximum tensile stress of reinforcing steel

f_y = yield stress of reinforcing steel

G_f = fracture energy of concrete

h_{ef} = effective embedment depth of anchor

k_c = coefficient for basic concrete breakout in tension

k_{st} = statistical parameter

$N_{b,m}$ = 50 percent fractile breakout strength of a single anchor

$N_{bg,m}$ = 50 percent fractile breakout strength for the group of anchors

N_{cbg} = nominal concrete breakout strength in tension of a group of anchors

P = applied load to specimen

P_u = maximum load applied to specimen

s = flexural reinforcement spacing

V_c = nominal punching shear strength

α_s = empirical constant to calculate V_c in slabs and footings

β = ratio of long side to short side dimensions of the column

ε_y = yield strain of reinforcing steel

λ = modification factor to reflect the reduced mechanical properties of lightweight concrete

λ_a = modification factor to reflect the reduced mechanical properties of lightweight concrete

λ_s = factor used to modify shear strength based on the effects of member depth

$\psi_{c,N}$ = factor used to modify tensile strength of anchors based on presence or absence of cracks in concrete

REFERENCES

ACI Committee 318 (2019). "Building Code Requirements for Structural Concrete and Commentary (ACI 318-19)," American Concrete Institute, Farmington Hills, MI, 623 pp.

ASCE 426 (1974). "The Shear Strength of Reinforced Concrete Members – Slabs," Joint ASCE-ACI Task Committee 426 on Shear and Diagonal Tension of the Committee on Masonry and Reinforced Concrete of the Structural Division, *Journal of the Structural Division*, V. 100, No. ST8, pp. 1543-1591.

Eligehausen, R., Mallée, R. & Silva, J. F. (2006). "Anchorage in Concrete Construction" Berlin: Ernst & Sohn, 2006.

Fuchs, W., Eligehausen, R., & Breen, J. (1995), "Concrete Capacity Design (CCD) Approach for Fastening to Concrete", ACI Structural Journal, V. 92, No. 1, January-February 1995.

Gaspar Rodriguez, D. (2018). Comparative study of punching shear and concrete breakout behavior in reinforced concrete foundation elements, M.S. Thesis, Civil and Environmental Engineering, University of California, Berkeley, 127 pp.

Hahn, G. & Meeker, W., (1991). Statistical Intervals: A Guide for Practitioners, John Wiley & Sons, 1991, pp. 397.

Ospina, CE, and Hawkins, NM (2017). "Effect of slab flexural reinforcement and depth on punching strength," *ACI Special Publication 315*, pp. 117-140.

RILEM TC (1994) "FMC 2 Size-effect method for determining fracture energy and process zone size of concrete, 1990. *RILEM Recommendations for the Testing and Use of Construction Materials*, pp. 102-106.

CHAPTER 2 - MOMENT TRANSFER AT COLUMN-FOUNDATION CONNECTIONS: PHYSICAL TESTS[2]

by Benjamin Worsfold, Jack Moehle, and John Silva

ABSTRACT

Steel and precast columns are commonly designed to transfer moment loads to concrete foundations through cast-in-place headed anchors. In design office practice in the United States, connection strength has been evaluated considering mechanisms emphasizing joint shear, strut-and-tie modeling, and anchoring-to-concrete. For any given connection, the strengths calculated with these three methods can differ by a wide margin. The application of these methods, including possible enhancements that improve strength estimates, is described. Laboratory tests were performed to provide benchmark physical data to determine the applicability of various design methods. The test specimens consisted of full-scale interior steel-column to concrete-foundation connections located away from foundation edges, with details typical of current construction practice on the West Coast of the United States. Strength in both tests was governed by concrete breakout failure. Strategically placed reinforcing increased the strength and displacement capacity of anchored connections governed by breakout. Design recommendations are provided.

Keywords: anchoring to concrete; beam-column joint; breakout; column-foundation connections; shear reinforcing; strut-and-tie; supplementary reinforcing

INTRODUCTION

Connections between structural columns and foundations are common in building construction. Whether the column is cast-in-place concrete, precast concrete, or structural steel, moment transfer at the foundation presents a challenge for designers as little consensus exists regarding what failure modes are relevant or which design provisions apply. This paper describes three moment transfer models that have

[2] Originally published as part of *ACI Structural Journal*, V. 119, No. 5, September 2022, DOI: 10.14359/51734799. Awarded The Wason Medal for Most Meritorious Paper of 2023 by the American Concrete Institute.

been considered by practicing structural engineers for steel columns anchored to foundations using cast-in-place anchors. These are: 1. Anchoring-to-concrete provisions (e.g., ACI 318-14 Ch. 17), 2. strut-and-tie modeling (e.g., ACI 318-14 Ch. 23), and 3. joint shear design provisions (e.g., ACI 352R-02). For any given connection, the strengths calculated with these three methods can differ by a large margin.

The ACI anchoring-to-concrete provisions historically reflect larger safety margins than is common in other parts of the code. This is in part due to the potential for a "single-point fastening" whereby loads can be carried by a connection providing no redundancy and little warning of failure. Various options for reducing conservatism are discussed such as including the beneficial effect of column flexural compression and the use of a median breakout strength rather than a 5-percent fractile value. These measures may allow designers to consider breakout failure in a manner that is more consistent with other methods and may lead to more economical designs, while preserving the overall required reliability.

Two full-scale interior steel-column to concrete-foundation connections located away from foundation edges were constructed and tested under reversed-cyclic lateral loading to better understand the failure mechanisms and design requirements. One of the test specimens was constructed without transverse reinforcement in the foundation, while the other test specimen had transverse reinforcement to increase strength and deformation capacity. Design recommendations are made based on the test results.

LITERATURE REVIEW

Fuchs et al. (1995) proposed the Concrete Capacity Design (CCD) method as a simplified model for calculating the peak breakout strength of anchors or anchor groups in plain concrete. This method forms the basis for many modern building codes, including ACI 318 and Eurocode EN 1992-4. Tests have shown that the breakout force does not increase linearly with the size of the failure area (Ožbolt et al. (1998)). This phenomenon is attributed to the size effect in concrete fracture (Bažant (2000)) and is incorporated into the CCD method by modifying the exponent on the effective depth. If the size effect is not considered, the breakout strength predicted for anchors with larger embedment may be unconservative.

Tests on anchors in cracked concrete tend to result in lower breakout strengths and lower stiffnesses than anchors tested in so-called uncracked concrete (Eligehausen et al. (2006)). Eligehausen and Balogh (1995) report that pre-existing cracks extending through the full anchor depth with a uniform crack width between 0.3 – 0.4 mm can reduce tension capacity governed by concrete breakout by about 25% (headed and undercut anchors) or 35% (torque-controlled expansion anchors) compared to the uncracked conditions. The authors recommend that, in general, the design of anchors should assume the cracked condition.

ACI 352R-02 describes recommendations for designing monolithic beam-column connections for structural frames. The geometry and force flow of a column-foundation connection can be thought of as similar to a roof connection confined on all four sides. Therefore, some engineers use the ACI 352 recommendations for the design of column-foundation connections.

Tanaka and Oba (2001) tested six concrete column-to-foundation connections comparing columns anchored with cast-in bent-out hooks and post-installed bonded reinforcing bars. Specimens governed by concrete cone failure show low displacement capacity and pinched hysteresis loops. The researchers also noted that the embedment of post-installed reinforcing bars required to avoid breakout failure was less than the prescribed development lengths.

Based on 16 full-scale column-foundation connection specimens and analytical simulations, Mahrenholtz et al. (2014) propose a design method that enhances the ACI 319 breakout strength equations. Two modification factors are proposed to consider 1) the degradation due to cyclic loading and 2) the beneficial effect of the column flexural compression force, which constrains the formation of the traditional breakout cone (as proposed by Herzog (2015)).

Analytical simulations by Mahadik et al. (2019) suggest that a column-foundation specimen that is simply supported places additional shear demands on the joint that may not be present in a specimen with continuous soil supports.

Kupfer et al. (2003) developed a strut-and-tie model for column-foundation connections that suggests vertical ties may be required in the foundation outside the joint for equilibrium.

Multiple researchers have investigated the beneficial effect of different reinforcing configurations on anchor behavior. Sharma et al. (2017a) and Sharma et al. (2017b) describe a series of physical tests of anchor groups with so-called supplementary reinforcing under tensile loads or shear loads towards an edge. They showed that relatively small amounts of reinforcing increase anchor group strength and displacement capacity. Based on finite element simulations (Nilforoush et al., 2017) and physical experiments (Nilforoush et al., 2018), a modification factor was proposed to consider the beneficial effect of surface reinforcement on breakout failure. However, no additional benefit was observed for surface reinforcing ratios above 0.3%. Papadopoulos et al. (2018) investigated headed reinforcing bars in column-slab connections for bridges. They demonstrated that shear reinforcing in the form of J-bars inside the joint and stirrups outside the joint prevented breakout failure and punching of the heads through the far side of the slab. The first row of stirrups outside the joint improved the behavior of the connection, while additional rows seemed to have no effect. The results led to detailing recommendations adopted by Caltrans in MTD 20-7 (Caltrans 2016).

RESEARCH SIGNIFICANCE

Full-scale laboratory tests of column-foundation connections with cast-in-place headed anchors focusing on the concrete failure modes are scarce, particularly for deep anchors where h_{ef} > 10-in [250 mm]. This project also investigates the influence of distributed reinforcing bars across the breakout failure zone. This research project provides benchmark physical data and evaluates alternate design methods.

FORCE TRANSFER AT A COLUMN-FOUNDATION CONNECTION

Fig. 1 illustrates an idealized case of a steel column transferring pure moment (no shear or axial loads) into a reinforced concrete foundation through a base plate and anchor bolts. In Fig. 1(a), let us assume that there are two lines of bolts, one on each side of the column. The moment is resisted by a tension-compression couple, as shown in Fig. 1(b). The tensile force T is resisted directly by the line of anchor bolts on the left side of the connection. The compressive force C is resisted by compression between the base plate and the grout/concrete interface. In a typical foundation, these actions are transferred into the foundation, which, in turn, transfers them to the surrounding soil and foundation elements.

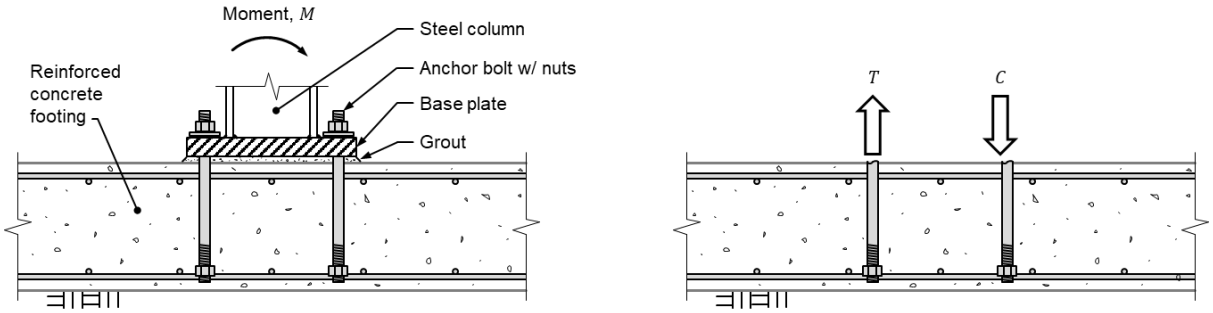

(a) Moment transfer at connection (b) Tension-compression couple

Fig. 1–Moment transfer between a steel wide-flange column and a reinforced concrete foundation

A fundamental design question is: “How is the tension-compression couple formed by T and C resolved in the concrete in the immediate vicinity of the applied forces, and how should the connection be assessed for structural adequacy?” The following three design options are considered here:

1. Design the connection using current design rules for beam-column joints.
2. Design the connection using a strut-and-tie model.
3. Design the connection considering anchoring-to-concrete provisions.

The following text considers each of these connection design options in turn. Moment transfer is assumed to be due to earthquake effects, which will dictate some of the strength and detailing requirements.

Design as a beam-column joint

In this approach, the connection is designed as a beam-column joint following ACI 318-19 or ACI 352R provisions. The joint is defined as the volume of concrete bounded by the depth of the foundation vertically and a horizontal area within the effective bearing area of the base plate. This joint is assumed to transfer horizontal joint shear through a diagonal strut, as shown in **Error! Reference source not found.**. Transverse reinforcement is provided following ACI 318-19 or ACI 352R provisions to confine the joint and thereby improve its ability to transmit joint shear under load and deformation reversals. Joint nominal shear strength in pounds is defined as:

$$V_n = \gamma\sqrt{f_c'}A_j \tag{1}$$

where γ = joint shear strength coefficient dependent on joint geometry and loading, f'_c = concrete compressive strength in psi, and A_j = cross-sectional area of a horizontal plane through the joint in square inches. The joint shear strength coefficient is taken as γ = 15 by considering the joint to have all four vertical faces confined and a discontinuous column subjected to lateral loading resulting from ground motion.

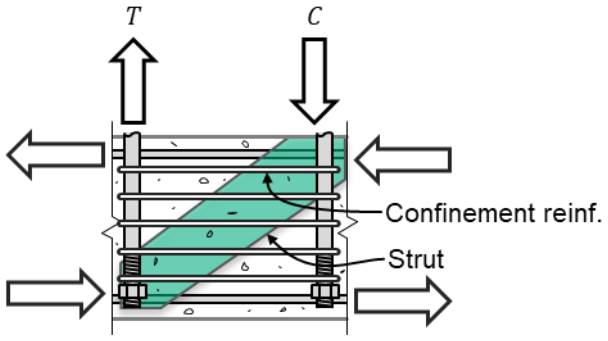

Fig. 2–Beam-column joint model

Design by the Strut-and-Tie Method

The strut-and-tie method was developed for regions near geometric discontinuities and points of load application, including beam-column joints (ACI 318-19). Fig. 3 illustrates a possible model for the application of the strut-and-tie method, including nodal zones, struts, and ties that are in equilibrium with the forces external to the discontinuity region. To facilitate effective nodal zone development, the anchor bolts may need to extend below the flexural tension-compression zone at the bottom of the foundation and be equipped with plate washers at the ends of the anchor bolts. This extension of the anchor bolts may be impractical from a construction perspective because concrete cover requirements would require thickening the foundation, either globally or locally, with associated cost implications. In a typical application, the discontinuity region might be designed to develop the full tensile strength of the anchor bolts on one side of the joint, with plate washers sized to keep stresses for nodal zones and struts within acceptable limits. According to ACI 318-19, the nominal axial compressive strength of a strut is given by:

$$F_{ns} = 0.85\beta_c\beta_s f_c' A_{cs} \quad (2)$$

where β_c = 1.0 because there is no adjacent bearing surface, β_s =0.75 for beam-column joints, and A_{cs} is the cross-sectional area at the end of the strut under consideration. The nodal zone at the lower left is anchoring two ties and one strut, making it a C-T-T node, so its strength is given by:

$$F_{nn} = 0.85\beta_c\beta_n f_c' A_{nz} \quad (3)$$

where β_n = 0.60 for beam-column joints and A_{nz} is the area of each face of the nodal zone. ACI 318-19 Sec. 23.11 specifies an additional factor for regions of a seismic force-resisting system assigned to Seismic Design Category D, E, or F. However, if the forces are limited by the yielding of the tension anchor, the additional factor is 1.0.

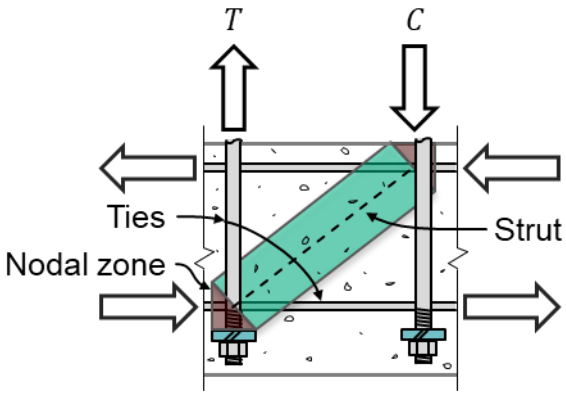

Fig. 3–Possible strut-and-tie model

Design using the Anchoring-to-Concrete Provisions

The ACI 318-19 provisions for anchoring to concrete include equations to predict concrete breakout failure, in this case characterized by cracks initiating at the bearing heads of the tension-loaded anchors and propagating towards the concrete surface at an angle of about 34 degrees (1.5:1) from the horizontal as shown in Fig. 4. This failure mode is recognizable by the appearance of a circular fracture pattern at the concrete surface and the subsequent pyramidal volume of detached concrete. According to ACI 318-19, for a group of anchors located away from free edges and subjected to concentric tension, the nominal breakout strength is given by:

$$N_{cbg} = \frac{A_{Nc}}{A_{Nco}} \ \psi_{ec,N}\, \psi_{ed,N}\, \psi_{c,N}\, \psi_{cp,N}\, N_b \tag{4}$$

where A_{Nc}/A_{Nco} = projected concrete failure area for the anchor group divided by failure area for a single anchor, $\Psi_{ec,N}$ = breakout eccentricity factor, $\Psi_{ed,N}$ = breakout edge effect factor, $\Psi_{c,N}$ = breakout cracking factor, $\Psi_{cp,N}$ = splitting modification for post-installed anchors, and

$$N_b = 24\sqrt{f_c'}\, h_{ef}^{1.5} \text{ (if } h_{ef} \leq 11\ in.\text{)} \text{ (lb, in.)} \tag{5}$$

$$N_b = 16\sqrt{f_c'}\, h_{ef}^{5/3} \text{ (if } 11\ in. \leq h_{ef} \leq 25\ in.\text{) (lb, in.)} \tag{6}$$

where h_{ef} = depth to the bearing surface of the anchor bolt. For this case, $\Psi_{ec,N} = \Psi_{ed,N} = \Psi_{cp,N} = 1.0$. A value of $\Psi_{c,N} = 1.0$ should be used if the concrete foundation element is expected to exhibit cracking under service loads near the anchors; otherwise, $\Psi_{c,N} = 1.25$. Shallow foundations subjected to large anchor forces associated with seismic demands may develop flexural stresses that exceed the modulus of rupture and, as such, could be considered cracked for anchor design. However, in cases where the anchor bearing surface is located well below the neutral axis, as shown in **Fig. 4**, the effect of cracking on anchor breakout strength of a headed bolt is likely to be marginal. For this reason, ACI 318 Sec. 17.10.5.4 specifically permits consideration of the uncracked concrete state, “where it can be demonstrated that the concrete remains uncracked”. It seems reasonable to apply this exception here.

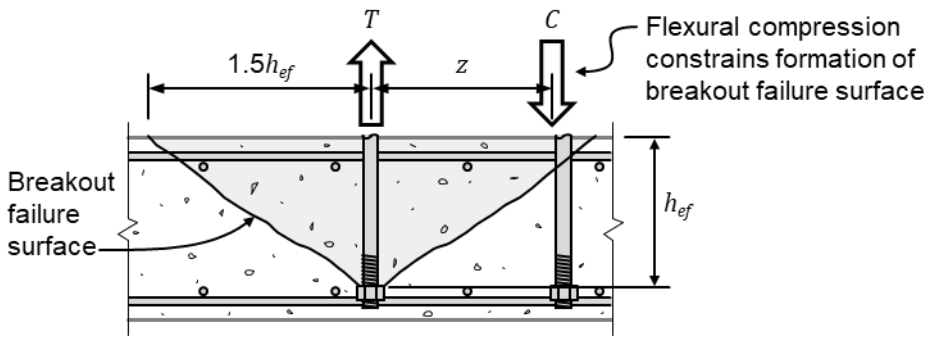

Fig. 4–Breakout failure

Fig. 4 illustrates that, for some connection geometries, the flexural compression force resultant C may bear against the failure cone such that the breakout failure will be constrained. This constraint has been observed to increase the breakout strength (Mahrenholtz et al., 2014; Herzog, 2015). Eurocode EN 1992-4 accounts for this effect by incorporating an additional factor in the breakout force calculation:

$$\Psi_M = 2 - \frac{z}{1.5\, h_{ef}} \geq 1.0 \tag{7}$$

where variable *z* is the distance between the tensile and compressive resultants (**Fig. 4**). This effect is not considered in ACI 318-19.

According to ACI 318-19, nominal strength for an anchor or anchor group is intended to correspond to a 5% fractile of the measured strengths. This design basis is in sharp contrast with design for other actions covered in the code, where the nominal strength is intended to correspond more closely with a mean or median strength. To convert a 5% fractile value to a median value, one may assume measured strengths follow a normal distribution with a covariance of 0.15 (Fuchs et al. 1995). The modification factor (f_{mean}) can be calculated using the standard normal distribution z-value for 5% fractile z = -1.645:

$$\boldsymbol{f_{mean} = \frac{1}{1+z*COV} = \frac{1}{1+(-1.645)*0.15} = 1.33} \tag{8}$$

OBSERVATIONS FROM LABORATORY TESTS

Two full-scale column-foundation connection tests were carried out to gain insights into the different design methods described previously and the influence of reinforcing bars on breakout failure. The test specimens comprised a steel wide flange column connected to a foundation slab by cast-in-place anchor bolts (see **Error! Reference source not found.** and Fig. 6). The column was subjected to reversed cyclic lateral loads with no additional axial load other than self-weight. Worsfold and Moehle (2019) and

Worsfold and Moehle (2021) provide detailed descriptions of the test specimens and experimental results for specimens M01 and M02, respectively.

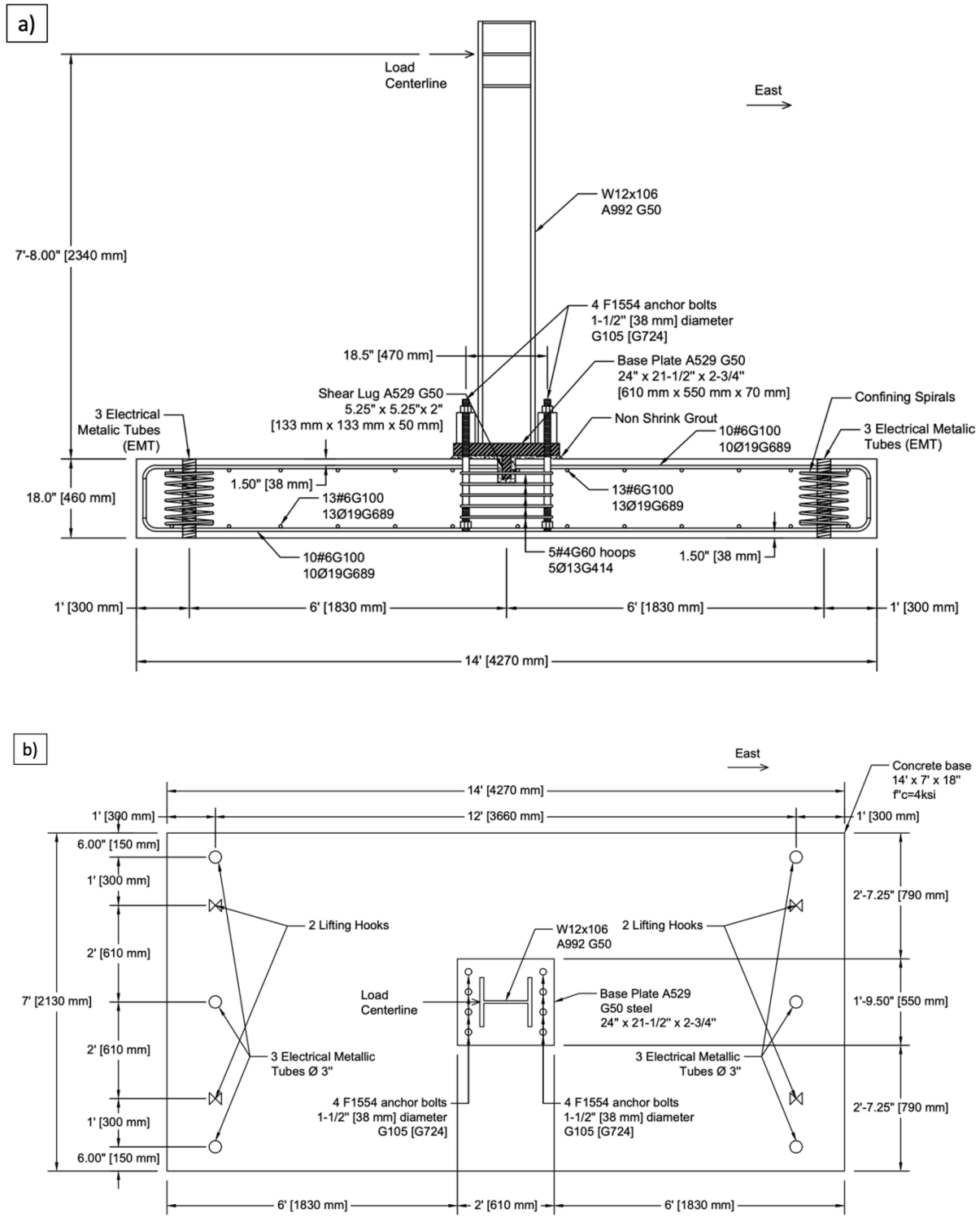

Fig. 5–Elevation view a) and plan view b) of test specimen M01

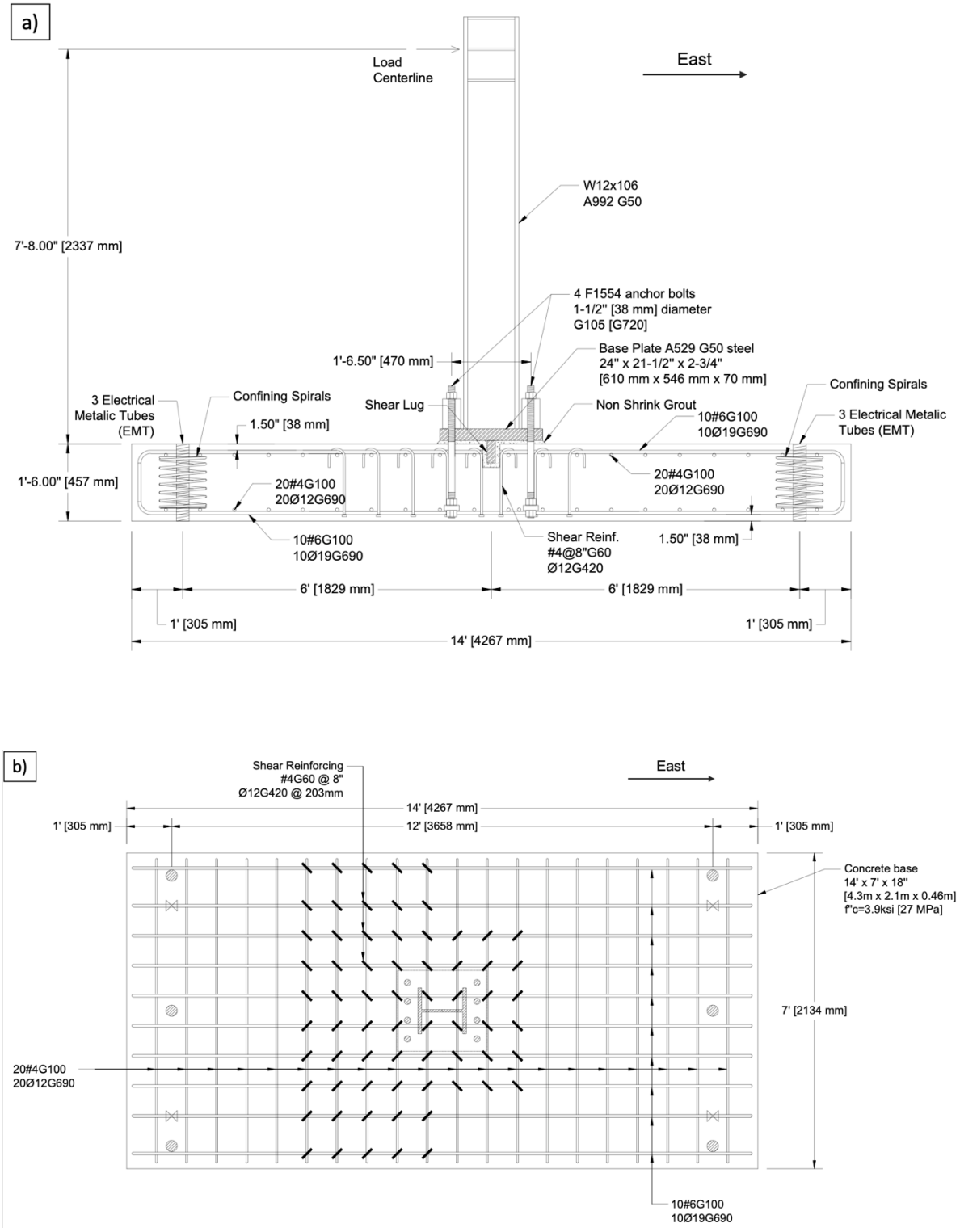

Fig. 6–Elevation view a) and plan view b) of test specimen M02

Test Specimen Design – Specimen M01

Test specimen M01 was designed so that strength would be limited by failure of the concrete foundation in the connection region. The steel column (W12x106 A992 G50) was welded to a 2-3/4-in. [70 mm] thick base plate (A529 G50) with a 5.25-in. x 5.25-in. x 2-in. [133-mm x 133-mm x 50-mm] shear lug (A529 G50) and a 0.75-in. [19-mm] layer of non-shrink grout. Four 1-1/2-in. [38-mm] diameter anchor bolts (F1554 G105) with heavy hex nuts as heads were cast into the 18-in. [457-mm] thick foundation on each side of the column with an effective embedment depth from the top of the slab to the bearing surface equal to 14.3 in. [363 mm]. Note that this embedment depth does not place the bearing surface of the nuts below the slab flexural reinforcement as may be required by some strut-and-tie models (see Fig. 3). The bearing area of each heavy hex nut was 2.6-in.^{2} [1690 mm^2]

The foundation slab was designed to resist the shear and moment resulting from developing the column moment yield strength. The normalweight concrete had a nominal maximum aggregate size of ¾ in. [19 mm] and measured compressive strength of 3700 psi [25.5 MPa] on test day. The compressive strength (f'_c), modulus of elasticity (E), and tensile capacity (f_t) were measured from 6-in. x 12-in. [152-mm x 305-mm] concrete cylinders (see Table 1). The fracture energy (G_f) was measured with three-point bending tests following RELIM recommendations TC89-FMT-FMC2. Slab flexural reinforcement was sized assuming nominal yield strength f_y = 60,000 psi [420 MPa]. However, Grade 100 [690 MPa] reinforcement was substituted to guard against yielding in case unexpected overloads or localized stress concentrations occurred. The joint was confined with 5#4 [Ø13 mm] Grade 60 [420 MPa] hoops, consistent with the requirement of ACI 352R for beam-column joint confinement, as well as requirements for distributed strut reinforcement from the ACI 318-19 strut-and-tie method.

Table 1–Concrete properties of the foundation slab for both specimens

Specimen	M01	M02
f'_c psi [MPa]	3700 [25.5]	3930 [27.1]
E ksi [GPa]	3470 [23.9]	3610 [24.9]
f_t psi [MPa]	380 [2.62]	438 [3.02]
G_f lb/in [N/m]	0.310 [54.3]	0.896 [157]
LA Abrasion Test ¾ in. [19 mm] aggregate	21%	21%

The steel column was subjected to quasi-static reversed cyclic lateral load applied at an elevation H = 7’-8” [2.34 m] above the top of the foundation slab in the strong direction of the column (east-west). Each load step involved two load cycles to a given drift ratio in the positive and negative directions (see **Error! Reference source not found.**). The test was paused when each new displacement goal was reached to document cracking. Axial load was limited to self-weight as this is a critical case for breakout failure and this simplifies the testing apparatus.

The slab was simply supported at the ends where it was post-tensioned to bearing pads located 6’-0” [1.83 m] from the center of the column to provide sliding and overturning resistance. We note that these support conditions are different from those in a soil-supported foundation. Soil support in a column-foundation connection may help confine the joint in which case the simply supported setup is considered more critical. Analytical studies by the authors (not reported here) suggest that soil support would not affect the breakout failure mode. Also, the simple supports result in a statically determinate structure allowing for a more direct interpretation of results. **Error! Reference source not found.** shows a photograph of the test setup.

Fig. 7–Test setup for both test specimens

Error! Reference source not found. summarizes the instrumentation for specimen M01. A load cell was placed on each of the eight anchors. Thirty-three strain gages were placed on the longitudinal

reinforcement as shown. Two hoops were instrumented with a strain gage at the mid-span of each leg for a total of eight gages. Two wire pots measured the column displacements at the elevation of the point of lateral force application in the N-S and E-W directions. Twenty-two vertical linear potentiometers measured the top surface displacement of the concrete slab and the base plate. Additional linear potentiometers monitored the sliding of the specimen and reaction blocks.

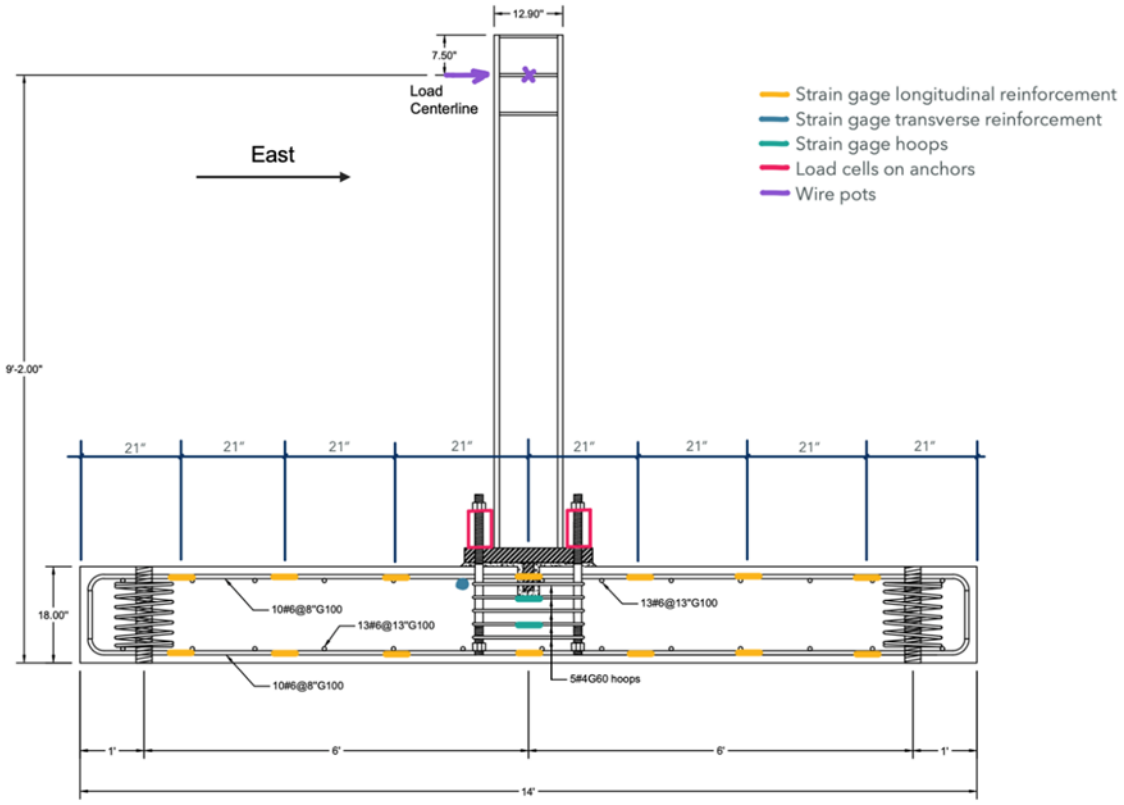

Fig. 8–Instrumentation as seen on an east-west cut specimen M01

Test Results – Specimen M01

Error! Reference source not found. shows the relationship between the column drift ratio and the force applied to the column free end. The drift ratio is defined as the displacement at the point of lateral force application divided by the height from the slab surface to the point of force application. The initial relationship is nearly linear up to a lateral force approaching 50 kips [222 kN] in each loading direction, after which resistance increased only gradually with increasing displacement. The departure from nearly

linear behavior was accompanied by flexural cracking in the slab and radial cracking along the top surface of the slab emanating from the anchor rods. The hysteresis loops show a pinching behavior.

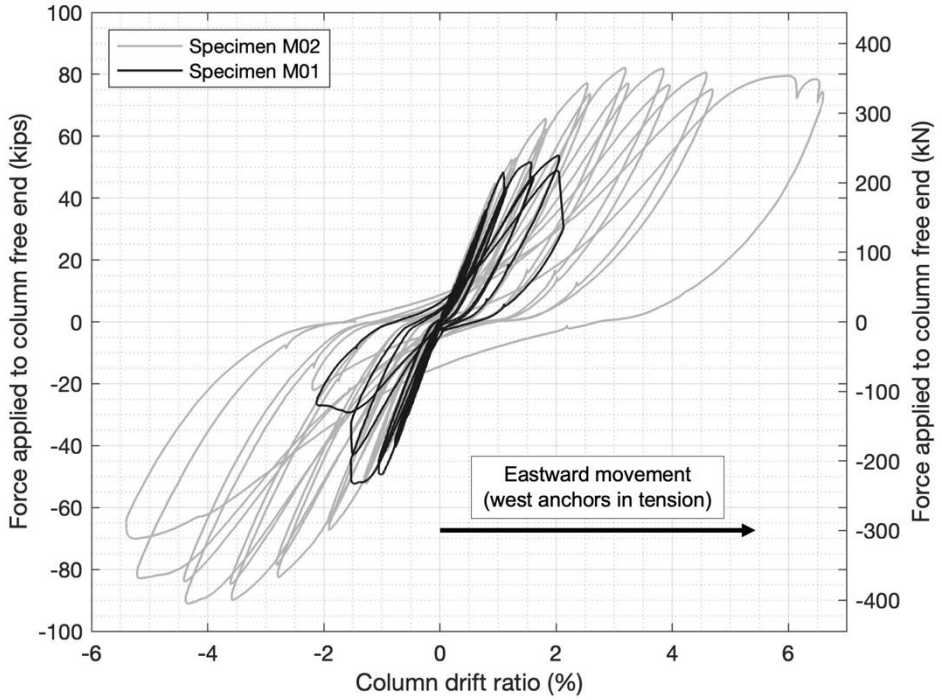

Fig. 9– Relationship between column drift ratio and the force applied to the column free end for both test specimens

Error! Reference source not found. plots the relationship between the column drift ratio and the force in the anchor groups as measured by the load cells on each anchor. The east anchor group failed first during load step nine at a peak anchor group force of 249 kips [1070 kN] and a drift ratio of 1.5%. The west anchor group failed during the next load step (step ten) at a peak anchor group force of 266 kips [1080 kN] and a drift ratio of 2.1% (see **Error! Reference source not found.**). The anchor group failures were sudden and displaced a cone-shaped segment of concrete (see **Error! Reference source not found.**). The post-breakout failures load cycle shows a residual strength of approximately 50% of the peak strength in either direction (see **Error! Reference source not found.**). The first breakout failure did not seem to impact the strength of the second breakout failure as the peak forces in both directions were similar. The observed ductility capacity in each direction is calculated as the drift ratio at breakout failure divided by the drift ratio when the specimen left the elastic range (see **Error! Reference source not found.**). The first breakout failure (east anchor group with ductility capacity of 1.42) likely caused the

stiffness of the system to drop, which increased the perceived ductility capacity of the opposite loading direction at failure (west anchor group with ductility capacity of 1.78).

Table 2–Peak measured forces and drift ratios

Anchor Group	Peak anchor group force (kip) [kN]	Peak column lateral force (kip) [kN]	Drift ratio at yield, DR_y(%)	Drift ratio at max force, DR_{br} (%)	Ductility Capacity, $\frac{DR_{br}}{DR_y}$
M01 - East (failed first)	240 [1070]	52.3 [233]	1.06	1.50	1.42
M01 - West (failed second)	266 [1180]	53.8 [239]	1.14	2.03	1.78
M02 - East	452 [2010]	91.1 [405]	0.92	4.34	4.72
M02 - West	446 [1980]	82.2 [366]	0.97	5.99	6.18

Note: For specimen M02 the yield drift ratio was taken as the max drift ratio during load step seven and the drift ratio at failure was taken as the drift ratio at the maximum anchor force.

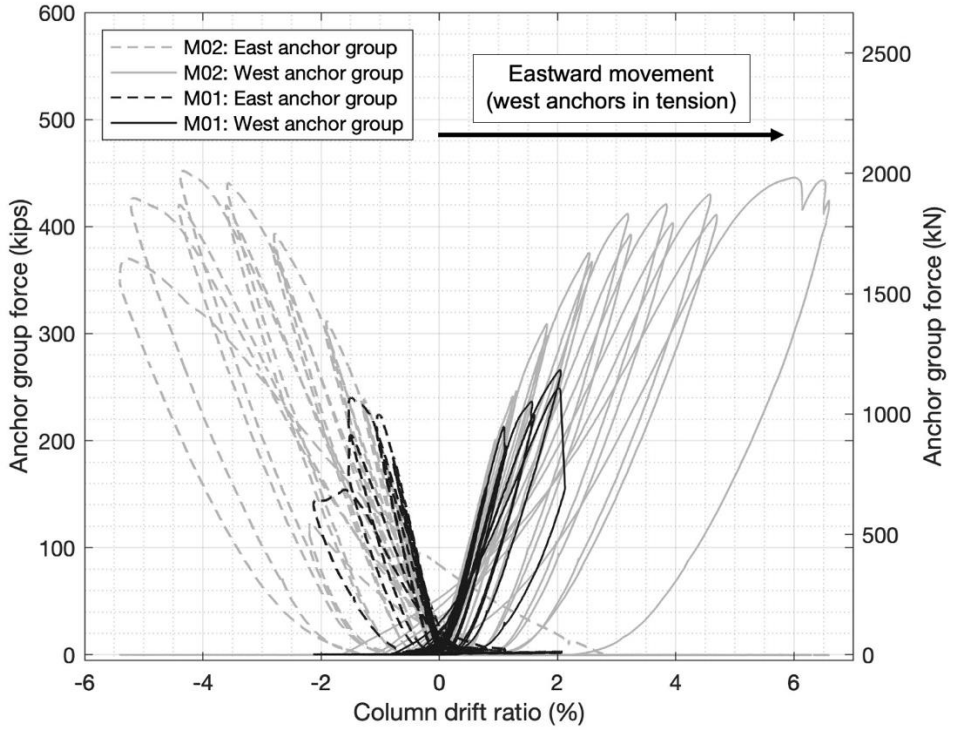

Fig. 10–Relationship between column drift ratio and force in anchor groups for both specimens

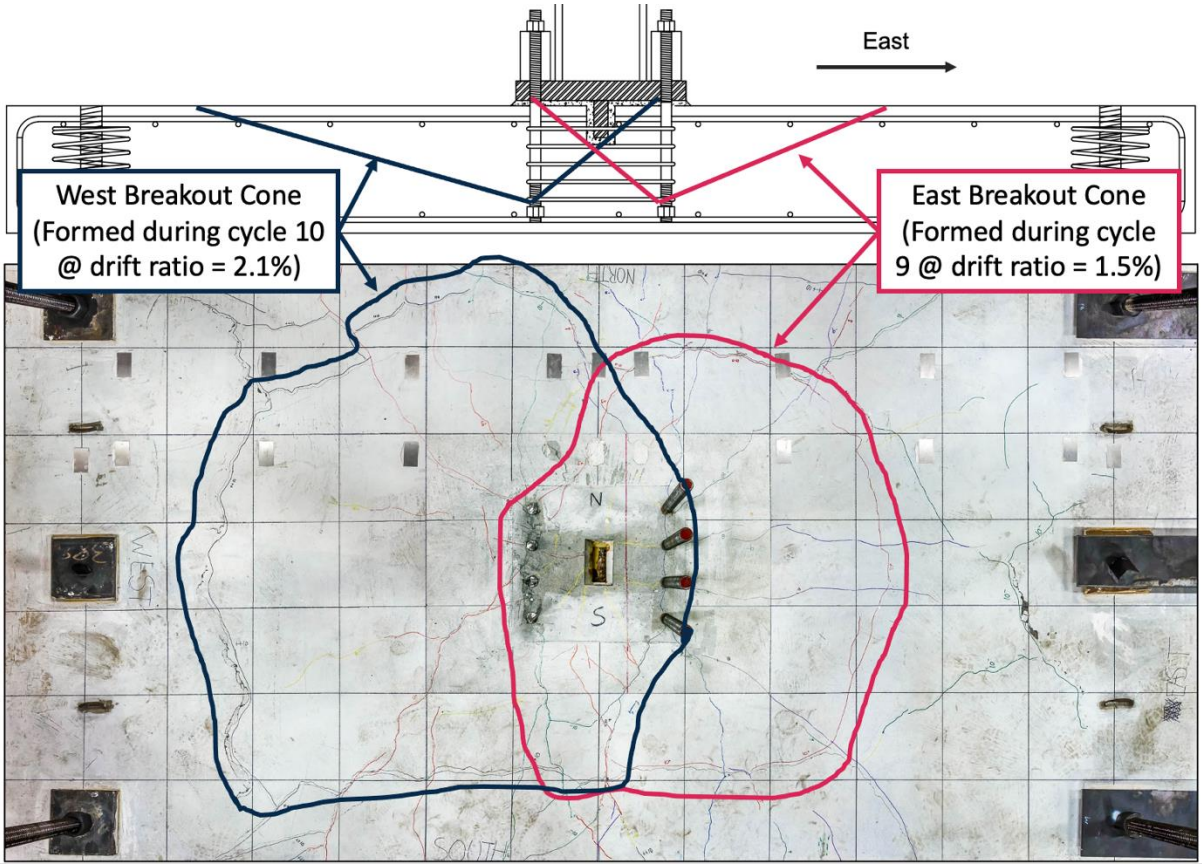

Fig. 11–Idealized cone geometry shown in elevation and observed cone geometry intersecting top surface in plan view, with 12-in. x 12-in. [305 mm x 305 mm] grid specimen M01

Error! Reference source not found. plots the column drift ratio against time and subdivides the drift ratio into contributions from the slab rotation, the relative base plate rotation, and the elastic column deflections due to moment and shear. The displacements due to the slab and the base plate rotation are calculated based on displacements measured with the vertical linear potentiometers on the top surfaces. The column elastic deflection is calculated with elastic theory knowing the force applied to the column free end. Initially, most of the displacement is due to the elastic deformation of the column and the rotation of the base plate. Extension of the anchors is the major contributor to the base plate rotation. As damage progresses in the concrete, the contribution of the slab rotation increases while the contribution of the elastic column decreases. After the breakout failures, the displacement due to elastic column deflection decreases (due to the reduced force) and the slab rotation increases because the breakout cones displace like rigid objects.

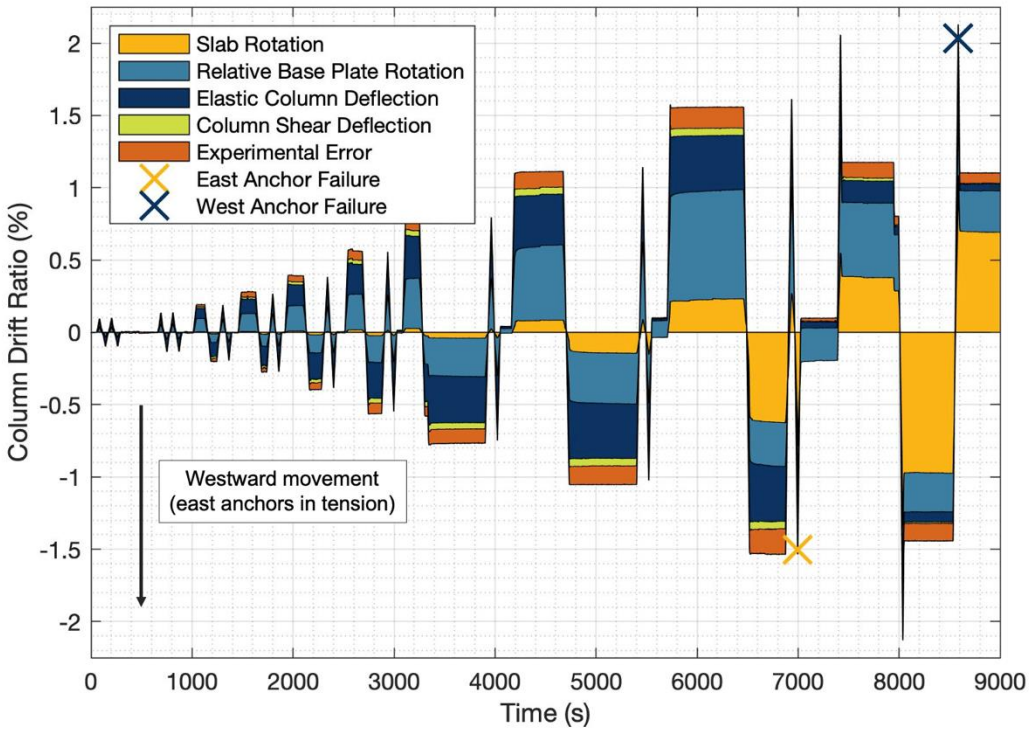

Fig. 12–Column drift ratio subdivided into contributions from the slab rotation, the relative base plate rotation, the elastic column deflection, the column shear deflection, and experimental error versus time, specimen M01

Error! Reference source not found. plots the strains in each leg of a top and a bottom hoop against the column drift ratio (see strain gage and hoop location in **Error! Reference source not found.**). The strains in the bottom hoop did not exceed 50% of the yield strain. In the top hoop, only the legs that crossed the concrete cone failure planes show appreciable strain; that is, the legs in the east-west direction (H6 and H8). A "V" shape is observed as loading in both directions causes tensile strains in the hoops, which is expected.

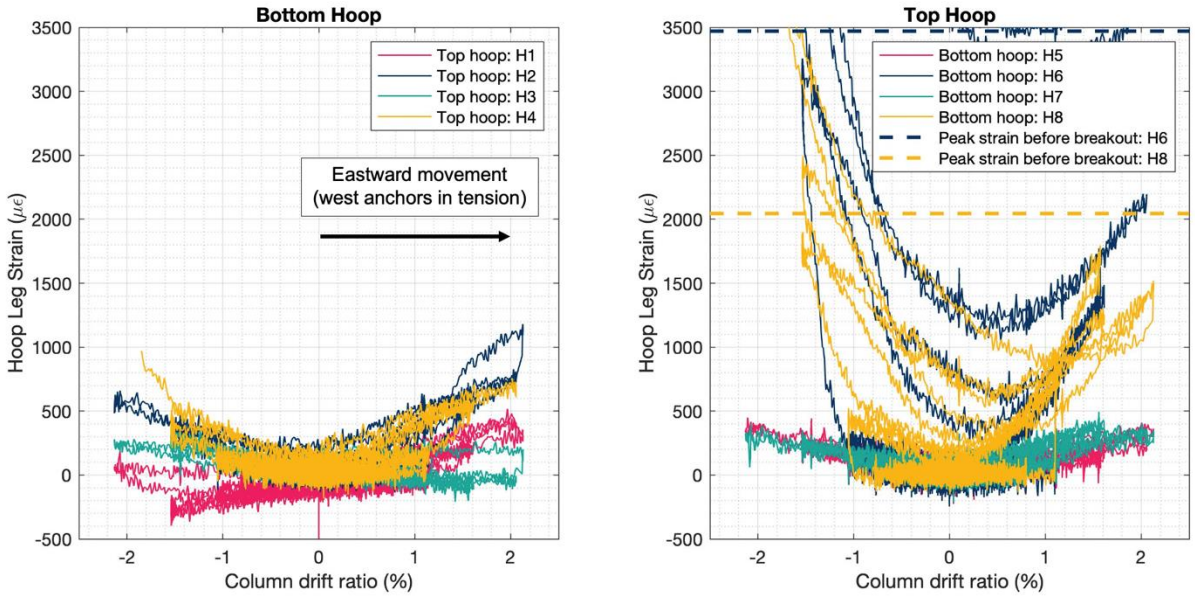

Fig. 13–Strains at the midpoint of each leg of a bottom and top hoop plotted against the column drift ratio. See strain gage location in **Error! Reference source not found.**. Positive drift ratio means eastward movement (west anchor group in tension) specimen M01

Surface cracks indicated that the breakout cones were asymmetric with a steeper slope towards the interior of the joint (see **Error! Reference source not found.**). This cone geometry is attributed to suppression of the unconstrained breakout surface because of flexural compression at the opposite side of the joint, as shown in Fig. 4. During the test, the longitudinal reinforcing bars and anchors remained in the elastic range. The bottom surface of the foundation slab showed minimal cracking. The anchors did not punch through the bottom of the slab. There was no evidence of joint crushing or joint dilation, as might be expected if there had been a beam-column joint failure.

Test Specimen Design – Specimen M02

Test specimen M02 was designed so that strength would be limited by failure of the concrete in the connection region. The steel column and baseplate fixture from the previous specimen were reused. Four 1-1/2-in. [38-mm] diameter anchor bolts (F1554 G105) with 1.25-in. x 3.5-in. 3.5-in. [32 mm x 89 mm x 89 mm] A36 steel plate washers were cast into the 18-in. [457-mm] thick foundation on each side of the column with an effective embedment depth from the top of the slab to the bearing surface of the plate washers equal to 14.3 in. [363 mm]. The bearing plate was sized to keep the bearing stress below ACI 318-19 limits (Sec. 17.6.3.2.2). The bearing area of each plate was 9.8-in.^{2} [6350 mm^2].

The foundation slab was designed to resist the shear and moment resulting from developing the column moment yield strength. The same concrete mixture design was used as for the previous specimen. On test day, the measured compressive strength was 3930 psi [27.1 MPa]. Other measured material properties are shown in Table 1. The fracture energy (G_f) was measured with three-point bending tests following RELIM recommendations TC50-FMC-FMC1. Slab flexural reinforcement was sized assuming nominal yield strength f_y = 60,000 psi [420 MPa]. However, Grade 100 [690 MPa] reinforcement was substituted to guard against yielding in case unexpected overloads or localized stress concentrations occurred. The shear reinforcing consisted of vertical #4 G60 A706 bars [Ø13 mm G420] in an 8-in. by 8-in. [203 mm by 203 mm] grid with 180° hooks on the top and heads on the bottom (see Fig. 6). The hook hung from the intersections of the longitudinal reinforcing mat and the head at the bottom was tied below the longitudinal steel. The shear reinforcing extended two rows farther on the west side than on the east side of the slab. No hoops were placed around the anchors.

The test setup for specimen M02 was identical to specimen M01 and was loaded in the same manner. The test was paused after each new displacement goal was reached to document cracking.

A load cell was placed on each of the eight anchors. Ten strain gages were placed on the longitudinal reinforcement as shown. One symmetric half of the shear reinforcing bars had a strain gage at mid-height for a total of thirty-four gages (see **Error! Reference source not found.**). Two wire pots measured the column displacements at the free end in the N-S and E-W directions. Thirteen vertical linear potentiometers measured the top surface displacement of the concrete slab and the base plate. Additional linear potentiometers monitored the sliding of the specimen and reaction blocks.

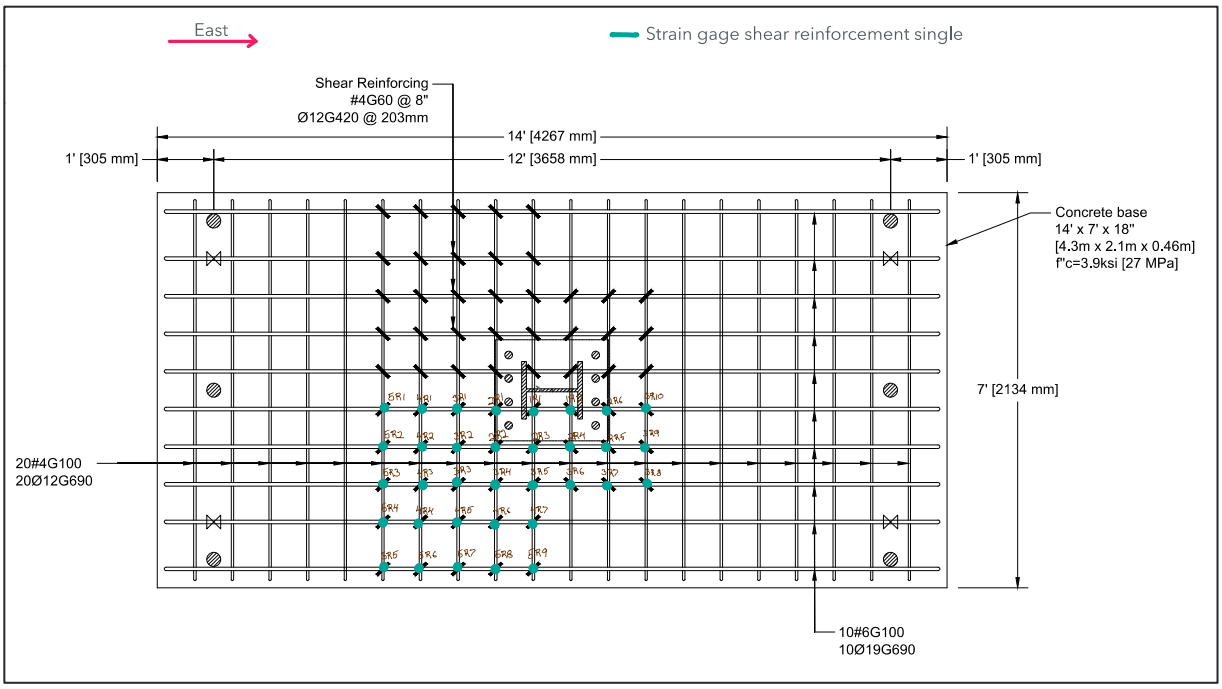

Fig. 14–Plan view of shear reinforcing strain gages specimen M02

Test Results – Specimen M02

Error! Reference source not found. shows the relationship between the column drift ratio and the force applied to the column free end. The initial relationship is nearly linear up to a lateral force approaching 50 kips [222 kN] in each loading direction, after which the force reached a plateau at about 80 kips [356 kN] in both directions. The departure from nearly linear behavior was accompanied by flexural cracking in the slab and radial cracking along the top surface of the slab emanating from the anchor rods. With a larger reinforced region, the west anchor group showed no drop in strength up to about a 6% drift ratio. In contrast, with a smaller reinforced region, the east anchor group began to lose strength after about a 4% drift ratio. The hysteresis loops show pinching. **Error! Reference source not found.** plots the relationship between the column drift ratio and the force in the anchor groups as measured by the load cells on each anchor. Each anchor group failed by displacing a cone-shaped segment of concrete (see **Error! Reference source not found.**). The anchor group failure occurred more gradually than for specimen M01. The peak force in the east group was 452 kips [2010 kN] and occurred at a drift ratio of 4.34%. The peak force in the west group was 446 kips [1980 kN] and occurred at a drift ratio of 5.99%. The observed ductility capacity in each direction is calculated as the drift ratio at maximum force divided

by the drift ratio when the specimen left the elastic range (see **Error! Reference source not found.**). The observed ductility capacity in the test was 4.72 for the east anchor group and 6.18 for the west anchor group.

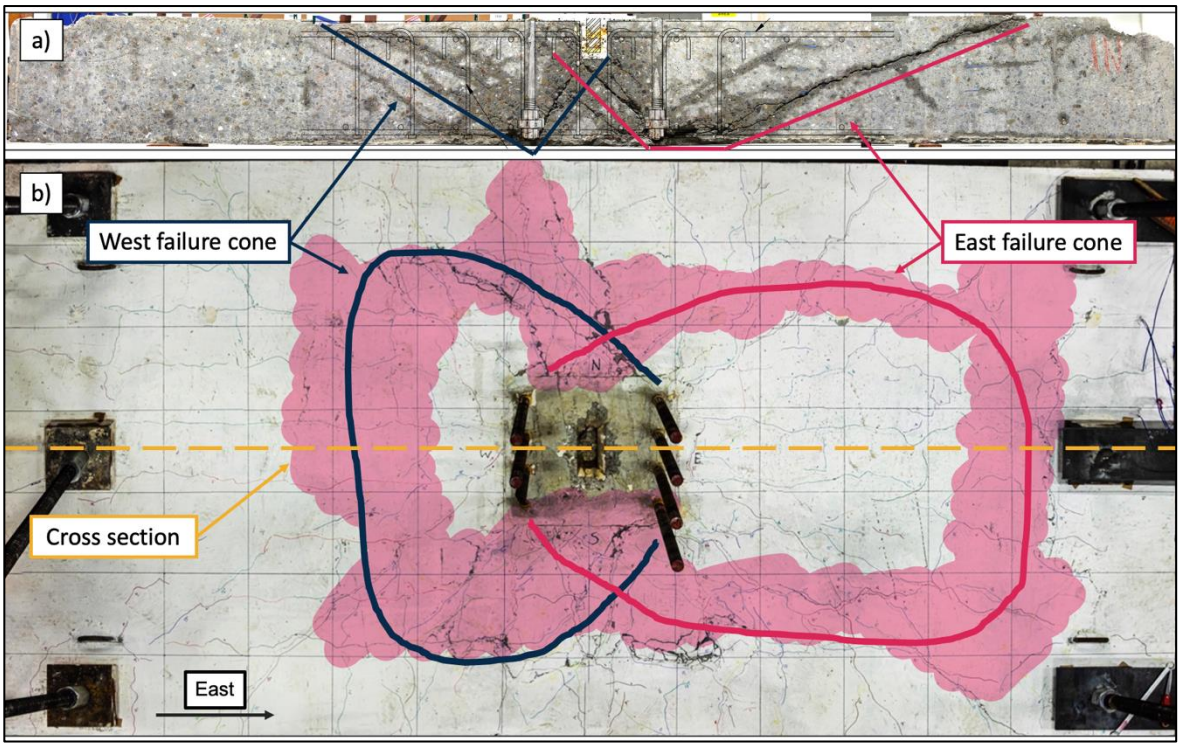

Fig. 15– a) Specimen cross section and b) plan view highlighting crack patterns and breakout cone geometry, with 12-in. x 12-in. [305 mm x 305 mm] grid for specimen M02. The shaded region produced a hollow sound when knocked.

Error! Reference source not found. plots the column drift ratio against time and subdivides the drift ratio into contributions from the slab rotation, the relative base plate rotation, and the elastic column deflections due to moment and shear. The calculations were done in the same manner as for specimen M01. Initially, most of the displacement is due to the elastic deformation of the column and the rotation of the base plate, which is due to elastic anchor extension. The contribution of the slab rotation increases as damage progresses in the concrete. Close to peak drift ratios, the slab rotation increases because the breakout cones have formed and move like rigid objects.

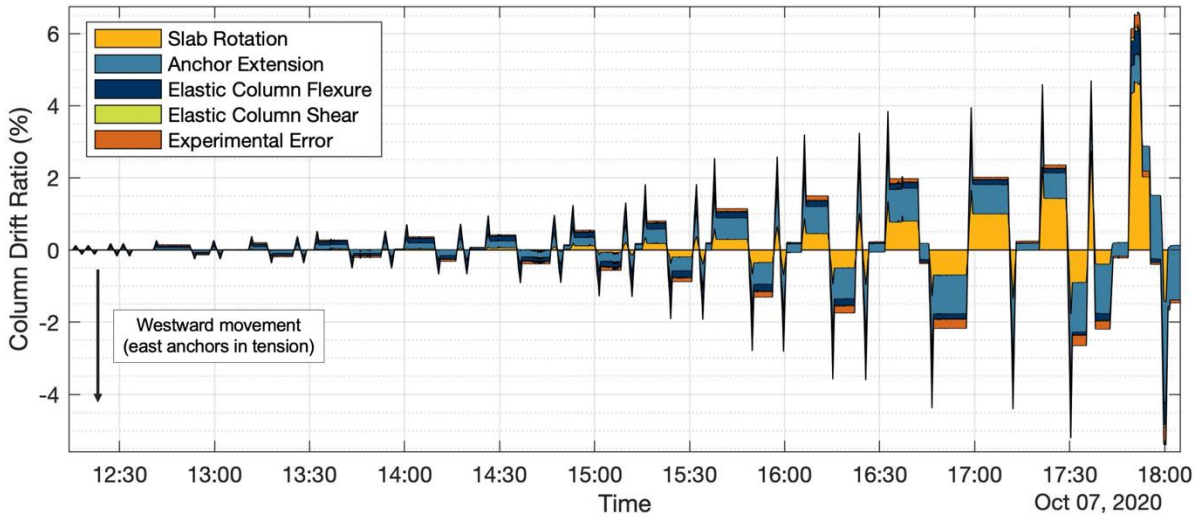

Fig. 16–Specimen M02 column drift ratio subdivided into contributions from the slab rotation, the relative base plate rotation, the elastic column deflection, the column shear deflection, and experimental error versus time

Error! Reference source not found. subdivides the shear reinforcing bars into rows based on the distance from the column center. **Error! Reference source not found.** shows the maximum strain felt by each shear reinforcing bar highlighting which bars yielded. Most bars in rows 1 and 2 yielded and exceeded 3% strain (maximum measurable strain of strain gage). The west side of the specimen had two additional rows of reinforcing (rows 4 and 5), which did not yield or show appreciable strains. **Error! Reference source not found.** plots the specimen force-drift ratio curve and highlights the point at which each shear reinforcing bar reached nominal yield strain (0.002). The initiation of yielding of the shear reinforcing coincided with the departure from linear behavior of the specimen. **Error! Reference source not found.** plots the shear reinforcing strain versus column drift ratio and highlights the first yield of each bar. The “V” shape of the strain graphs indicates that the bars experienced tensile strains when the column was loaded in either direction.

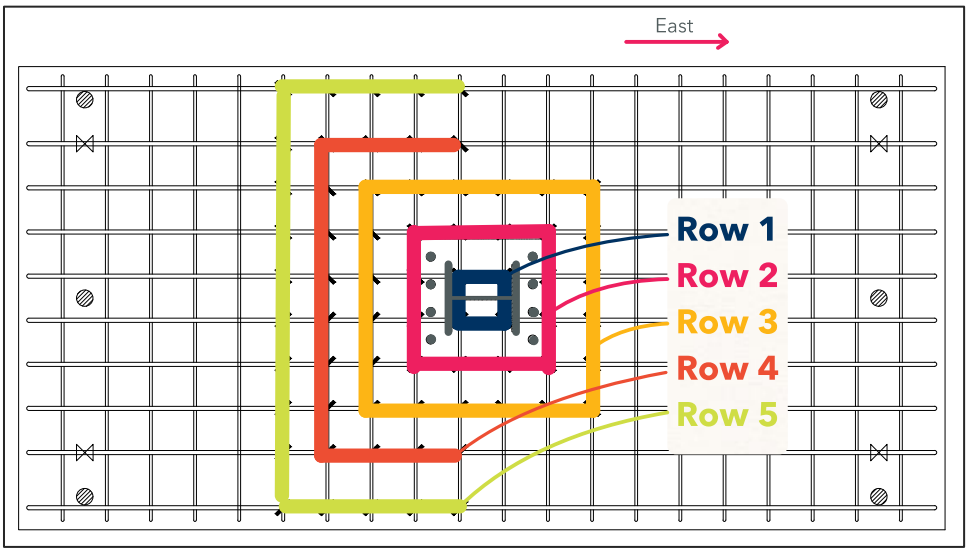

Fig. 17–Specimen M02 plan view separating the shear reinforcing bars into rows

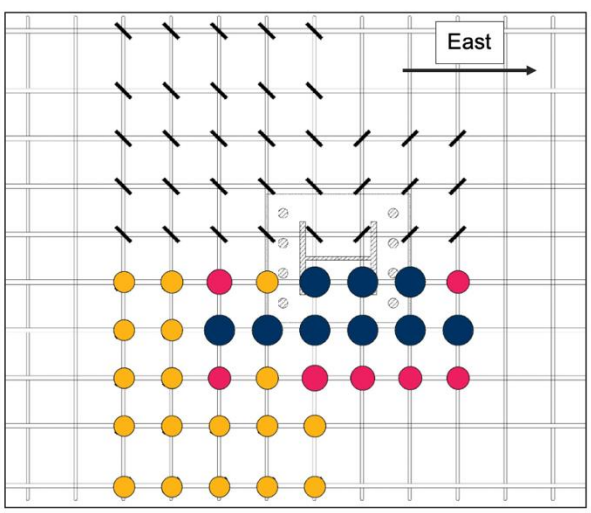

Marker Color	Bar State	Max Strain (μstrain)
	Elastic	0-2000
	Yielded	2000-31,000
	Damaged	>31,000

Notes:
- Marker area is proportional to max strain
- Shear reinforcing in rows 4 and 5 showed no significant strain
- Strain gages can only measure up to about 3%

Fig. 18–Specimen M02 plan view showing maximum strain felt by each shear reinforcing bar

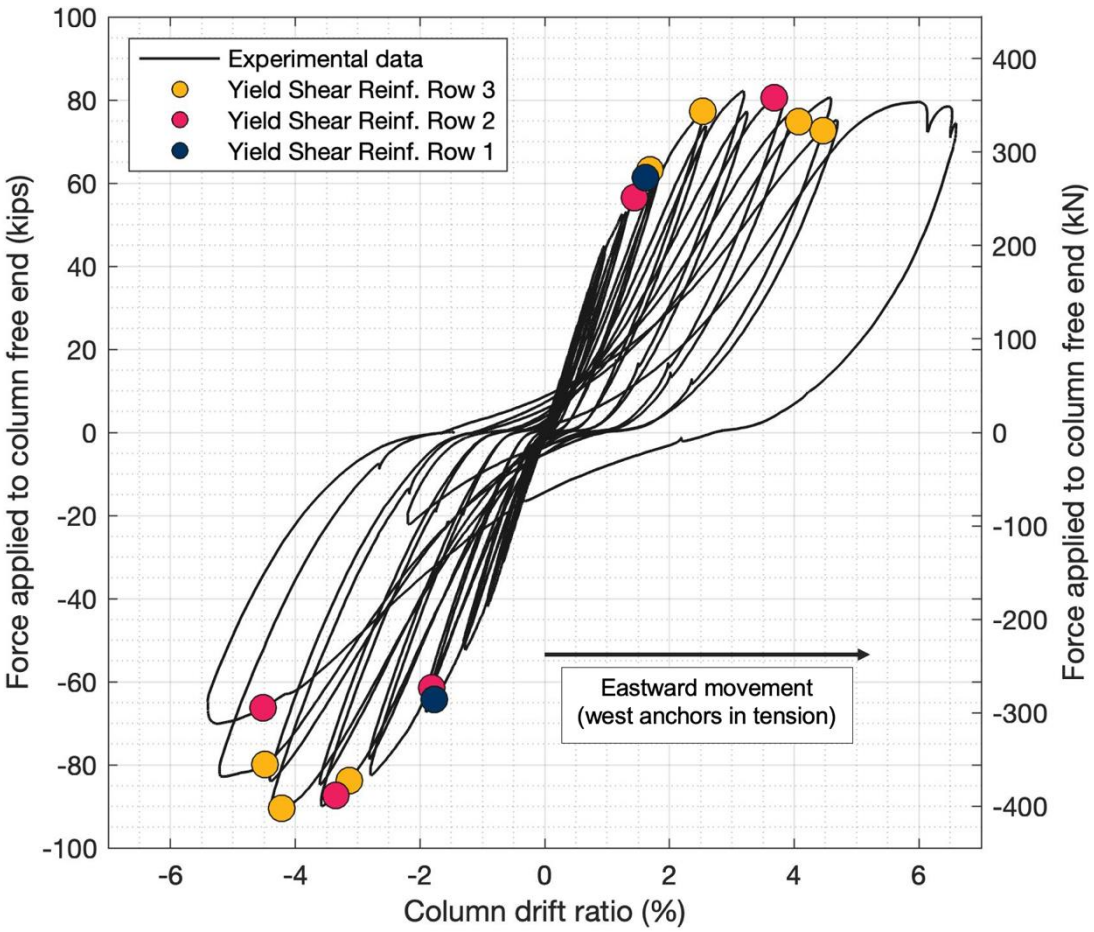

Fig. 19–Specimen M02 force versus drift ratio curve highlighting instances when the shear reinforcing bars first reached the nominal yield strain for G60 [G420] bars

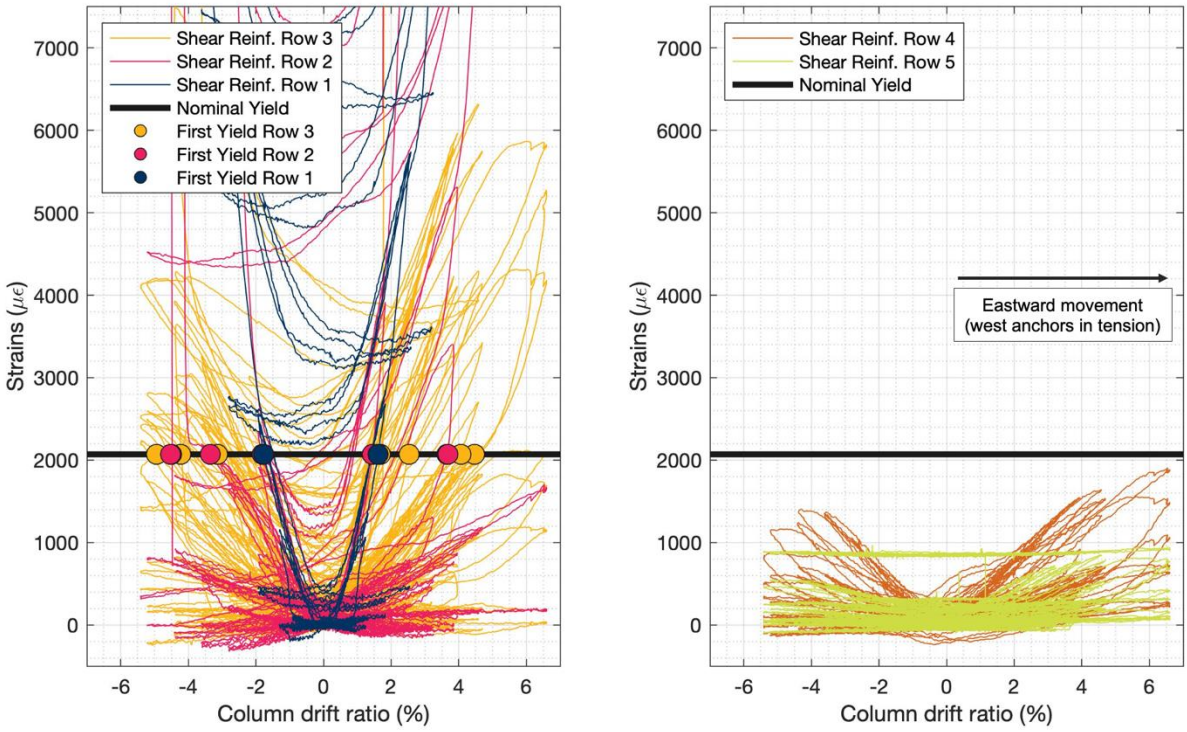

Fig. 20–Specimen M02 strain in shear reinforcing bars versus column drift ratio subdivided into rows. The first yield of each bar is highlighted.

Photographs of the specimen cross section (see **Error! Reference source not found.**) indicate that the breakout cones were asymmetric with a steeper slope towards the interior of the joint. This cone geometry is attributed to suppression of the unconstrained breakout surface because of column flexural compression at the opposite side of the joint, as shown in Fig. 4. During the test, the longitudinal reinforcing bars and anchor rods remained in the elastic range. The bottom surface of the foundation slab showed minimal cracking. The anchors did not punch through the bottom of the slab.

DISCUSSION

Each specimen provided two data points corresponding to the failure of the east and west anchor groups. All four anchor groups failed in a concrete breakout mode. Other possible failure modes associated with slab flexure, one-way shear, or joint shear were not observed.

An analysis of the connection strength of test specimen M01 was performed considering beam-column joint shear and anchoring-to-concrete provisions. The calculated strength using the strut-and-tie method is not presented since the bearing surfaces of the anchor bolts were not ideally positioned or sized

for developing a proper strut-and-tie model.

Beam-column joint nominal shear strength was calculated with equation (1), assuming that the effective horizontal area of the joint was defined by lines located one nominal concrete cover dimension, or 1.5 in. [38 mm], outside the joint hoops of specimen M01, resulting in

$$V_n = 15\sqrt{3700}(20.5")(24") = 449\ kips\ [2000\ kN] \quad (9)$$

Assuming an internal moment arm in the foundation slab equal to $0.9d$ and ignoring self-weight, the corresponding horizontal column force can be calculated from equilibrium to be P = 86.4 kips [384 kN]. Using AISC Design Guide 1 provisions, the internal moment arm for the tension-compression couple of the base plate is z = 19.6 in. [498 mm]. Thus, the force in the set of four anchor bolts in tension (T_n) corresponding to the nominal joint shear strength is given by equation (9) is

$$T_n = PH/z = (86.3k)(92")/19.6" = 402\ kips\ \ [1790\ kN] \quad (10)$$

where H is the vertical distance between the point of force application and the top surface of the slab.

The tensile capacity of the group of four anchor bolts was also calculated using the ACI 318-19 anchoring-to-concrete provisions. For this purpose, we assume uncracked concrete as described previously. We also use the additional factor Ψ_M from equation (7) to account for the proximity between the tensile and compressive forces (**Fig. 4**) and the factor 4/3 to bring the 5% fractile anchor strength to the median value. The internal moment arm for the tension-compression couple of the base plate is calculated to be z = 20.5 in. [521 mm] using AISC Design Guide 1 procedures. Thus, using equation (4), the nominal median breakout capacity of the four anchor bolts in tension is:

$$T_n = 1.33N_{cbg}$$

$$= 1.33\frac{A_{Nc}}{A_{Nco}}\psi_{ec,N}\psi_{ed,N}\psi_{c,N}\psi_{cp,N}\psi_M N_b$$

$$= 1.33\frac{2480\ in.^2}{1840\ in.^2}(1)(1)(1.25)(1)\left(2 - \frac{20.5\ in.}{1.5 * 14.3\ in.}\right)\left(16\sqrt{3700\ psi}\right)(14.3\ in.)^{5/3}$$

$$= 192\ kips\ [860\ kN]$$

The measured tensile strengths corresponding to observed breakout failures were 240 kips [1070 kN] for the east anchor group and 266 kips [1180 kN] for the west anchor group.

The calculated strengths and the measured values for specimen M01 are summarized in **Error! Reference source not found.**. From the values given, it can be determined that the mean measured strength is approximately 1.3 times the strength calculated by the anchoring-to-concrete method, indicating that the mean breakout calculation is conservative for this case even with inclusion of the Ψ_M

adjustment. Comparison of the nominal breakout strength (5% fractile) without adjustment for the compression block (Ψ_M) yields a ratio of measured strength to calculated nominal strength of 1.8. Including the strength reduction factor ϕ = 0.70, the ratio of measured to design strength becomes 2.6, and if the cracking factor $\Psi_{c,N}$ is taken equal to 1.0, as may be inferred from language in ACI 318-19, then the ratio of measured peak strength to design strength rises to 3.3. On the other hand, the beam-column joint shear calculation yields a ratio of mean measured strength to nominal strength based on the beam-column joint nominal shear strength of 0.62, indicating that failure occurred well before nominal joint shear strength was reached.

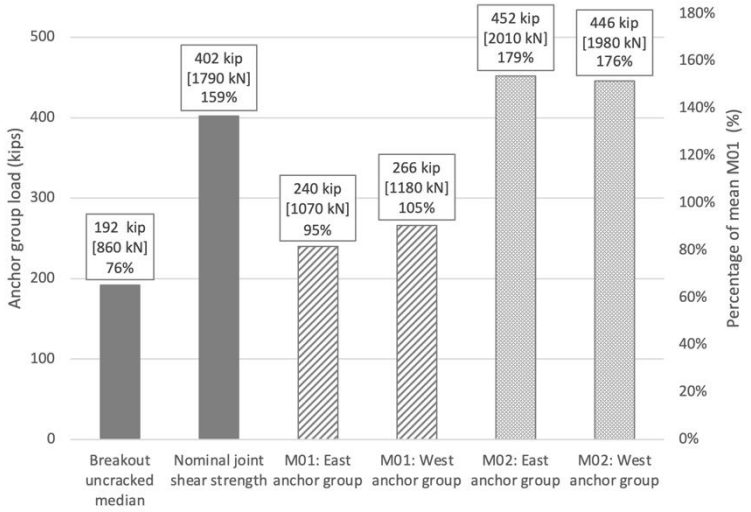

Fig. 21–Nominal median peak anchor group forces according to breakout equations (assumed uncracked and including Ψ_M) and joint shear equations. The peak measured strengths of specimens M01 and M02 are also shown. Note: ϕ = 1 and the breakout calculations were multiplied by a factor of 4/3 to bring the result from a 5% fractile value to a median value.

This example demonstrates the conservatism of the anchoring-to-concrete provisions for large-scale column-foundation connections as specified in ACI 318-19. The use of a 5% fractile value for design of concrete anchors is rooted in concerns about risk and failure consequences associated with attachments anchored by one or a small number of anchors where force redistribution is unlikely, and failure is sudden. When used to design large structural elements anchored by multiple anchor groups, the provisions result in a higher degree of conservatism than is commonly provided for similar connections with hooked or headed reinforcing bars. The use of a median strength value, rather than a 5% fractile, should be considered along with an appropriate strength reduction factor for anchors used in structural applications.

Strain gauge data from specimen M01 indicate that the joint hoops (Fig. 5) were not effective in confining the joint or increasing the breakout strength. For the bottom hoop, **Error! Reference source not found.** shows low strains in all legs. For the top hoop, the two legs that crossed the cone failure plane yielded but this occurred well after the initiation of the breakout failure.

Specimen M02 incorporated an 8-in. by 8-in. [203 mm by 203 mm] shear reinforcing grid of #4 G60 [Ø13 mm G420] bars with a 180-degree hook on one side and a head on the other. Both ends engaged longitudinal reinforcing. After controlling for concrete strength, the addition of shear reinforcing in specimen M02 increased the breakout force by 72% and displacement capacity by a factor of 3 on average compared to specimen M01 (see **Error! Reference source not found.**). The increased peak force is comparable to the calculated beam-column joint strength (see **Error! Reference source not found.**). The strength increase is consistent with the strut-and-tie model developed by Kupfer et al. (2003) for column-foundation connections which suggests tension ties outside the joint are required for equilibrium. Contrary to current assumptions in ACI 318-19 and EN 1992-4 design equations, relatively small amounts of shear reinforcing can improve the connection behavior. Most shear bars near the anchors developed strains well beyond the nominal yield strain (>3%) even though they were not fully developed on both sides of the potential breakout cone as would be required for ACI 318-19 anchor reinforcement. This observation suggests that anchoring shear reinforcing bars following the requirements for anchoring transverse reinforcement (ACI 318-19 Sec. 25.7.1.3) may be sufficient to develop the nominal yield stress.

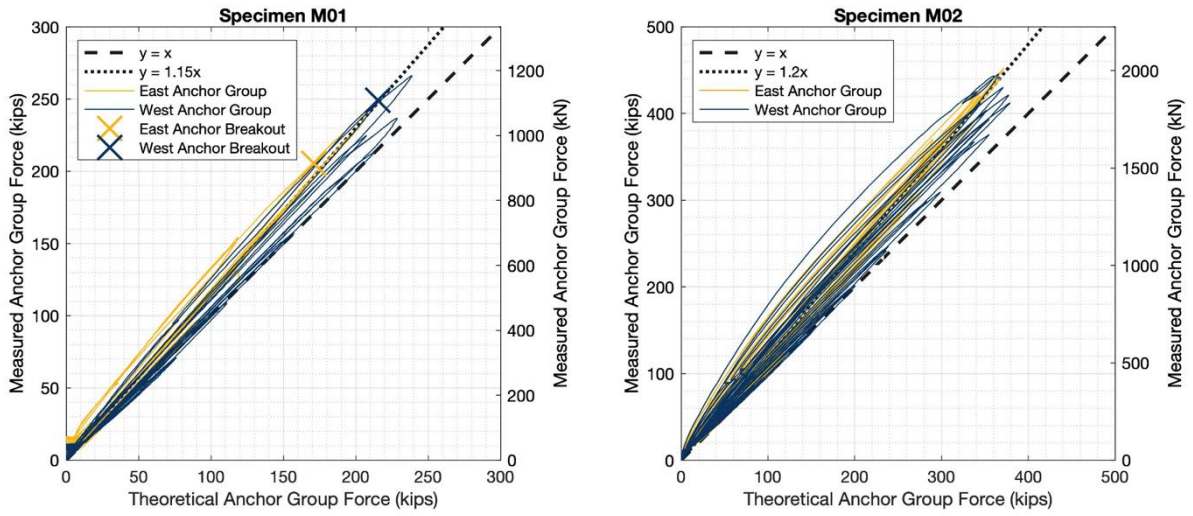

Fig. 22–Comparison between the theoretical AISC and the measured anchor group forces; assuming uniform bearing pressure distribution under base plate for theoretical; experimental forces from load cells on anchors

Both specimens exhibited pinched hysteresis loops (see **Error! Reference source not found.**), indicating a non-ductile concrete breakout failure mode similar to those observed by Tanaka and Oba (2001). Increasing the breakout failure strength may allow the designer to provide an alternate more ductile failure mode (for example, anchor or column yielding).

For the east anchor group of specimen M02, the east face of the failure cone is located beyond the outer perimeter of the shear reinforcing bars (see **Error! Reference source not found.**). If one assumes the shear reinforcing bars form part of the anchor group, the calculated strength of this larger secondary breakout cone increases by a factor of 1.72 due to the increased group factor. This strength increase is almost exactly that observed between specimen M01 and M02 (72%). The calculated increase in strength for the secondary breakout cone on the west side is about 3.14 due to the larger reinforced area. This secondary breakout failure cone was observed on the west side but did not govern.

The additional rows of shear reinforcing on the west side of test specimen M02 did not increase the load capacity but did increase displacement capacity from a drift ratio of about 4% to about 6% and prevented the formation of a secondary breakout cone initiating where the shear reinforcing ended. The observation that stirrups beyond $0.75h_{ef}$ from the anchor centerline did not increase anchor force is consistent with Eurocode provisions for supplementary reinforcement (EN 1992-4 7.2.1.2 (2) c)).

Neither specimen showed substantial cracking along the bottom surface. This suggests that the absence of continuous soil pressure under the test specimens did not have a substantial effect on the observed concrete breakout failure mode which governed the strength. The influence of soil support on other failure mechanisms should be investigated further.

For both specimens, the failure cones were asymmetric with a steeper slope towards the interior of the joint (see **Error! Reference source not found.** and **Error! Reference source not found.**). This cone geometry is attributed to suppression of the unconstrained breakout surface because of flexural compression at the opposite side of the joint, as shown in **Fig. 4**. The Ψ_M factor from equation (7) seems appropriate to account for the breakout strength increase associated with the flexural compression force. This factor requires the calculation of the internal lever arm (z). This value can be approximated by either A) assuming the compression resultant is located below the column flange (z = 15.2-in. and Ψ_M = 1.29), B) assuming the compression resultant is located at the opposite edge of the base plate (z = 21.25-in. and Ψ_M = 1.01), or C) assuming uniform bearing pressure below the base plate and calculating z from the forces applied to the column following AISC Design Guide 1 recommendations (z = 20.5-in. and Ψ_M = 1.04). **Error! Reference source not found.** plots the measured anchor group forces versus those calculated following AISC recommendations. In general, the measured forces are higher, suggesting that the experimental internal level arm is about 15% lower than the theoretical AISC value for specimen M01 (z = 18-in. and Ψ_M = 1.16) and 20% lower for specimen M02 (z = 17.3-in. and Ψ_M = 1.19). Measuring z from the centroid of the tensile anchors to the far edge of the base plate may be assumed as a conservative and straightforward approximation unless a more detailed calculation is performed.

ACI 318-19 commentary Sec. R25.4.4.2c suggests that breakout failure in a beam-column joint can be precluded in a joint by keeping anchorage length greater than or equal to 1/1.5 times the effective depth of the member introducing the anchor force into the joint, presumably due to the restraining influence of the compression field. However, for both test specimens, breakout failure occurred even though this recommendation was satisfied. The ratio of breakout failure to joint shear failure was on the order of 2.1.

Designing specimen M01 considering only the beam-column joint strength and ignoring breakout strength would have been unconservative (see **Error! Reference source not found.**). This observation suggests that both failure modes, breakout and joint shear, should be checked to produce safe designs.

With additional shear reinforcing, the breakout failure force of specimen M02 became comparable to the beam-column joint strength. The experiments did not test whether further additions of shear reinforcement would result in further increases in strength or whether strength would be limited by beam-column joint shear strength. The formation of a secondary failure cone beyond the outer perimeter

of the shear reinforcing, analogous to the requirement for two-way slabs with shear reinforcement, should also be considered.

SUMMARY AND CONCLUSIONS

Two full-scale test specimens of interior steel-column-to-concrete foundation connections with cast-in-place anchor bolts were constructed and tested. Each test specimen provided two data points corresponding to the peak forces of each anchor group. The columns were tested under incrementally increasing cyclic lateral loading resulting in moment transfer from the column to the foundation element. All four tested anchor groups failed in a brittle concrete breakout mechanism due to tensile force transfer from the anchor bolts to the foundation. This observation challenges the assumption that breakout failures will not govern the behavior of large-scale connections, provided they have adequate capacity joint shear capacity. The pinched hysteresis loops are indicative of concrete failure. There was no evidence of failure or distress associated with other force-limiting mechanisms.

For specimen M01 without shear reinforcing, the nominal breakout strength of the tension anchor bolt group was calculated using anchoring-to-concrete provisions of ACI 318-19. The measured breakout strength was 1.8 times the code-based nominal strength, indicating the conservatism of the ACI 318-19 provisions for this case. Part of the conservatism is because the ACI 318-19 provisions for anchoring to concrete take the 5% fractile of resistance for design rather than the median value, as is more common for other nominal strengths. ACI 318-19 also currently neglects the positive influence of the flexural compression field developed under the base plate, which can act to retard the formation of the concrete breakout surface. Finally, ACI 318-19 requires calculating the reduced breakout capacity considering cracked concrete ($\Psi_{c,N}$ equal to 1.0), even though an assumption of uncracked concrete ($\Psi_{c,N}$ equal to 1.25) may be justified for headed anchors if the bearing surface of the anchor bolt is within the flexural compression region of the foundation. These three effects should be considered in future revisions to ACI 318.

Calculations for test specimen M01 also demonstrated that the beam-column joint shear strength was never realized because it was preempted by tension breakout failure. For specimens M01 and M02, the breakout failure governed even though the anchorage length was greater than 1/1.5 times the effective depth of the member introducing the anchor force into the joint. This observation runs contrary to ACI 318-19 commentary Sec. R25.4.4.2. ACI 318 should consider revised guidance or new code requirements emphasizing the importance of checking breakout failures in addition to checking joint shear strength. A good practice would be to check both breakout strength and beam-column joint shear strength and use the lower value as the limit for design. This observation may also be relevant for beam-column joint design.

The addition of a distributed grid of shear reinforcing in the breakout cone region can increase the breakout strength and displacement capacity. Increasing the breakout strength may allow the designer to provide a more desirable ductile failure mode like anchor yielding. Even though only the shear reinforcing within 0.75 h_{ef} of the anchors seems capable of increasing the breakout strength, additional rows can increase displacement capacity and prevent secondary breakout failure cones beyond the outermost row of shear reinforcement. ACI 318-19 and the Eurocodes should consider including provisions that combine the strength of concrete and reinforcing for the breakout failure mode.

ACKNOWLEDGMENTS

The authors express their gratitude to the ACI Foundation Concrete Research Council, AISC, and the Hilti Corporation for financing this and other ongoing research projects at UC Berkeley relating to concrete anchorage. Special thanks to Ron Klemencic, chairman and CEO of Magnusson Klemencic Associates, Level 10 Constructions, Cascade Steel, and PJ's Rebar Inc. for donations of materials and manual labor. This study was greatly improved through discussions with the following individuals: Rafael Sabelli (director of seismic design at Walter P. Moore), James Malley (senior principal of Degenkolb Engineers), and Dr. Roberto Piccinin (VP for code development and research at Hilti Corporation).

NOTATION:

A_j = cross-sectional area of a horizontal plane through the joint in square inches

A_{cs} = is the cross-sectional area at the end of the strut under consideration

A_{Nc} = projected failure area of a single anchor or an anchor group in question

A_{Nco} = projected concrete failure area of a single anchor if not affected by edges ($9h_{ef}^2$)

A_{nz} = area of each face of the nodal zone

d = distance between the extreme compression fiber to centroid of longitudinal tension reinforcement

DR_{bo} = drift ratio at breakout failure

DR_y = drift ratio at when leaving the elastic range

E = concrete modulus of elasticity

f'_c = concrete compressive strength

f_{mean} = conversion factor from 5% fractile to median value

f_t = concrete tensile strength

f_y = nominal yield stress steel

G_f = concrete fracture energy

F_{nn} = nominal compressive strength of a nodal zone

F_{ns} = nominal axial compressive strength of a strut

H = vertical distance between the top surface of the slab and the point the force is applied

h_{ef} = anchor effective embedment depth

N_b = basic concrete breakout strength of a single anchor in tension in cracked concrete

N_{cbg} = nominal concrete breakout strength in tension of a group of anchors

P = horizontal force applied to the column free end

T_n = tensile force in anchor group

V_n = nominal horizontal joint shear strength

z = lever arm between tensile and compressive force resultants

β_c = strut and node confinement modification factor for the strut-and-tie method

β_n = nodal zone coefficient for the strut-and-tie method

β_s = strut coefficient for the strut-and-tie method

γ = joint shear strength coefficient that depends on joint geometry and loading

ϕ = strength reduction factor

$\Psi_{ec,N}$ = modification factor for anchor groups loaded eccentrically in tension

$\Psi_{ed,N}$ = modification factor for edge effects of anchors in tension

$\Psi_{c,N}$ = modification factor for anchors in uncracked concrete under service loads

$\Psi_{cp,N}$= modification factor for concrete splitting with post-installed anchors

Ψ_{M} = modification factor for bearing pressure of base plate by Herzog (2015)

REFERENCES

AISC, 2006, “Design Guide 1: Base Plate and Anchor Rod Design,” Vol. 2, 63 pp.

ACI 318 (2019). “Building Code Requirements for Structural Concrete (ACI 318-19) and Commentary ACI (ACI 318R-19),” American Concrete Institute, Farmington Hills, MI, 624 ACI

ACI 352R (2002). “Recommendations for Design of Beam-Column Connections in Monolithic Reinforced Concrete Structures (Reap 2010), American Concrete Institute, Farmington Hills, MI, 38 pp.

Bažant, Z., (2000) “Size effect,” International Journal of Solids and Structures 69-80, Elsevier Science Ltd.

Caltrans, 2016. Memo to DesignMTD (MTD) 20-7, Seismic Design of Slab Bridges, California Department of Transportation, Sacramento, CA.

Eligehausen, R., Bouska, P., Cervenka, V., and Pukl, R., 1992, “Size Effect of the Concrete Cone Failure Load of Anchor Bolts,” In Z. P. Bazant (Ed.), Fracture Mechanics of Concrete Structures (pp. 517-525). London, New York: Elsevier Applied Science.

Eligehausen, R. and Balogh, T., 1995, “Behavior of Fasteners Loaded in Tension in Cracked Reinforced Concrete,” ACI-Structural Journal, V. 92, No. 3, May-June 1995, p. 365-379

Eligehausen, R., Mallée, R., and Silva, J. F., 2006, “Anchorage in Concrete Construction,” Berlin: Ernst and Sohn.

European Committee for Standardization, 2018, EN 1992-4:2018, “Design of concrete structures. Design of fastenings for use in concrete”, Brussels, European Committee for Standardization.

Fuchs, W.; Eligehausen, R.; and Breen, J., 1995, “Concrete Capacity DesCCD (CCD) Approach for Fastening to ConcreACI” ACI Structural Journal, V. 92, No. 1, Jan.-Feb., pp. 73-94.

Herzog, M., 2015, “Beitrag zur Vereinheitlichung der Bemessung im Stahlbetonbau und in der Befestigungstechnik (Contribution to the standardization of design in reinforced concrete construction and fastening technology),” Stuttgart, Germany: Institut für Werkstoffe im Bauwesen der Universität Stuttgart, 457 pp.

Kupfer H, Munger F, Kunz J, Jahring A., 2003, “Hauptaufsatze-Nachtraglich verankerte gerade Bewehrungsstabe bei Rahmenknoten (Anchorage of post installed straight bars for frame node connections),” Bauingenieur. Berlin: Julius Springer [1920]- 1997.; 2003;78(1):24–37.

Mahadik, V., Sharma, A., and Hofmann, J. (2019), Re-evaluation of existing tests on RC connections using post-installed reinforcing bars. Elsevier https://doi.org/10.1016/j.engstruct.2019.109970

Mahrenholtz, C., Akguzel, U., Eligehausen, R., and Pampanin, S., 2014, "New Design Methodology for Seismic Column-to-Foundation Anchorage Connections" *ACI Structural Journal*, V. 111, No. 5, Sep.-Oct., 1179-1189 pp.

Nilforoush, R., Nilsson, M., Elfgren, L., Ožbolt, J., Hofmann, J., and Eligehausen, R., 2017, "Influence of Surface Reinforcement, Member Thickness, and Cracked Concrete on Tensile Capacity of Anchor Bolts," ACI-Structural Journal, V. 114, No. 6, November-December 2017, p. 1543-1556.

Nilforoush, R., Nilsson, M., and Elfgren, L. 2018, "Experimental Evaluation of Influence of Member Thickness, Anchor-Head Size, and Orthogonal Surface Reinforcement on the Tensile Capacity of Headed Anchors in Uncracked Concrete," ASCE Journal of Structural Engineering, January 2018, p. 14 DOI: 10.1061/(ASCE)ST.1943-541X.0001976

Ožbolt, J., Eligehausen, R., and Reinhardt, H.W., 1998, "Size effect on the concrete cone pull-out load," International Journal of Fracture 95: 391–404, 1999.

Papadopoulos, V., Murcia-Delso, J., Benson Shing, P., 2018, Development of Headed Bars in Slab-Column Joints of Reinforced Concrete Slab Bridges. ACI-Structural Journal, V. 115, No. 5, September 2018, p. 1393-1406.

RILEM TC, 1985, "Determination of the fracture energy of mortar and concrete by means of three-point bend tests on notched beams," Materials and Structures, Vol. 18, No. 106, July – August 1985, RILEM, Paris, France, pp. 99-101

RILEM TC, 19FMC "FMC 2 Size-Effect Method for Determining Fracture Energy and Process Zone Size of Concrete, 1990," RILEM Recommendations for the Testing and Use of Construction Materials, RILEM, Paris, France, pp. 102-106.

Sharma, A. Eligehausen, R., and Asmus, J., 2017a, Comprehensive Experimental Investigations on Anchorages with Supplementary Reinforcement. Conference Proceedings, 3rd International Symposium on Connections between Steel and Concrete, Stuttgart, Germany, Sep. 27-29, 2017

Sharma, A. Eligehausen, R., and Asmus, J., 2017b, Comprehensive Analytical Model for Anchorages with Supplementary Reinforcement. Conference Proceedings, 3rd International Symposium on Connections between Steel and Concrete, Stuttgart, Germany, Sep. 27-29, 2017

Tanaka R, Oba K., 2001, "Experimental study on seismic performance of beam members connected with post-installed anchors," Proceedings of the Symposium on Connections between Steel and Concrete, Stuttgart, Germany. p. 576–85.

Worsfold, B. and Moehle, J., 2019, "Laboratory Tests of Column-Foundation Moment Transfer Connections with Headed Anchors," Structural Engineering, Mechanics, and Materials (SEMM) Report, University of California, Berkeley, UCB/SEMM-2019/01, 171 pp.

Worsfold, B. and Moehle, J., 2021, “Laboratory Tests of Column-Foundation Moment Transfer Connections with Shear Reinforcement,” Structural Engineering, Mechanics, and Materials (SEMM) Report, University of California, Berkeley, UCB/SEMM-2022/01, 255 pp.

CHAPTER 3 - MOMENT TRANSFER AT COLUMN-FOUNDATION CONNECTIONS: ANALYTICAL STUDIES[3]

by Benjamin Worsfold and Jack Moehle

ABSTRACT

Steel and precast columns are commonly designed to transfer moments to foundations through cast-in-place headed anchors. The concrete breakout failure mode is not routinely checked, even though recent tests have shown it can limit the connection's strength. This paper describes how physical test data are used to calibrate finite element models of column-foundation connections to investigate critical variables. When designing column-foundation connections with cast-in-place anchors, both beam-column joint shear strength and concrete breakout failure strength should be calculated, with the connection strength taken as the smaller of the two values. Results suggest that properly detailed distributed shear reinforcement in the foundation can increase connection strength and displacement capacity if the connection is controlled by the concrete breakout failure mode. This effect is ignored by current building codes.

Keywords: anchoring to concrete; breakout; column-foundation connections; finite element method; headed anchor; shear reinforcement; supplementary reinforcement

INTRODUCTION

Connections between structural columns and foundations are common in building construction. Whether the column is structural steel, cast-in-place concrete, or precast concrete, moment transfer to foundations presents a challenge for designers. Little consensus exists concerning what failure modes should be checked and if concrete breakout failure is applicable. Recent tests by Chicchi et al. (2020) suggest that brittle breakout failure can govern large-scale connections. Neither ACI 318-19 nor Eurocode EN 1992-4 allow for the beneficial effects of shear reinforcement as a means of increasing concrete breakout strength, even though research has shown that small amounts of added shear reinforcement can significantly improve behavior (e.g., Sharma et al., 2017b; Papadopoulos et al., 2018). Instead, designers

[3] Originally published as part of *ACI Structural Journal*, V. 120, No. 2, February, 2023, DOI: 10.14359/51737146

must use either the concrete breakout strength without considering shear reinforcement or use anchor reinforcement to carry the full breakout force across the critical failure surface. Additionally, ACI 318-19 anchoring-to-concrete provisions use larger safety margins than is common in other equations in the code, leading to anchorage lengths that may seem long compared with equivalent development lengths for hooked or headed reinforcement. Some designers have reasoned that the joint shear strength of column-foundation connections is similar to that of a beam-column joint where the column terminates at a roof level with beams framing into all four column faces. The joint area can be estimated as the nominal area between the anchor groups.

This paper describes Finite Element (FE) models of concrete anchors built using the software ATENA and calibrated with physical test data from Ninĉević et al. (2019), Gaspar and Moehle (2021), and Worsfold et al. (2022a). FE modeling guidelines were distilled and used to perform a blind prediction of a full-scale column-foundation connection by Worsfold and Moehle (2022). FE parametric studies were performed with the calibrated models to investigate critical variables affecting the failure modes of concrete breakout and beam-column joint (BCJ) failure. The beneficial influence of shear reinforcement on the breakout failure was investigated, as well as requirements for placement and development of the reinforcement.

RESEARCH SIGNIFICANCE

Full-scale physical tests of column-foundation connections focusing on the concrete failure modes are scarce and resource intensive. FE models calibrated with physical tests have been shown to be a viable alternative that permits the study of failure modes and critical variables. The influence of distributed shear reinforcement on the concrete breakout failure zone is investigated.

LITERATURE REVIEW

The beneficial effect of different reinforcement configurations on anchor behavior has been observed in physical experiments and analytical simulations (Eligehausen et al., 2006). Sharma et al. (2017a) and Sharma et al. (2017b) studied anchor groups welded to a common plate and observed that relatively small amounts of reinforcement increased the anchor group strength and displacement capacity. They proposed a design equation to consider this effect. It is unknown if this model functions adequately for other reinforcement configurations or for anchors not welded to a common plate.

Papadopoulos et al. (2018) tested physical specimens of column-slab connections for bridges under axial load and moment. Shear reinforcement inside and outside the joint was effective at preventing

breakout type failures and increased displacement capacity. Detailing recommendations have been adopted into Caltrans in MTD 20-7 (Caltrans 2016). No general model for the influence of shear reinforcement on breakout failure is proposed.

Kupfer et al. (2003) developed a strut-and-tie model for column-foundation connections that suggests vertical ties may be required outside the joint for equilibrium in the foundation.

Neither ACI 318-19 nor Eurocode EN 1992-4 allow the shear reinforcement strength to be added to the concrete breakout strength. If reinforcing bars are included, both codes require that the designer select strength based on either the concrete strength or the reinforcement strength, whichever is larger. In EN 1992-4, only bars located less than 0.75 times the effective embedment depth (for tension loading) or the edge distance (for shear loading) from the anchors are assumed effective. Punching shear tests by Simões et al. (2016) found that shear reinforcement placed farther than 0.78*d* from the column edges was ineffective.

Bruckner (2007) matched experimental anchor test results with FE MASA3D models where the anchors were 3D elements. The anchor shaft included a bond layer between the steel and the concrete. The head bearing surface was fixed to the concrete. All other surfaces of the anchor head (side and bottom faces) had no contact with the surrounding materials. Reinforcement bars were modeled exclusively with 1D elements.

Based on physical experiments and finite element simulations with the program MASA, Nilforoush et al. (2018) propose anchor strength modification factors to consider the effect of surface reinforcement, member thickness, and anchor head size. ACI 318-19 indirectly restricts head size by limiting the nominal bearing stress to $8 f'_c$.

FINITE ELEMENT SOFTWARE

In this study, the authors use the finite element software ATENA (V5.7.0). The concrete material model in this program is based on the smeared crack approach and crack band method for both tension and compression with the combined fracture-plastic model proposed by Červenka and Pappanikolaou (2008). This formulation decomposes the strain vector into the elastic (ε_e), plastic/crushing (ε_p), and fracture (ε_f) strains:

$$\varepsilon = \varepsilon_e + \varepsilon_p + \varepsilon_f \tag{11}$$

The Menetrey and William (1995) relation is used for compression. In tension, the concrete is elastic up to the maximum tensile stress (f_t). Beyond this peak, the softening curve uses the crack band approach of Bažant and Oh (1983) and follows the exponential crack opening curve from Hordijk (1991). The area under this crack opening law is the fracture energy (G_f), defined as the energy needed to fully

open a crack of unit area such that stress is no longer carried across the crack. Normal stress across the crack drops to zero when the crack width reaches w_c, which ATENA defines as:

$$w_c = 5.15 * \frac{G_f}{f_t} \tag{12}$$

Each finite element can have a maximum of one crack (per orthogonal direction). The crack width (w_t) is calculated by multiplying the fracture strain (ε_f) and the crack band width (L_t):

$$w_t = \varepsilon_f L_t \tag{13}$$

The crack band width of each element is measured perpendicular to the crack and then modified as proposed by Červenka et al. (1995) with equations (14) to reduce the inherent sensitivity to mesh size and orientation in smeared crack models.

$$L_t' = \gamma L_t$$
$$\gamma = 1 + (\gamma_{max} - 1)\frac{\theta}{45} \tag{14}$$

with γ_{max} = 1.5 and θ is the crack angle. Červenka et al. (2018) propose upper and lower limits on the crack band width to diminish mesh size sensitivity. Fine meshes may produce too many cracks, while coarse meshes may produce too few. An incorrect number of cracks decreases the model's ability to accurately simulate softening. Models with fine meshes were observed to increase strength and ductility. They propose a lower limit for the crack band width (L_t) of 1.5 d_{max} and an upper limit equal to the reinforcement spacing.

CALIBRATION OF FINITE ELEMENT MODELS

Single anchor tests

A series of single cast-in-place headed anchor tests was performed by Ninĉević et al. (2019) with an anchor rod diameter of 0.79-in. [20 mm] and an effective depth of 4-in. [100 mm]. See test setup **Error! Reference source not found.**(a). The measured force-displacement curves for two concrete mixes are shown in **Error! Reference source not found.**(a) (Mixture E1 with f'$_c$ = 4120 psi [28.4 MPa]) and **Error! Reference source not found.**(b) (Mixture E3 with f'$_c$ = 4790 psi [33.0 MPa]). The measured displacements included part of the deformation of the loading apparatus.

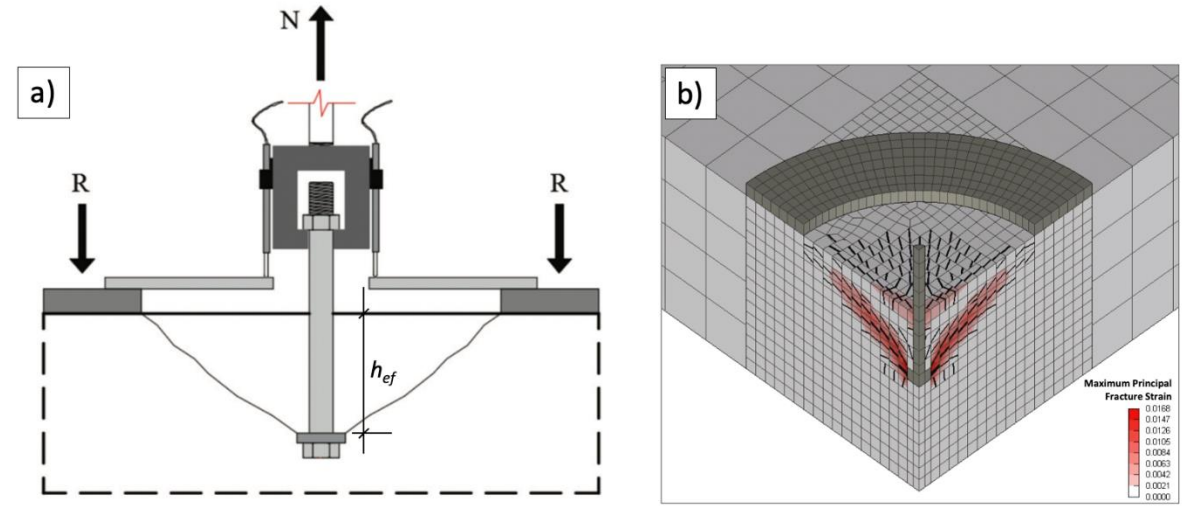

Fig. 1–(a) Test setup and typical concrete cone failure from Ninčević et al. (2019) and (b) example FE model showing crack patterns and principal tensile strains

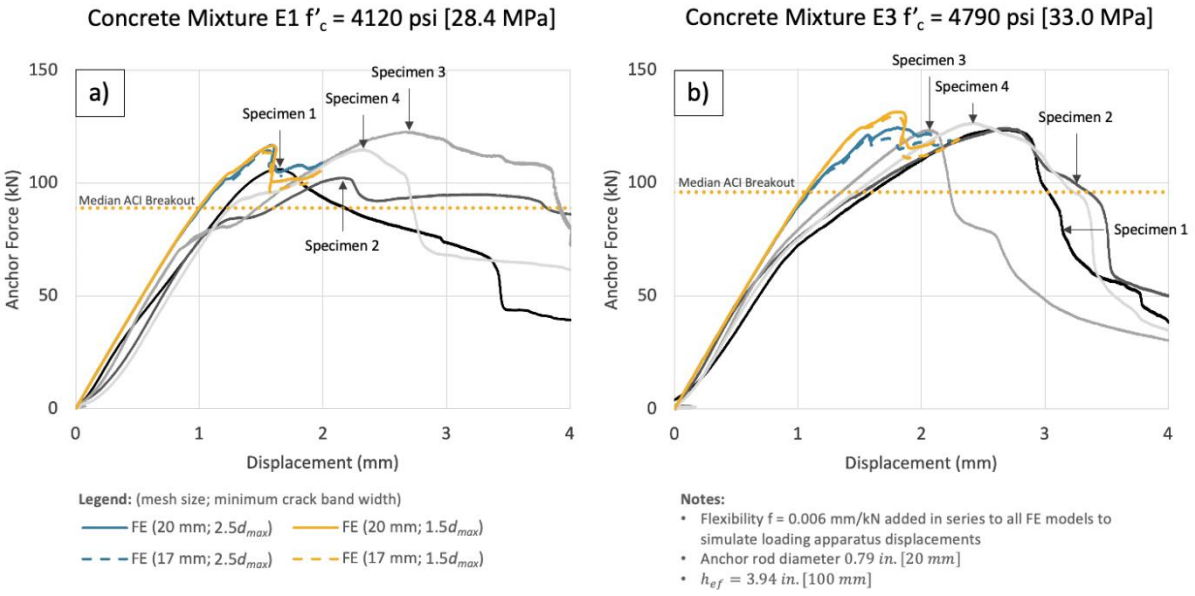

Fig. 23–Select single anchor physical test results from Ninčević et al. (2019) and calibrated FE models for two different concrete mixtures (a) E1-28d (b) and E3-28d

FE models were calibrated to fit the experimental data while balancing precision and run time. The modeling approach highlights are summarized in Table 3. In general, the material properties were taken as the software defaults except where noted. The doubly symmetric test setup allowed so only a quarter of the specimens need be modeled. The concrete is modeled with 3D 8-node hexahedra elements

and a 2 x 2 integration scheme. Regions of undamaged concrete were modeled with a coarser mesh which had no appreciable effect on the results other than reducing calculation times. The anchor was modeled as a 3D solid-elastic steel object fixed to the concrete at the bearing surface (similar to Bruckner (2007)). No other anchor surface is in contact with the concrete. Tests including sliding contact interfaces between the concrete and the anchor shaft increased the calculation time by up to a factor of 30 without an appreciable effect on the peak anchor forces or concrete crack patterns. Modeling anchor rods as 1D truss elements fixed to the concrete at both ends reduced the calculation time but increased mesh size sensitivity.

Table 3–Select modeling parameters for headed anchors with ATENA

Model Property	Notes
Anchor	3D solid-elastic steel fixed to the concrete at the bearing surface (no other contacts)
Mesh size	d_{max} < mesh size < h_{ef} / 5
Stop analysis	End run once failure cone has formed and cracks approach w_c.
Rotated crack	0.80
Fracture Energy (G_f)	FIB Model Code 1990
Elements	8-node hexahedra
Integration scheme	2 x 2
Minimum crack band	1.5 to 2.5 d_{max}

The inherent sensitivity to mesh size and orientation with smeared crack approaches can be reduced following recommendations from Červenka et al. (2018). Elements should not be smaller than the maximum aggregate size to not violate the assumption of homogeneity. Large elements can reduce run times but should be small enough to accommodate at least five elements along the anchor embedment depth (h_{ef}) to accurately reproduce experimental concrete cone fracture patterns. A model run should be stopped if a failure cone has formed and crack widths are approximately equal to w_c (fully open cracks). Some models allowed to run beyond this state resulted in artificial strengthening, as they developed compression struts between the anchor head and the supports. This effect may result because the model does not completely detach the failure cone as would happen in physical tests.

The cracks that produce the concrete cone are generally not the first cracks to occur in the member. It is essential to allow for crack rotation as the state of triaxial stress evolves during loading and stresses redistribute as cracks propagate. A rotated crack value of 0.8 was found to adequately reproduce crack patterns and observed behavior. To visualize concrete cone failures clearly, crack patterns in this paper show primary, secondary, and tertiary cracks overlaid with the principal fracture strains.

If fracture energy is not input manually, ATENA V 5.7.0 will default to the FIB Model Code 2010 equation:

$$G_f = 73\,(f_{cm})^{0.18} \tag{15}$$

where f_{cm} is the concrete strength in MPa and G_f is the fracture energy in N/mm. This approach is independent from aggregate size and was found to overestimate the fracture energy for concrete mixes with small aggregate sizes resulting in anchors with excessive strength and ductility. The FIB Model Code 1990 approach is recommended as it incorporates the aggregate size and results in fracture energies closer to the values measured by Ninĉević et al. (2019):

$$G_f = G_{f0}\left(\frac{f_{cm}}{f_{cm0}}\right)^{0.7} \tag{16}$$

where G_{f0} is a reference fracture energy proportional to the aggregate size (d_{max}) and f_{cm0} is a reference compressing strength equal to 1450 psi [10 MPa].

An appropriate range for the minimum crack band width was found to span from 1.5 and 2.5 times d_{max}, which agrees with the recommended value of $1.5d_{max}$ from Červenka et al. (2018). Higher minimum crack band widths tend to drop the peak force as fewer cracks appear, concentrating the fracture strain in a smaller region. This limit is important in these models because the mesh size is close to the maximum aggregate size.

The direction of the plastic flow (β) was set to 0.0 as these are monotonic tests where volume dilation (β > 0) or contraction (β < 0) are not expected to play significant roles. Dilation was observed to decrease crack widths resulting in larger displacements.

The single anchor breakout models were not sensitive to parameters relating to the concrete compressive behavior, which is expected, as tensile behavior dominates. The concrete tensile capacity (f_t) was found to have a minor influence on the anchor behavior. Note that if the fracture energy (G_f) remains constant, varying the tensile capacity will not change the total energy required to fully open a crack. The element sizes are relatively small, so the maximum crack band spacing has little influence on the results. The shear factor (s_F) has a negligible influence on the results which is expected as the anchor force-resisting mechanism does not rely on shear stress carried across the cracks.

Concerning the numerical solution strategy, an elastic predictor with relatively small step sizes (≈ 1 / 140 mm), a relatively large number of iterations (≈ 300), and strict convergence criteria (< 0.1%) was found to perform adequately. Refining the solution strategy did not noticeably improve results or runtime (for example, line search, repeating unconverted steps with smaller step sizes, or selecting iterations with lower iteration numbers when at an unconverted step). This calibration phase also observed that mesh incompatibility along the crack path can increase mesh size sensitivity.

Error! Reference source not found. plots the measured force-displacement curves from

Ninčević et al. (2019) and the calibrated FE models for two concrete mixtures. The median uncracked concrete breakout strength is labeled “Median ACI Breakout”. The uncracked breakout strength is calculated as per ACI 318-19 and multiplied by a factor of 1.33 to move from a 5% fractile to a median value. This modification factor is calculated using the standard normal distribution z-value for a 5% fractile (-1.645) and assuming measured strengths follow a normal distribution with a covariance of 0.15 (Fuchs et al. 1995). The flexibility of the loading apparatus was estimated as 0.006 mm / kN and added in series to all FE results. Four FE models are shown per concrete mix, varying mesh size (17 mm and 20 mm) and minimum crack band width (1.5 and 2.5 times d_{max}). The variation in mesh size and minimum crack band width had relatively little effect on the results. The initial stiffness is similar to experimental values. For each concrete mixture, the average FE peak anchor forces are within 3% of the average measured values. The FE models are not able to simulate the descending branch.

Axial anchor group tests

Three cast-in-place headed anchor group tests were performed by Gaspar and Moehle (2021) with eight anchors per group at an effective depth of 7-in. [178 mm] and an anchor diameter of 0.75-in. [19 mm] in the test setup shown in **Error! Reference source not found.**(a). The anchors were configured along the perimeter of a 12-in. x 12-in. [305 mm x 305 mm] square pattern with one rod at each corner and another rod at the center point of each face. The measured force-displacement curves for specimens B01, B02, and B03 (f'_c = 4170 psi [28.7 MPa]; f'_c = 4920 psi [33.9 MPa]; f'_c = 5140 psi [35.4 MPa], respectively) are shown in **Error! Reference source not found.**. The measured displacements include settlement of the supports and setup flexibility.

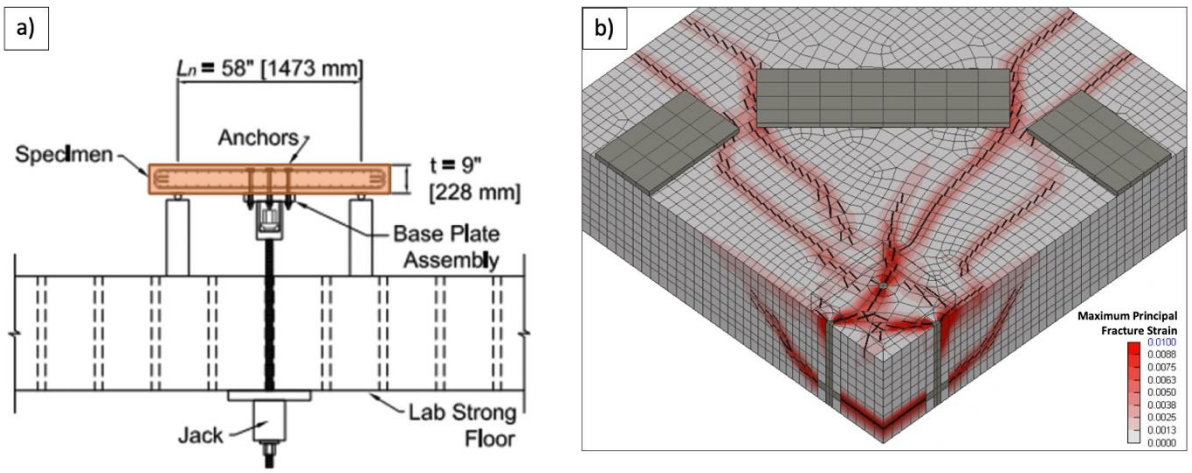

Fig. 24–(a) Test setup for anchor group specimens from Gaspar and Moehle (2021) and (b) example FE model showing crack patterns and principal tensile strains for specimen B02

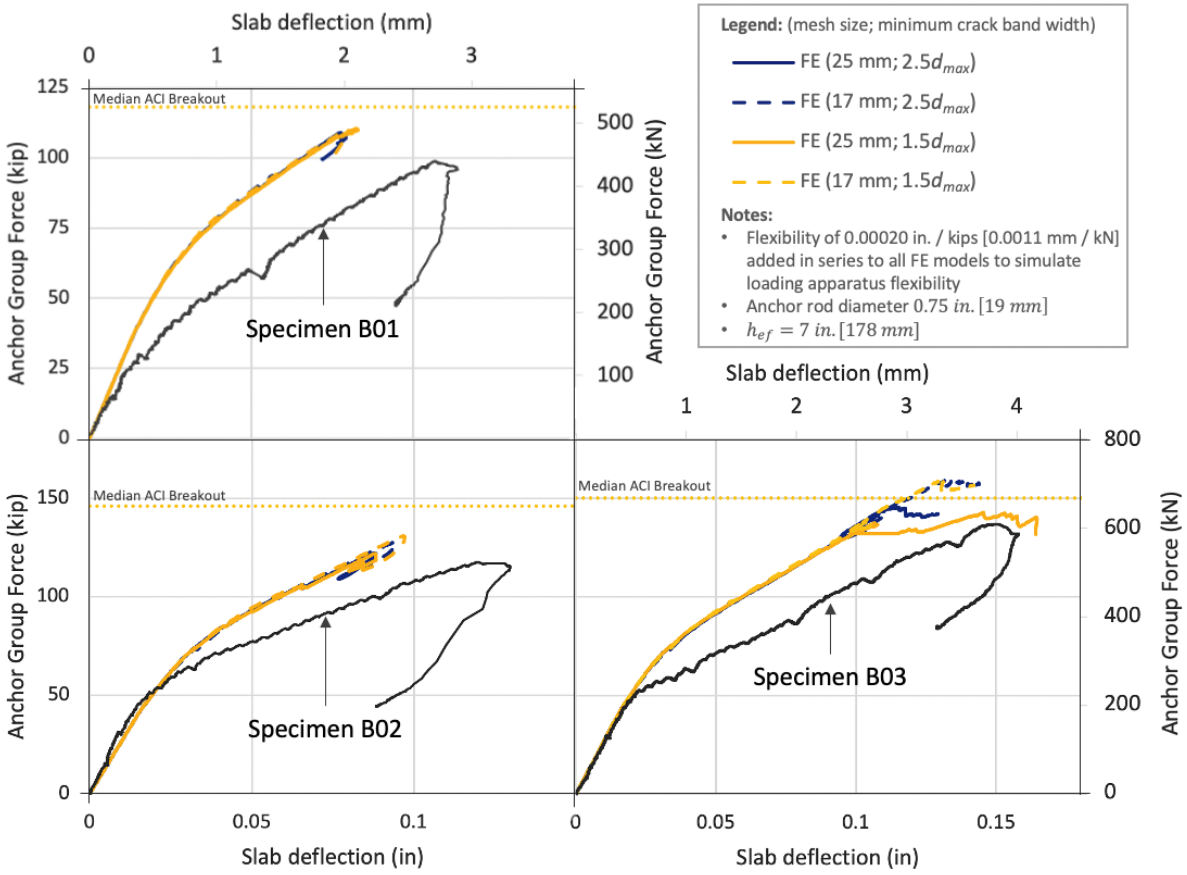

Fig. 25– Anchor group force versus slab deflection for three physical anchor group tests from Gaspar and Moehle (2021) and calibrated FE models

These tests were simulated following the modeling observations from the single anchor calibration phase. The anchors were fixed to a common loading plate. The support plates were fixed to the slab surface while being allowed to pivot about their centerlines. The longitudinal reinforcement was modeled as 1D truss elements perfectly fixed to the concrete elements. Bond failure is not expected but would be represented by the fracture of concrete elements around the reinforcing bars. Specimen B03 included four reinforcing bars placed perpendicular to the anchor shafts against the head bearing surfaces. These “trim bars” were modeled as 3D objects fixed to the concrete as the anchors relied on their flexural stiffness to provide dowel action. When the trim bars were modeled as 1D truss elements, they had no effect.

Error! Reference source not found. shows four FE models per specimen, varying mesh size (17 mm and 20 mm) and minimum crack band width (1.5 and 2.5 times d_{max}). For all three test specimens, the peak FE anchor forces were within 15% of the measured peak strengths. The variation in mesh size and minimum crack band width had relatively little effect on the results. The models reproduced both the flexural surface cracks that appeared relatively early in the test and the group failure cone, which appeared suddenly when approaching peak strength (see **Error! Reference source not found.**(b)). In both FE simulations and physical tests, flexural cracking caused a distinct change in stiffness for all three specimens. The flexibility of the loading apparatus was estimated as 0.00020 in. / kips [0.0011 mm / kN] and added in series to all FE results. The focus of this calibration phase was to match peak anchor forces and crack patterns. Matching the displacements would require modeling the complete test setup.

Moment anchor group tests (M01)

A column-foundation connection specimen with cast-in-place headed anchors was tested by Worsfold et al. (2022) with an anchor effective depth of 14.3-in. [360 mm], anchor rod diameters of 1.5-in. [38 mm], and f'_c = 3700 psi [25.5 MPa] (see **Error! Reference source not found.**(a)). Each anchor group consisted of four anchors in a line spaced 5-in. [127 mm] on center. The measured anchor force to column drift ratio curves for the east and west anchor groups are shown in **Error! Reference source not found.**. The median uncracked concrete breakout strength is labeled “Median ACI Breakout”. The column was loaded laterally in a cyclic manner with increasing displacement amplitudes. No additional axial force was included other than self-weight. For additional details on specimen M01 see test report Worsfold and Moehle (2019).

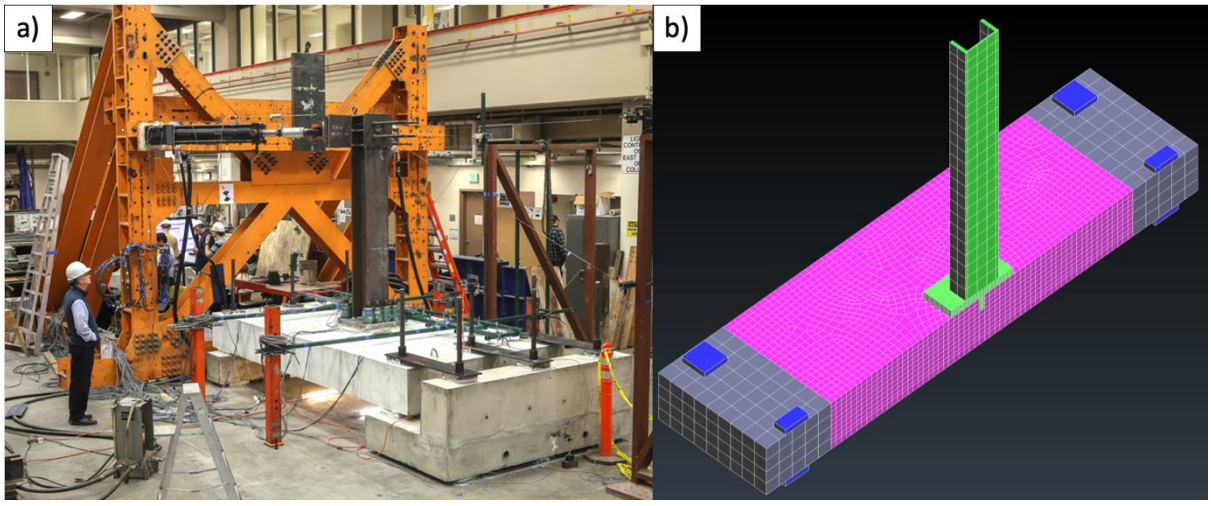

Fig. 26–(a) Test setup and (b) FE model for specimens M01 and M02

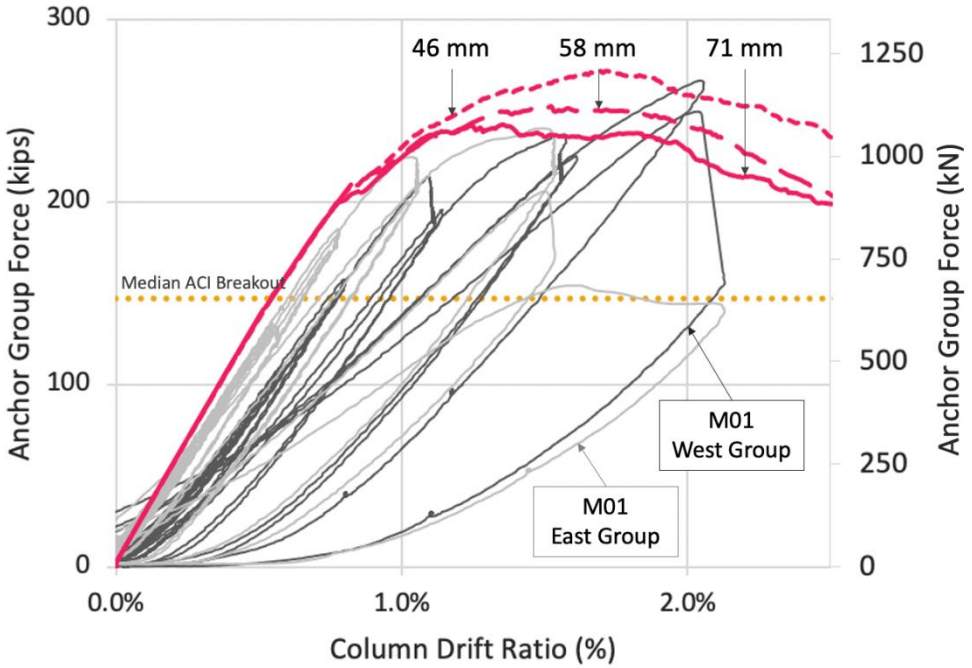

Fig. 27–Anchor group force-column drift ratio for specimen M01 from Worsfold et al. (2022) including FE models with different mesh sizes

This column-foundation connection was modeled using the FE modeling guidelines described in the previous sections (see **Error! Reference source not found.**(b)). The column, base plate, shear lug, and anchor rods were modeled as elastic steel as they are not expected to yield. The anchors are fixed to the baseplate. Longitudinal reinforcement and hoops around the anchors within the joint were modeled as 1D elements fixed to the concrete. A compression-only interface connects the base plate and shear lug to the concrete allowing for sliding and uplift. The plastic flow direction (β) was set to +0.25 to allow for dilation, so the monotonically loaded FE models would better describe the envelope of the cyclic test. The mesh sizes used (71 mm, 58 mm, and 46 mm) are large enough to not be noticeably affected by the minimum crack band width of $2.5d_{max}$ = 48 mm.

Error! Reference source not found. plots the force-displacement curves of the monotonically loaded FE models against the cyclic experimental data. Notice an increase in strength with decreasing mesh size as is expected with smeared crack approaches. The range of peak anchor forces resulting from this mesh size study is similar to the difference between the east and west anchor group forces. Notice that the initial elastic FE stiffness in **Error! Reference source not found.** matches the observed stiffness reasonably well with an offset for the west anchor group.

Error! Reference source not found. shows cross sections of the FE models plotting crack patterns and principal fracture strains for the largest and smallest mesh sizes (71 mm and 46 mm). Concrete breakout failures were observed, which matches the experimental failure mode. Notice flexural cracks at the locations of the maximum moment under the double curvature deformed shape. Some flexural cracks cross the anchor group plane.

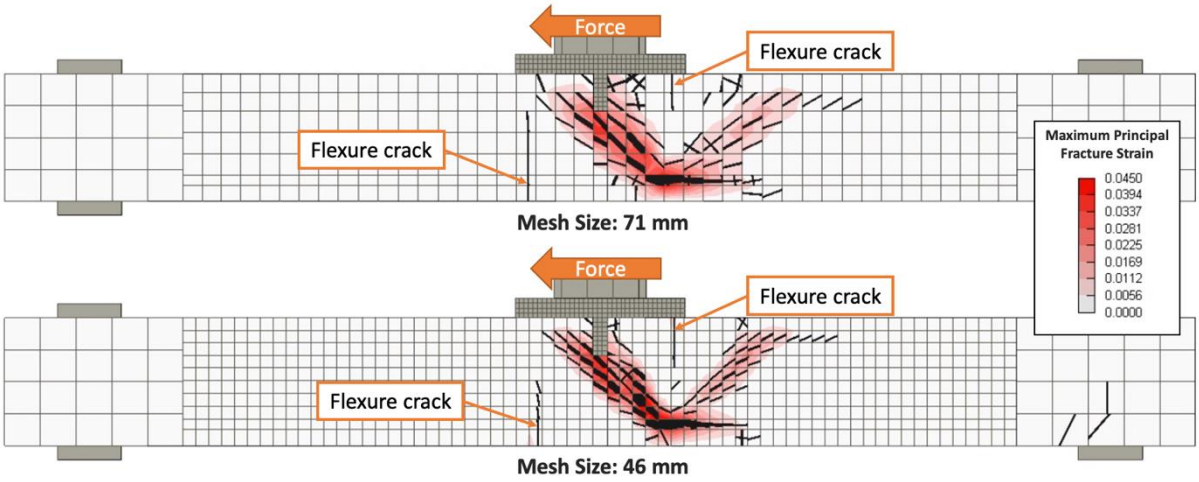

Fig. 28–Crack patterns and principal fracture strain for calibrated FE models of specimen M01 for two mesh sizes

Blind prediction for a moment transfer test specimen (M02)

Worsfold et al. (2022) tested an additional column-foundation connection (Specimen M02) with geometry similar to that of specimen M01 but with shear reinforcing added to the foundation in the form of vertical #4 G60 A706 bars [Ø13 mm G420] in an 8-in. by 8-in. [203 mm by 203 mm] grid (see **Error! Reference source not found.**). The anchor rod diameters were 1.5-in. [38 mm] and f'_c = 3930 psi [27.1 MPa]. To explore the required distribution of shear reinforcement, the grid extends over a larger region in the west half of the foundation slab than the east. The measured anchor group force to column drift ratio curves for the east and west anchor groups are shown in **Error! Reference source not found.**. The dotted lines represent the median cracked concrete breakout strength ("Median ACI Breakout") and the median beam-column joint strength ("Median ACI BCJ") per ACI 318-19 assuming a nominal strength coefficient of 15 [1.2]. For additional details on specimen M02 see test report Worsfold and Moehle (2022).

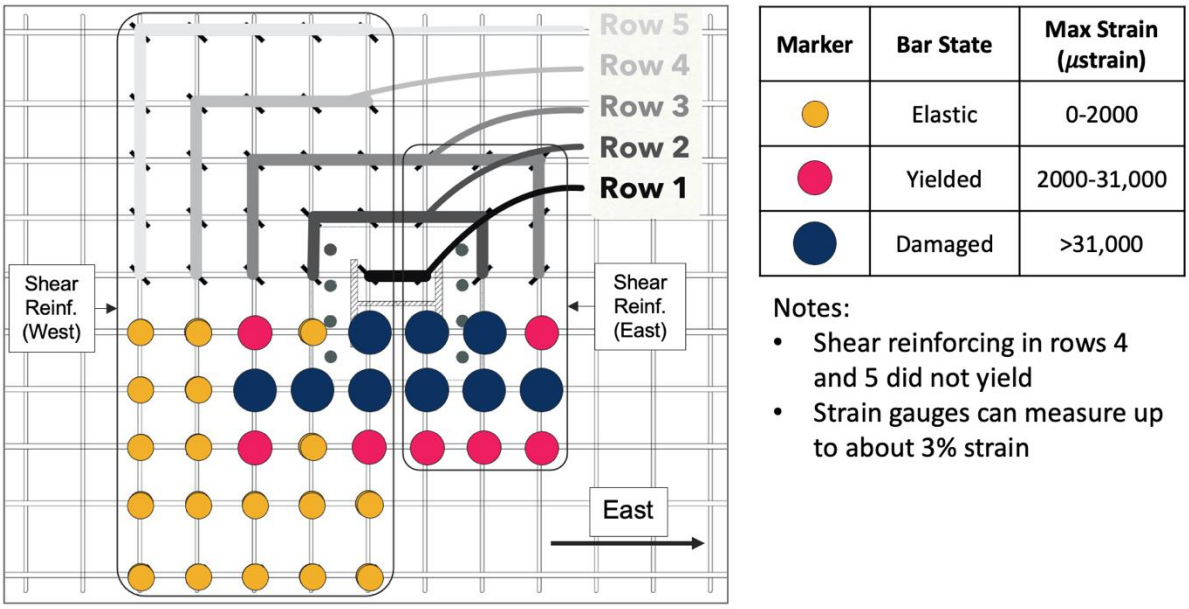

Fig. 29– Specimen M02 plan view showing the final state of each instrumented bar and subdividing the shear reinforcing into rows.

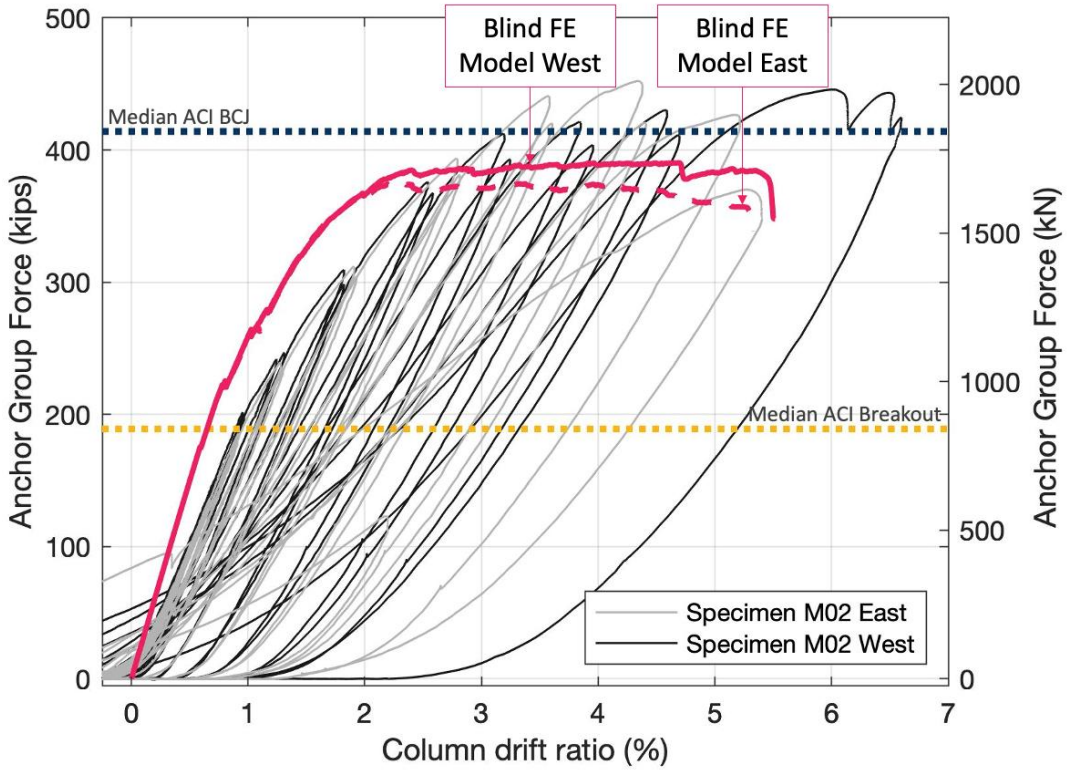

Fig. 30– Anchor group force versus column drift ratio plot for specimen M02 including FE blind predictions

Before specimen M02 was tested, FE models were constructed using as-built drawings and measured material properties. As can be seen in **Error! Reference source not found.**, these so-called blind FE models were stiffer than the experimental results. The blind FE peak anchor group forces were on average about 17% lower than the corresponding experimental values.

Error! Reference source not found. compares a cross section of physical specimen M02 with the crack patterns from the blind prediction models for monotonic loading in both directions. In the physical specimen, each anchor group formed a principal failure cone initiating at the anchor head and a secondary cone initiating at the second row of shear reinforcing bars. For both the physical specimen and the FE models, the primary cone governed for the west anchor group (larger reinforced region) while the secondary cone governed for the east anchor group (smaller reinforced region).

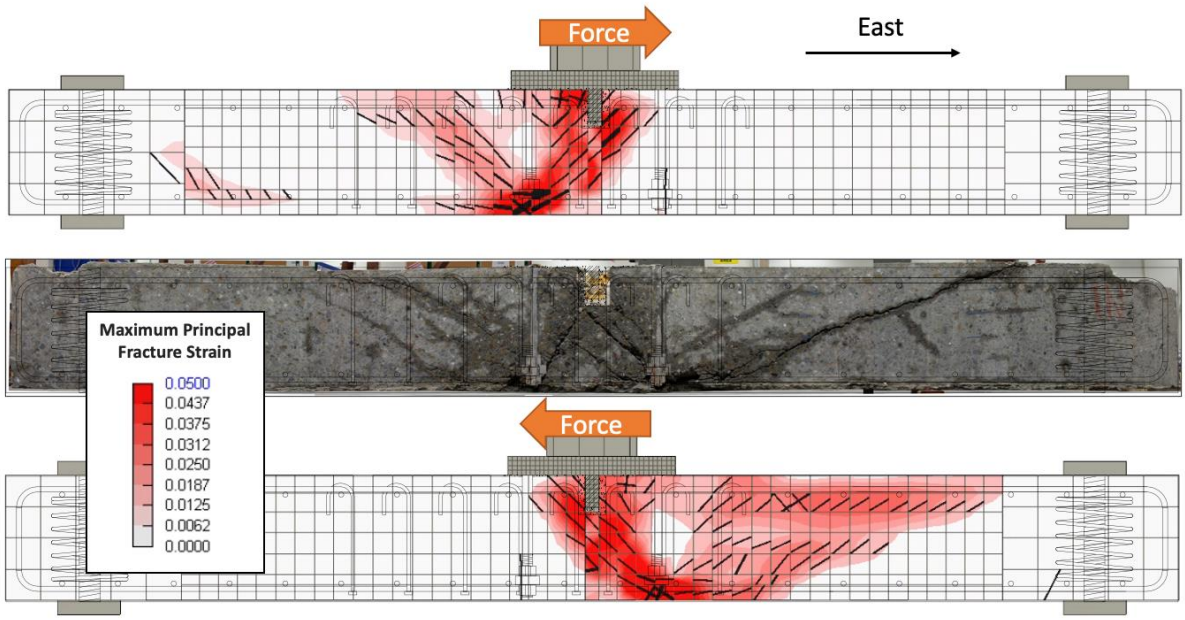

Fig. 31– Physical specimen cross section and FE blind prediction crack patterns for monotonic loading in each direction with reinforcement overlaid

Error! Reference source not found. subdivides the shear reinforcement into rows according to the distance from the anchors. In the physical specimen, only the shear reinforcement near the anchor group yielded (rows 1, 2, and 3). These bars were within 0.75 h_{ef} from the anchor group. The FE blind models showed the same trend (see Error! Reference source not found.).

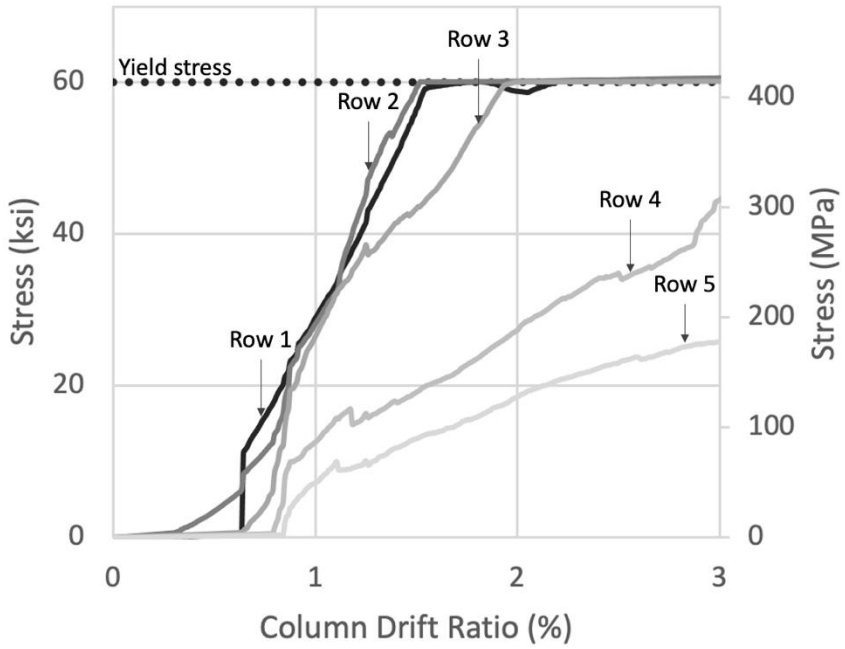

Fig. 32–FE results for M02 blind prediction model. The maximum stress in each row of shear reinforcement per row is plotted against the column drift ratio.

The shear reinforcement bars in specimen M02 were 15-in. [380 mm] long and engaged the top longitudinal reinforcement with a 180-degree hooks while the bottom terminated with a head (see **Error! Reference source not found.**). In the FE blind predictions, the shear reinforcement is fixed to the concrete along the full length. According to ACI 318-19, the development lengths of the hooked and headed shear reinforcing bars are both 6-in. [150 mm]. The shear reinforcement will satisfy ACI 318-19 anchor reinforcement requirements only where the failure plane intersects the middle 3-in. [76 mm] segment of the bar. Nonetheless, many bars that were not developed yielded (see **Error! Reference source not found.**).

The longitudinal bars in test specimen M02 were designed as G60 [420 MPa] but were substituted for G100 [690 MPa] to avoid premature longitudinal yielding. FE models with G60 [420 MPa] and G100 [690 MPa] longitudinal reinforcement showed no appreciable difference as breakout failure governs in both cases.

PARAMETRIC STUDIES

The calibrated FE models described previously were used to perform parametric studies. These studies explored critical variables to investigate the effects of shear reinforcement on column-foundation connections with cast-in-place anchors.

Boundary conditions

The foundation slab of test specimens M01 and M02 spanned between supports located near the ends of the slab (see **Error! Reference source not found.**). These hinge supports represent inflection points of a continuous foundation slab when subjected to lateral loading. Parametric studies were conducted using FE models to investigate the effect of distributed soil support on the test results. Three models were created: two had compression-only soil springs simulating a stiffer soil (1100 psi / in. [300 MPa / m]) and a softer soil (200 psi / in. [54 MPa / m]), while a third model fixed the foundation slab along the bottom surface. In all cases, the tie-down rods at the ends of the slab were kept in place to avoid overturning and simulate the reactions felt due to continuity of the foundation slab. The crack patterns in **Error! Reference source not found.**(a) show that concrete breakout failure governed regardless of the boundary condition. The fixed base resulted in an unnatural breakout cone geometry, apparently due to tensile stresses developed along the base of the foundation slab. The force-displacement curves for all boundary conditions are similar except for the model with a fixed base (see **Error! Reference source not found.**(b)). These observations suggest that the simply supported column-foundation boundary condition used in the tests was adequate to represent breakout failure modes expected for soil-supported foundation slabs.

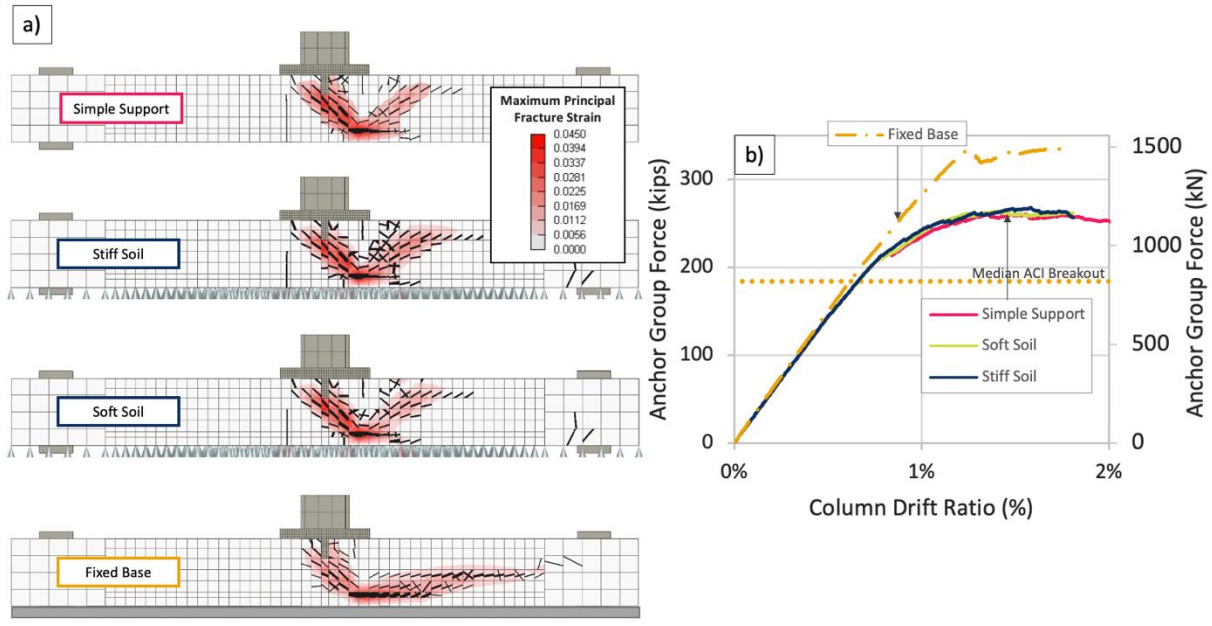

Fig. 12–(a) Crack patterns and (b) force-displacement curves for various FE models comparing boundary conditions

Shear reinforcement stress-strain relationship

The M02 FE blind prediction models used an elastoplastic relationship for the shear reinforcement bars with a nominal yield stress of 60 ksi [420 MPa]. FE models incorporating the measured stress-strain curve with a yield stress of 75 ksi [520 MPa] and ultimate stress of 105 ksi [720 MPa] did not increase the peak anchor strength, suggesting that concrete failure governs.

Shear reinforcement ratio (ρ_{tr})

The shear reinforcement of test specimen M02 consisted of #4 G60 bars [Ø13 mm G420] in an 8-in. by 8-in. grid [200 mm by 200 mm] for a shear reinforcement ratio of $\rho_{tr} = 0.2\text{-in.}^2/(8\text{-in.})^2 = 0.31\%$. **Error! Reference source not found.** plots the force-displacement curves for FE models with different shear reinforcement ratios. The dotted lines represent the median cracked concrete breakout strength and the median beam-column joint strength per ACI 318-19. In all FE models, the shear reinforcement extended throughout the whole slab. A strong correlation is observed between the shear reinforcement ratio (ρ_{tr}) and the peak force in the anchor group. The displacement capacity also increases with ρ_{tr}. Note that the strengths seem to max out in the vicinity of the median beam-column joint strength suggesting joint shear failure.

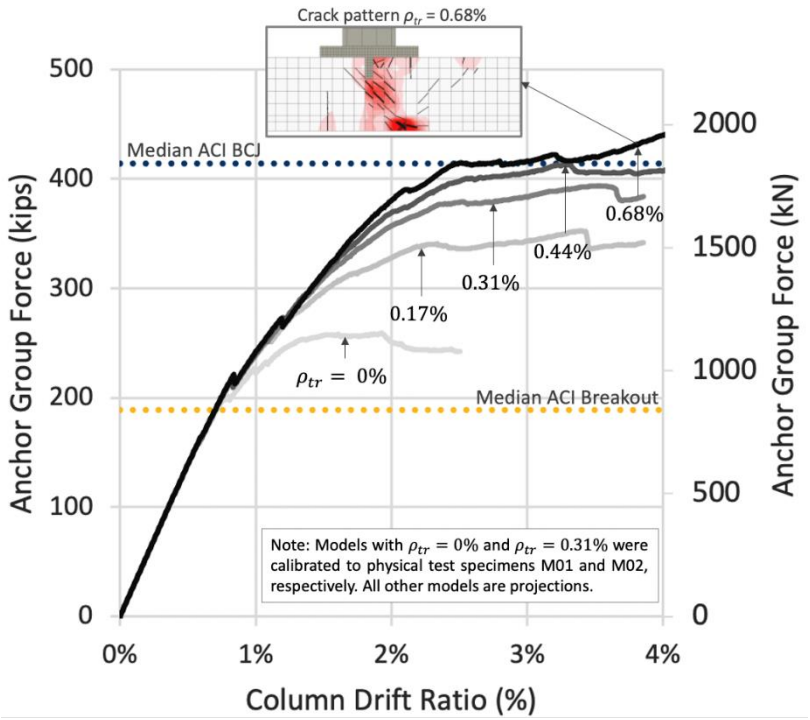

Fig. 33–Force in anchor group versus column drift ratio for FE models varying shear reinforcement ratio (ρ_{tr}). Crack patterns shown for model with ρ_{tr} = 0.68%.

Size of the region with shear reinforcement

Specimen M02 had a larger reinforced region on one side than on the other (see **Error! Reference source not found.**). Multiple FE models were run varying the size of the reinforced region. **Error! Reference source not found.** plots the peak anchor group force relative to the unreinforced case versus the distance from the anchors to the farthest shear reinforcement bar. The models suggest that shear reinforcement placed farther than about 1.5 h_{ef} from the anchor group has no appreciable effect on peak anchor forces. Good detailing practice might extend the shear reinforcement farther from the anchor group to guard against reduced strength for flatter breakout cones that extend past terminated shear reinforcement.

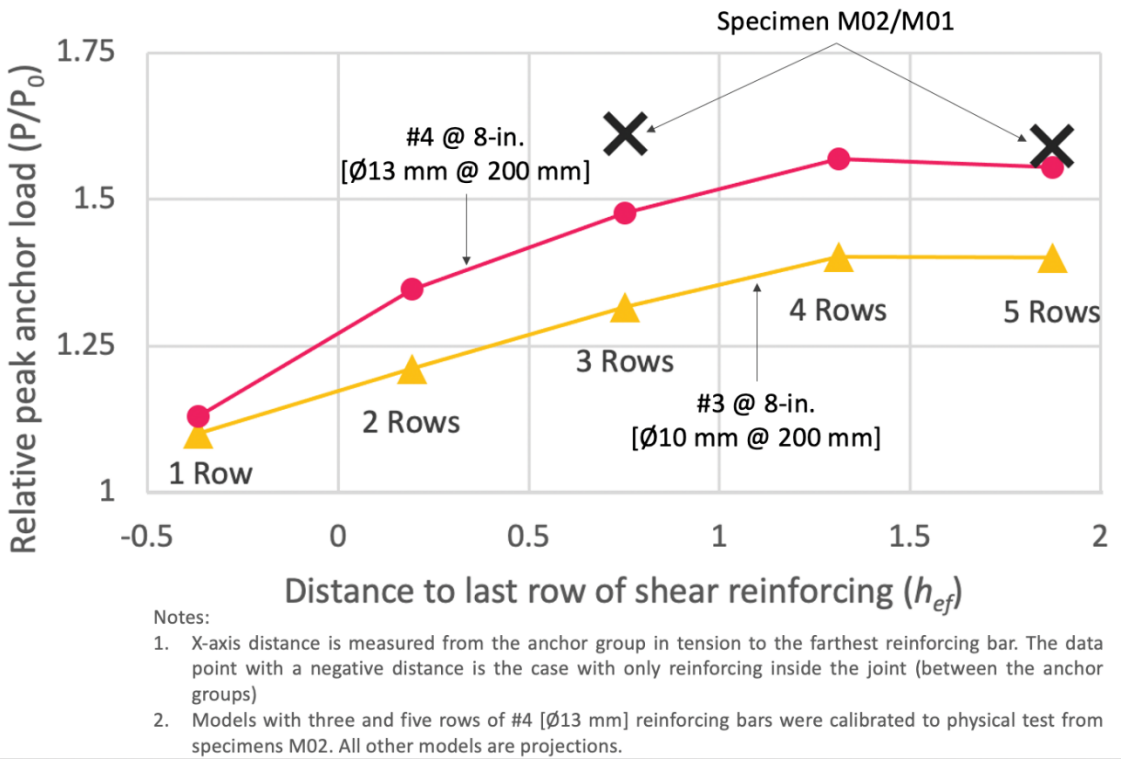

Notes:

1. X-axis distance is measured from the anchor group in tension to the farthest reinforcing bar. The data point with a negative distance is the case with only reinforcing inside the joint (between the anchor groups)
2. Models with three and five rows of #4 [Ø13 mm] reinforcing bars were calibrated to physical test from specimens M02. All other models are projections.

Fig. 34–Relative peak anchor group force versus the size of the region with shear reinforcement

Joint-confining hoops

Specimen M01 included hoops that confined the joint, while specimen M02 did not. FE models were created with various shear reinforcement ratios with and without hoops. Joint hoops comprised 5 #5 G60 [5Ø10 G420], which satisfies the requirements of ACI 318-19 for interior joints of special moment frames. Confining the joint with hoops produces a relatively small and uniform increase in strength of about 3.5% across the tested range of ρ_{tr} (0% - 0.56%). With or without hoops, the connection strength in each case was limited by breakout failure. This observation is consistent with the test results for specimen M01 for which strains in the joint hoop reinforcement were below yield until well after the initiation of breakout failure.

Shear reinforcement grid location

For specimen M02, the grid of shear reinforcement was placed such that the distance from the anchors to the closest shear reinforcement bar was equal in both the east and west halves of the specimen as shown in **Error! Reference source not found.**. **Error! Reference source not found.** plots force-drift ratio

curves for various FE models where the uniform grid of shear reinforcing was shifted such that the anchors were located either near a shear reinforcement bar (solid lines) or equidistant from adjacent shear reinforcement bars (dashed lines). The yellow lines correspond to a #3 @ 8-in. grid [Ø10 mm @ 200 mm] where shifting the grid has no appreciable effect. The blue lines correspond to a #3 @ 10.5-in. grid [Ø10 mm @ 270 mm]. In this case, placing the anchors far from the shear reinforcing bars results in approximately a 7% increase in strength. Limiting the grid spacing to about 0.75 h_{ef} will help keep this effect small such that the designer need not be concerned with the exact location of the reinforcement grid relative to the anchor group.

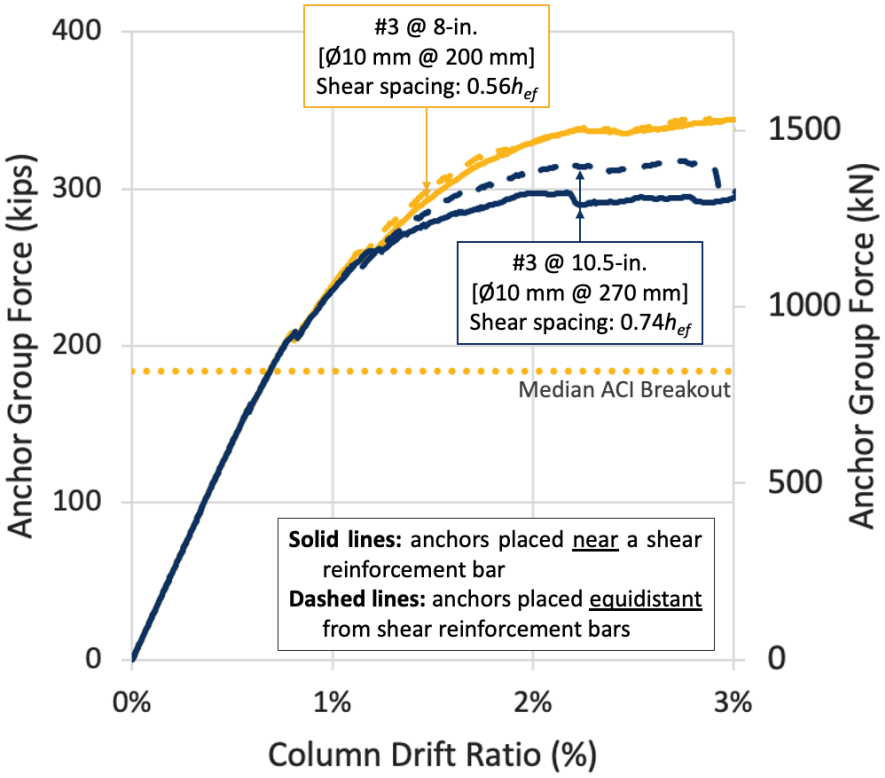

Fig. 35–FE models with two different shear reinforcement ratios (ρ_{tr}) varying the location of the reinforcement grid. All models shown are projections as no physical data are available for these cases.

Joint aspect ratio

Physical specimens M01 and M02 had joint aspect ratios near 1:1, calculated as z / h_{ef} where z is the horizontal distance between the tensile and compressive resultant forces from the column. FE models

were developed to investigate how the beneficial effect of shear reinforcement changes for different joint aspect ratios. The slab was thickened and the anchors were extended towards the bottom of the slab to achieve joint aspect ratios near 1.5:1 and 2:1. **Error! Reference source not found.**(a) and (b) show the force-drift ratio curves of these models with different amounts of shear reinforcement. Similar to the trend observed with the 1:1 join, adding shear reinforcement to the more slender joints increased the connection strength and displacement capacity. Note that the strengths seem to max out in the vicinity of the median beam-column joint strength suggesting joint shear failure.

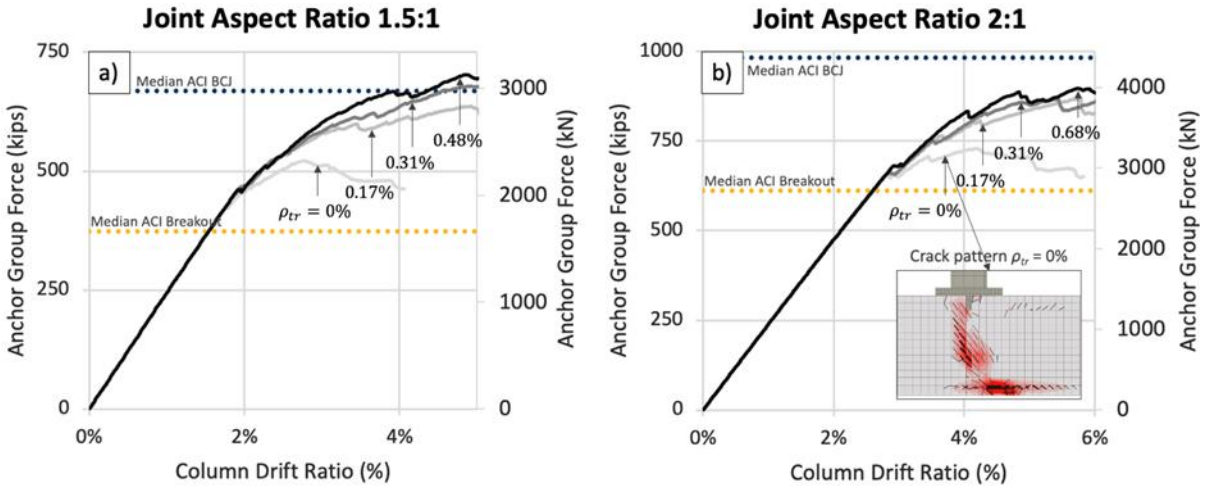

Fig. 36–FE models with different shear reinforcement ratios (ρ_{tr}) for joint aspect ratios of (a) 1.5:1 and (b) 2:1. Crack pattern shown for model with 2:1 joint aspect ratio and ρ_{tr} = 0%. All models shown are projections as no physical data are available for the cases with slender joint aspect ratios.

SUMMARY AND CONCLUSIONS

A series of physical tests was used to calibrate Finite Element (FE) models of cast-in-place anchors for single anchor axial tests, anchor group axial tests, and anchor group moment tests. Modeling guidelines developed from the calibrations were used to perform a blind prediction of another group anchor moment test (Specimen M02). The calibrated results and the blind prediction adequately matched the observed strengths, displacements, crack patterns, and shear reinforcement strains. Some observations from the calibration process follow:

1. A minimum crack band width between 1.5 and 2.5 times the maximum aggregate size was observed to reduce mesh size sensitivity, which is consistent with previous observations.

6. Modeling anchors as 3D objects fixed only to the concrete at the bearing surfaces, reduced mesh size sensitivity without an excessive increase in calculation time compared to modeling anchors as 1D elements.
7. A rotated crack model was necessary to adequately simulate the redistribution of triaxial stress as the breakout cracks propagate from the anchor head to the concrete surface.
8. The FIB Model Code 2010 equation for fracture energy (Gf) overestimated Gf. Improved results were obtained using the FIB Model Code 1990 equation that considers maximum aggregate size.

A series of parametric studies were performed with the calibrated FE models to investigate the effect of shear reinforcement on the breakout failure mode of column-foundation connections with cast-in-place anchors. Some observations follow:

9. Breakout failure of column-foundation connections was insensitive to whether the foundation was supported on soil springs or spanned simply between concentrated supports.
10. Physical test results and FE model results demonstrate that distributed shear reinforcement can increase the tension breakout strength and displacement capacity of column-foundation connections transferring moment.
11. In the physical specimen, many shear reinforcement bars yielded even though they were not developed on both sides of the potential breakout cone surface as would be required by ACI 318-19 anchor reinforcement provisions.
12. The engagement of the shear reinforcement decreased with increasing distance from the anchor bolts, such that shear reinforcement beyond approximately 1.5 h_{ef} was not effective in increasing connection strength or displacement capacity.
13. Secondary breakout cones may govern if distributed shear reinforcing does not extend up to at least 1.5 h_{ef} from the anchors.
14. Where shear reinforcement grid spacing was kept smaller than about 0.75 h_{ef}, the breakout strength was insensitive to the exact location of the shear reinforcement, whereas when the spacing exceeded about 0.75 h_{ef} the breakout strength was sensitive to bar placement.
15. Joint shear strength may govern the behavior of connections with high amounts of shear reinforcement loaded primarily with moment. This failure mode can limit the effectiveness of shear reinforcement.
16. Sizing the joint and confining it with hoops in accordance with ACI 318-19 requirements for joints of special moment frames does not preclude the possibility of breakout failure.

17. When designing column-foundation connections with cast-in-place anchors, both beam-column joint shear strength and concrete breakout failure strength should be calculated, with the connection strength taken as the smaller of the two values.

ACKNOWLEDGMENTS

The authors express their gratitude to the ACI Foundation Concrete Research Council, the American Institute of Steel Construction (AISC), and the Hilti Corporation for financing this and other ongoing research projects at UC Berkeley relating to concrete anchorage. Special thanks to Ron Klemencic, chairman and CEO of Magnusson Klemencic Associates, Level 10 Constructions, Cascade Steel, and PJ's Rebar Inc. for donations of materials and manual labor. This study was greatly improved through discussions with the following individuals: Rafael Sabelli (director of seismic design at Walter P. Moore), James Malley (senior principal of Degenkolb Engineers), John Silva (senior director of codes and standards for Hilti North America), Roberto Piccinin (VP for code development and research for Hilti), and Vladimir Červenka and Jan Červenka (director and executive director respectively of Červenka Consulting).

NOTATION

d = member effective depth

d_{max} = aggregate size

f'_c = concrete compressive strength

f_{cm} = concrete compressive strength

f_{cm0} = reference concrete compressive strength equal to 10 MPa

f_t = concrete tensile strength

G_f = fracture energy

G_{f0} = reference fracture energy FIM Model Code 1990

h_{ef} = effective depth of anchor

L_t = crack band width

L_t' = modified crack band width

s_F = shear factor

w_c = crack width after which no normal stress can travel across the crack in ATENA

w_t = crack width

z = horizontal distance between the tensile and compressive resultant forces of a column

β = direction of the plastic flow

γ = crack band orientation factor

γ_{max} = upper limit to crack band orientation factor

ε = total strain

ε_e = elastic strain

ε_f = fracture strain

ε_p = plastic strain

θ = crack angle taken as the minimum average angle between the crack and the sides of the element $\theta \in 0$, 45.

ρ_{tr} = shear reinforcement ratio

REFERENCES

ACI 318, 2019, Building Code Requirements for Structural Concrete (ACI 318-19) and Commentary (ACI 318R-19), American Concrete Institute, Farmington Hills, MI, 624 pp.

Bazant, Z.P., Oh, B.H., 1983, Crack band theory for fracture of concrete. Materials and Structures, RILEM 16 (3), 155–177.

Bruckner, M. (2007), Anwendung von Ankerstäben in Rahmenecken, Rahmenendknoten und Stütze-Fundament-Verbindungen (Use of tie rods in frame corners, frame end nodes and column-foundation connections), Doctoral thesis, University of Stuttgart, 2007.

Caltrans, 2016. Memo to Designers (MTD) 20-7, Seismic Design of Slab Bridges, California Department of Transportation, Sacramento, CA.

Červenka, V., Pukl, R., Ožbolt, J., and Eligehausen, R., 1995, Mesh Sensitivity Effects in Smeared Finite Element Analysis of Concrete Fracture, Fracture Mechanics of Concrete Structures, Proceedings FRAMCOS-2, EADIFICATIO Publishers, D-79104 Freiburg, p.1387-1396

Červenka, J., Červenka, V., Laserna S., 2018, On crack band model in finite element analysis of concrete fracture in engineering practice, Engineering Fracture Mechanics 197 (2018), p. 27-47

Červenka J, Papanikolaou V.K., 2008, Three-dimensional combined fracture-plastic material model for concrete. Int. J. Plast. 2008; 24:2192–220. doi:10.1016/j.ijplas. 2008.01.004.

Chicchi, R., Varma, A. H., Seo, J., Bradt, T., & McCarty, E., 2020, "Experimental testing of tension-loaded deformed anchors in concrete," ACI Structural Journal, 117(5), 133-146.

Eligehausen, R., Mallée, R., and Silva, J. F., 2006, "Anchorage in Concrete Construction," Berlin: Ernst and Sohn.

European Committee for Standardization, 2018, EN 1992-4:2018, "Design of concrete structures. Design of fastenings for use in concrete", Brussels, European Committee for Standardization.

FIB Bulletin 65: Model Code 2010, Final draft – Volume 1, Lausanne, Switzerland, March 2012, ISBN 978-2-88394-105-2, p. 350

FIB Bulletin 213/214: Model Code 90, Lausanne, Switzerland, 1993, ISBN 978-0-7277-1696-5, p. 460

Fuchs, W.; Eligehausen, R.; and Breen, J., 1995, Concrete Capacity Design (CCD) Approach for Fastening to Concrete, ACI Structural Journal, V. 92, No. 1, Jan.-Feb., pp. 73-94.

Gaspar, D. and Moehle, J., 2021, Comparative Study of Punching Shear and Concrete Breakout, ACI Structural Journal, V. 118, No. 2, March 2021, pp. 183-192.

Hordijk, D.A., 1991, Local approach to fatigue of concrete, PhD Thesis, Delft University of Technology, 1991.The Netherlands.

Kupfer H, Munger F, Kunz J, Jahring A., 2003, Hauptaufsatze-Nachtraglich verankerte gerade Bewehrungsstabe bei Rahmenknoten (Anchorage of post installed straight bars for frame node connections), Bauingenieur. Berlin: Julius Springer [1920]- 1997.; 2003;78(1):24–37.

Menetrey, Ph., and Willam, K.J., 1995, Triaxial failure criterion for concrete and its generalization, ACI Structural Journal, 92 (3), pp. 311-318.

Nilforoush, R., Nilsson, M., and Elfgren, L., 2018, Experimental Evaluation of Influence of Member Thickness, Anchor-Head Size, and Orthogonal Surface Reinforcement on the Tensile Capacity of Headed Anchors in Uncracked Concrete. ASCE Journal of Structural Engineering, January 2018, p. 14 DOI: 10.1061/(ASCE)ST.1943-541X.0001976

Ninĉević, K., Czernuschka, L., Marcon, M., and Wan-Wendner, R., 2019, Age and Cure Dependence of Concrete Cone Capacity in Tension, ACI Structural Journal, V. 116, No. 4, pp. 1-10.

Papadopoulos, V., Murcia-Delso, J., Benson Shing, P., 2018, Development of Headed Bars in Slab-Column Joints of Reinforced Concrete Slab Bridges. ACI-Structural Journal, V. 115, No. 5, September 2018, p. 1393-1406.

Sharma, A., Eligehausen, R., and Asmus, J., 2017a, Comprehensive analytical model for anchorages with supplementary reinforcement, Proceedings 3rd International Symposium on Connections between Steel and Concrete (ConSC 2017) September 27-29, Stuttgart, p. 253-265

Sharma, A., Eligehausen, R., Asmus, J., 2017b, Comprehensive experimental investigations on anchorages with supplementary reinforcement, Proceedings 3rd International Symposium on Connections between Steel and Concrete (ConSC 2017) September 27-29, Stuttgart, p. 242-252

Simões, J., Bujnak J., Fernández Ruiz, M., Muttoni, A., 2016, Punching shear tests on compact footings with uniform soil pressure, Structural Concrete

Worsfold, B., Moehle, J., and Silva, J., 2022, Moment transfer at column-foundation connections: physical tests, ACI-Structural Journal, V. 119, No. 5, September 2022

Worsfold, B. and Moehle, J., 2019, Laboratory Tests of Column-Foundation Moment Transfer Connections with Headed Anchors, Structural Engineering, Mechanics, and Materials (SEMM) Report, University of California, Berkeley, UCB/SEMM-2019/01, 171 pp.

Worsfold, B. and Moehle, J., 2022, Laboratory Tests of Column-Foundation Moment Transfer Connections with Shear Reinforcement, Structural Engineering, Mechanics, and Materials (SEMM) Report, University of California, Berkeley, UCB/SEMM-2022/01, 243 pp.

CHAPTER 4 - SHEAR-REINFORCED CONCRETE BREAKOUT DESIGN METHODOLOGY FOR MOMENT TRANSFER AT COLUMN-FOUNDATION CONNECTIONS[4]

by Benjamin L. Worsfold and Jack P. Moehle

ABSTRACT

Recent studies have shown that the strength of column-foundation connections carrying moment can be limited by the concrete breakout failure mode. Distributed shear reinforcement in the concrete breakout cone region has been observed to increase the strength and displacement capacity of structural connections governed by breakout. However, the ACI 318-19 building code does not allow designers to consider this strength increase. Rather, the code allows the use of anchor reinforcement provided that the concrete contribution to strength is ignored. This paper proposes a design methodology to calculate the breakout strength considering the additive effect of concrete and reinforcement. Physical test data and finite element simulations from previous studies were used to calibrate the proposed strength equations. Detailing requirements are discussed.

Keywords: anchoring to concrete; anchor reinforcement; breakout; column-foundation connection; finite element modeling; shear reinforcement; supplementary reinforcement

INTRODUCTION

Previous physical tests [1] [2] [3] [6] [15] [17] [18] have demonstrated that the strength of column-foundation connections with moment transfer can be limited by brittle concrete breakout failure. While this failure mode is identified in ACI 318-19 [12] and the Eurocode EN 1992-4 [13], it is not routinely checked in many design offices. Physical tests and finite element (FE) simulations [4 -5] [7-11] [19] [20] have shown that strategically placed reinforcement can increase the strength and displacement capacity of anchor groups. The codes permit the use of so-called anchor reinforcement (ACI 318-19) or supplementary reinforcement (Eurocode EN 1992-4) to transfer forces from the anchors to the receiving member. However, when using these provisions, the strength of the concrete must be omitted. Neither

[4] Originally published as part of *Engineering Structures*, V. 283, article id. 115783, May 2023, DOI: 10.1016/j.engstruct.2023.115783.

code includes a methodology that would allow designers to combine the strength of the reinforcing bars and the concrete.

This paper describes a selection of previous physical tests and FE simulations of steel-column-to-concrete-foundation moment connections with cast-in-place anchors strengthened with a grid of distributed shear reinforcement. This data set is used to calibrate a design methodology that specifies a grid of uniformly distributed reinforcement around the tension anchors and calculates breakout strength as the sum of strengths provided by the concrete and the distributed reinforcement. Detailing recommendations are discussed.

LITERATURE REVIEW

Sharma et al. [9] [10] report tests performed on 2x2 anchor groups welded to a common plate under tensile loads with additional reinforcement placed parallel to the anchors. The peak anchor force and displacement capacity increased even though the reinforcement was not sized to carry the full anchor force. A design model was developed that combines the strength of the concrete and the reinforcement. This detailed model considers yielding of the reinforcement, bond failure, strut crushing, and pryout failure. Similar models have been proposed by other researchers [11] [21].

Papadopoulos et al. [8] investigated headed reinforcing bars in column-slab connections for bridges through physical tests and finite element simulations. They demonstrated that shear reinforcement in the form of "J-bars" inside the joint and stirrups outside the joint prevented breakout failure. These results led to detailing recommendations adopted by Caltrans in MTD 20-7 (Caltrans 2016 [14]).

Mahrenholtz et al. [6] proposed modification factors to the ACI 318 breakout strength equations based on 16 full-scale column-foundation connection specimens and analytical simulations. Two modification factors were proposed to consider 1) the degradation due to cyclic loading and 2) the beneficial effect of the column flexural compressive force, which constrains the formation of the potential breakout cone (as proposed by Herzog [15]).

CONCRETE BREAKOUT AND REINFORCEMENT IN CURRENT BUILDING CODES

The ACI 318-19 [12] and the Eurocode EN 1992-4 [13] describe methods to calculate the strength of the concrete breakout failure derived from the Concrete Capacity Design (CCD) method developed by Fuchs et al. (1995) [16]. In ACI 318-19, the nominal breakout strength is given by:

$$N_{cbg} = \frac{A_{Nc}}{A_{Nco}} \; \psi_{ec,N} \, \psi_{ed,N} \, \psi_{c,N} \, \psi_{cp,N} \, N_b \qquad (17)$$

where A_{Nc}/A_{Nco} = projected concrete failure area for the anchor group divided by the reference projected area of a single anchor, $\Psi_{ec,N}$ = eccentricity factor, $\Psi_{ed,N}$ = edge factor, $\Psi_{c,N}$ = cracking factor, $\Psi_{cp,N}$ = splitting factor, and N_b = the 5% fractile basic concrete breakout strength of a single anchor.

The ACI 318-19 building code recognizes two ways anchors can benefit from reinforcement. The Code defines the concept of anchor reinforcement (see Figure 1) as that which is used to transfer the full anchor design force into the structural member. The concrete strength is ignored. The bars must be developed on both sides of the potential failure cone. The Code also defines the separate concept of supplementary reinforcement as that which is configured and placed similarly to anchor reinforcement but is not designed to carry the full anchor force. In this case, the reinforcement strength is ignored, requiring the concrete to carry the full anchor force with a slight increase to the strength reduction factor. Neither the anchor reinforcement nor the supplementary reinforcement concepts allow designers to combine the strength contributions from the concrete and reinforcement.

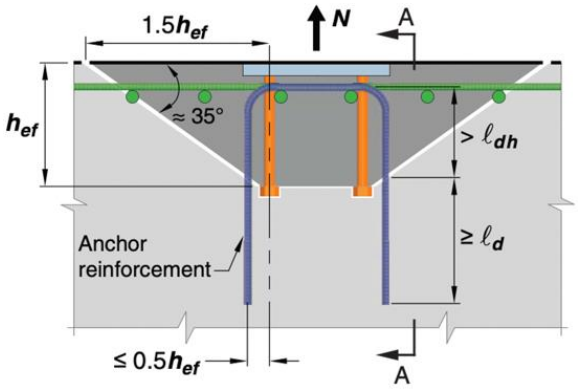

Figure 1. Example of anchor reinforcement for tension from ACI 318-19 [12]

For column-to-foundation connections transferring moment, the flexural compressive force resultant from the column may fall within the potential breakout failure cone and it may thereby constrain the development of the failure cone. This effect has been observed to increase breakout strength ([1] [4] [5] [6] [15]). Eurocode EN 1992-4 accounts for this effect by incorporating a breakout modification factor:

$$\Psi_M = 2 - \frac{z}{1.5\ h_{ef}} \geq 1.0 \tag{18}$$

where z is the distance between the tensile and compressive resultants of the column and h_{ef} is the effective depth of the anchors. This effect is not considered in ACI 318-19.

PREVIOUS PHYSICAL TESTS

In a previous paper [1], the authors describe how two full-scale column-foundation connections were tested to investigate the effect of shear reinforcement on the concrete breakout failure mode [2] [3]. A summary of the test results is presented below. The specimens consisted of a steel wide-flange column with a base plate attached to a foundation through groups of cast-in anchor bolts (see Figure 2). The foundation was simply supported on two concrete blocks near the east and west ends and prestressed to the laboratory floor. Specimen M01 had no shear reinforcement, while specimen M02 included a grid of #4@8in. [⌀12@203mm] shear reinforcement. These bars, sometimes called "candy cane" bars, hung from the top reinforcement mat with 180° hooks and had heads on the bottom. The shear reinforcement to the west of the column extended to about $1.5h_{ef}$ from the anchors, while the shear reinforcement to the east extended to about $0.75h_{ef}$. The column was subjected to quasi-static reversed cyclic lateral loading. Axial load was limited to self-weight. Additional details can be found in the previous paper [1] and test reports [2] [3].

Figure 3 shows the relationship between the anchor group force and the column drift ratio. The peak anchor force in the shear-reinforced specimen M02 is about twice that of the unreinforced specimen M01. The displacement capacity of specimen M02 is about three times that of specimen M01. The west anchor group on the side of specimen M02 with a larger reinforced region displayed a larger displacement capacity without force degradation. Figure 4 shows the crack patterns in cross section and plan view for reinforced specimen M02. Both anchor groups presented a primary failure cone with the vertex located at the anchor head and a larger secondary failure cone encompassing additional rows of shear reinforcement. Note that the primary failure cone governed for the west anchor group with a larger reinforced region, while the secondary cone governed for the east anchor group with a smaller reinforced region. This suggests that secondary failure cones can govern and must be considered in design.

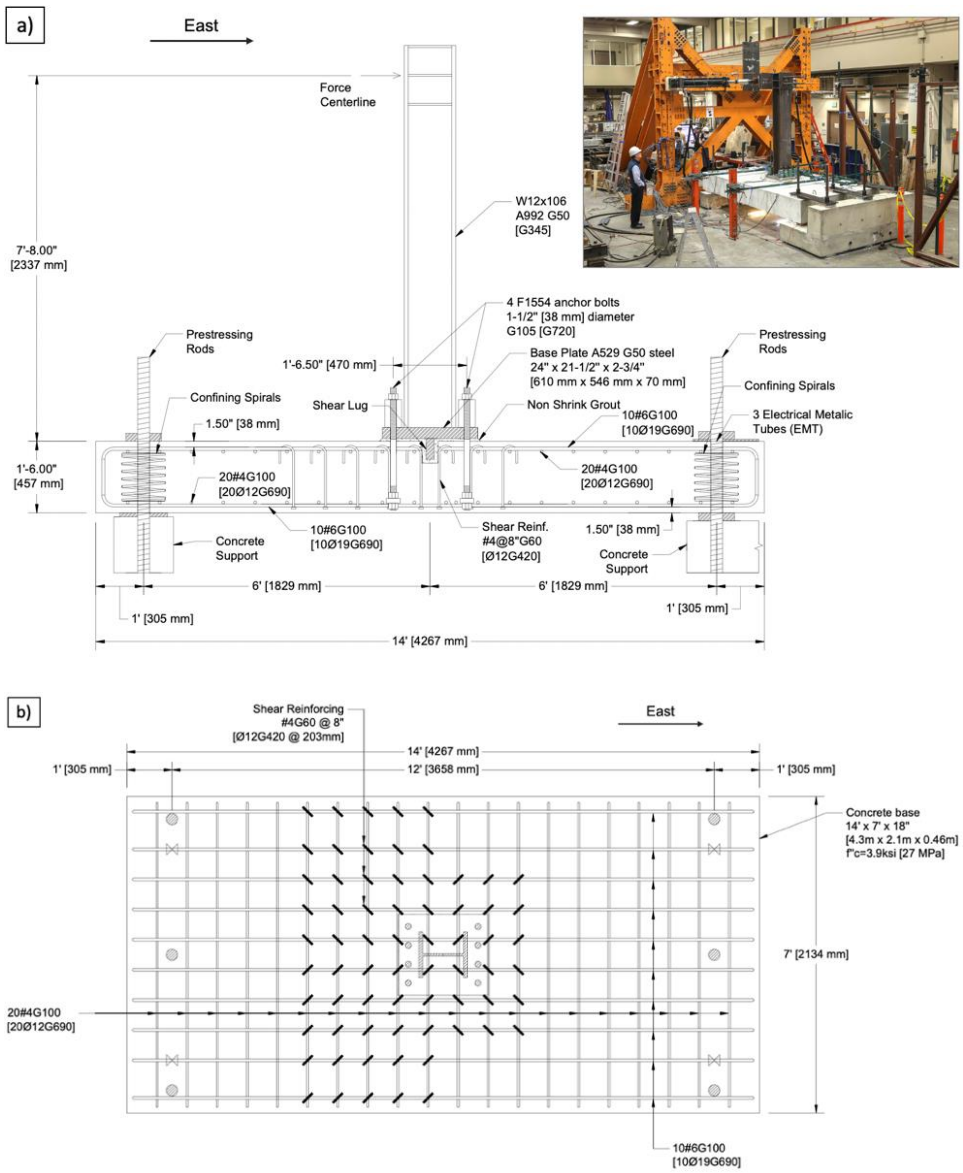

Figure 2. Elevation (a) and plan view (b) of test specimen M02; photo inset of test setup [1]

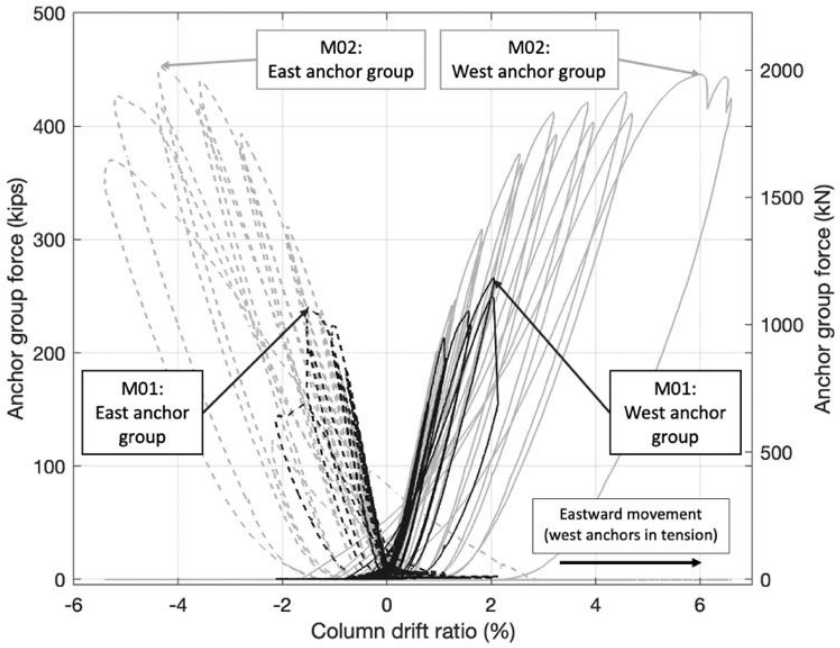

Figure 3. Anchor group force versus column drift ratio for specimens M01 and M02 [1]

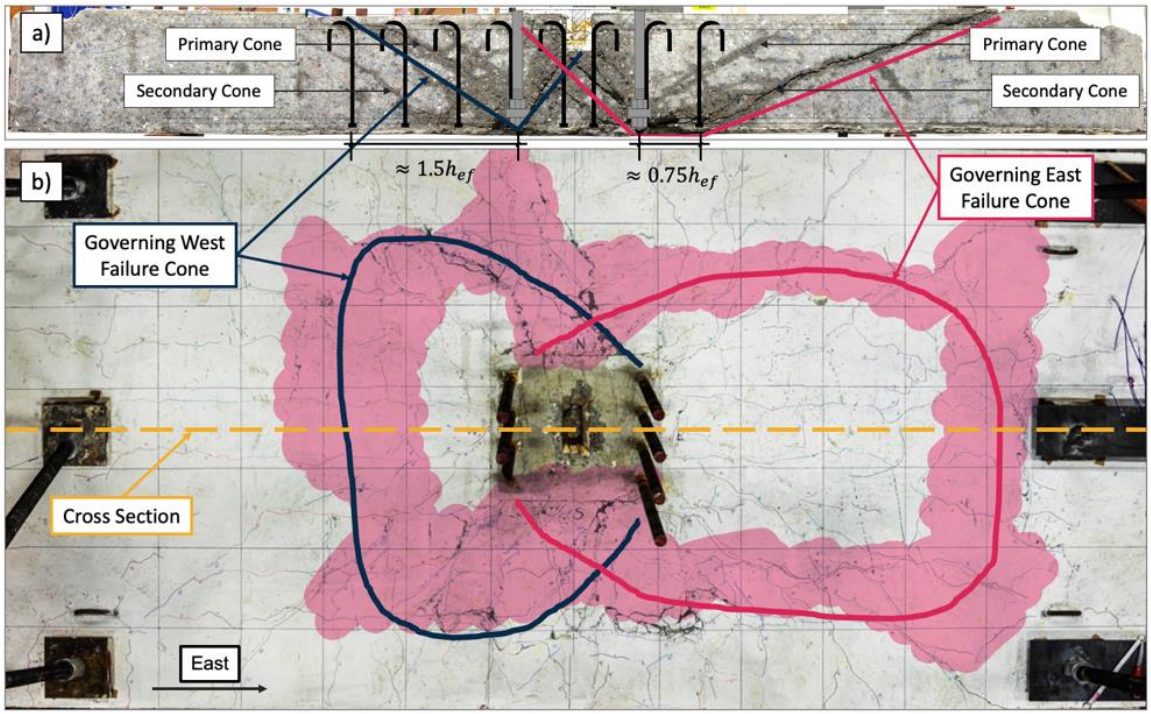

Figure 4. Specimen M02 crack patterns in (a) cross section and (b) plan view highlighting the breakout cones. The shaded region produced a hollow sound when tapped. [1]

PREVIOUS FINITE ELEMENT SIMULATIONS

In a previous paper [4], the authors used physical test data of single anchors and anchor groups loaded either axially or in moment to calibrate 3D finite element (FE) models with the software ATENA and perform parametric studies. The modeling approach is summarized in Table 3. See Worsfold and Moehle (2022b) for calibration and validation details. A subset of the models is selected and summarized in

Table 5 for further discussion.

Table 4–Select FE modeling parameters for headed anchors with ATENA [4]

Model Property	Notes
Anchor	3D solid-elastic steel only fixed to the concrete at the bearing surface
Mesh size	d_{max} < mesh size < h_{ef} / 5
Stop analysis	End analysis once failure cone has formed and cracks approach w_c.
Rotated crack	0.80
Fracture Energy (G_f)	FIB Model Code 1990
Elements	8-node hexahedra
Integration scheme	2 x 2
Minimum crack band	1.5 to 2.5 d_{max}

Table 5. Finite element model selections

Model Number	h_{ef}		Rebar size		s (in.)		ρ_{tr} (%)	Peak anchor force		Notes
	(in.)	(mm)	(psi)	(SI)	(in.)	(mm)		(kip)	(kN)	
154	14.3	360	NA	NA	NA	NA	0.00	259	1150	
156	14.3	360	3	10	8	203	0.17	353	1570	
157	14.3	360	3	10	6	152	0.31	394	1750	
190	14.3	360	4	13	8	203	0.31	387	1720	Study on size of reinfroced region
191	14.3	360	4	13	8	203	0.31	408	1820	
155	14.3	360	4	13	8	203	0.31	389	1730	Base models
153	14.3	360	4	13	8	203	0.31	392	1740	
179	14.3	360	4	13	8	203	0.31	374	1660	Elastoplastic shear reinfrocement
181	14.3	360	4	13	8	203	0.31	392	1740	
184	14.3	360	4	13	8	203	0.31	399	1770	Finer mesh
186	14.3	360	4	13	8	203	0.31	388	1730	
193	14.3	360	4	13	6.75	171	0.44	414	1840	
158	14.3	360	4	13	6	152	0.56	443	1970	
194	14.3	360	5	16	6.75	171	0.68	453	2020	
204	23.3	590	NA	NA	NA	NA	0.00	522	2320	
225	23.3	590	3	10	11.5	292	0.08	593	2640	
212	23.3	590	3	10	8	203	0.17	660	2930	
205	23.3	590	4	13	8	203	0.31	746	3320	
206	23.3	590	5	16	8	203	0.48	770	3430	
201	32.3	820	NA	NA	NA	NA	0.00	730	3250	
226	32.3	820	3	10	16	406	0.04	765	3410	
213	32.3	820	3	10	8	203	0.17	868	3860	
200	32.3	820	4	13	8	203	0.31	925	4110	
203	32.3	820	5	16	6.75	171	0.68	986	4390	

A previous study on the size of the shear-reinforce region is summarized below [4]. Figure 5 plots the peak anchor force (P) divided by the strength of the unreinforced case (P_0) for test specimen M02 and for multiple FE models increasing the size of the shear-reinforced region. Two shear reinforcing ratios are considered ($\rho_{tr} = 0.11in^2/(8in)^2 * 100 = 0.17\%$ and $\rho_{tr} = 0.20in^2/(8in)^2 * 100 = 0.31\%$). The FE

results suggest that each successive increase to the size of the shear-reinforced region results in a smaller increase to the peak anchor force. Physical specimen M02 showed no effect on peak strength from bars located beyond about 0.75 h_{ef} while the FE models showed a minor increase.

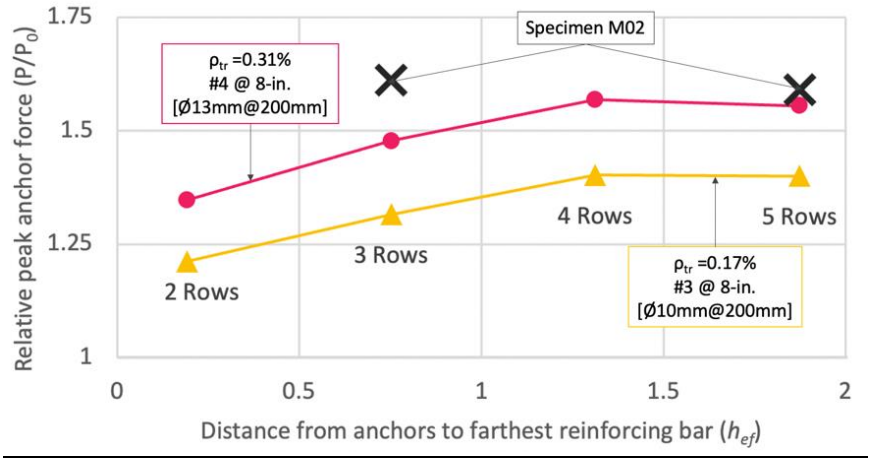

Figure 5. Peak measured anchor force (P) relative to that of the unreinforced case (P_0) versus the size of the shear-reinforced region [4]

SHEAR-REINFORCED BREAKOUT STRENGTH

In general, if an axially loaded anchor group is placed within a grid of distributed shear reinforcement, Figure 6(a) qualitatively sketches the expected stress distribution in the bars. The bell-shaped stress distribution can be substituted for a rectangular form of equal force supposing uniform yield stress. This rectangular region can be called the effective area (A_{eff}) of the anchor group. The increase in anchor force due to the presence of distributed shear reinforcement (N_s) can be calculated as:

$$N_s = A_{eff}\, \rho_{tr}\, f_{yt} \tag{19}$$

where ρ_{tr} is the shear reinforcing ratio and f_{yt} is the nominal yield stress.

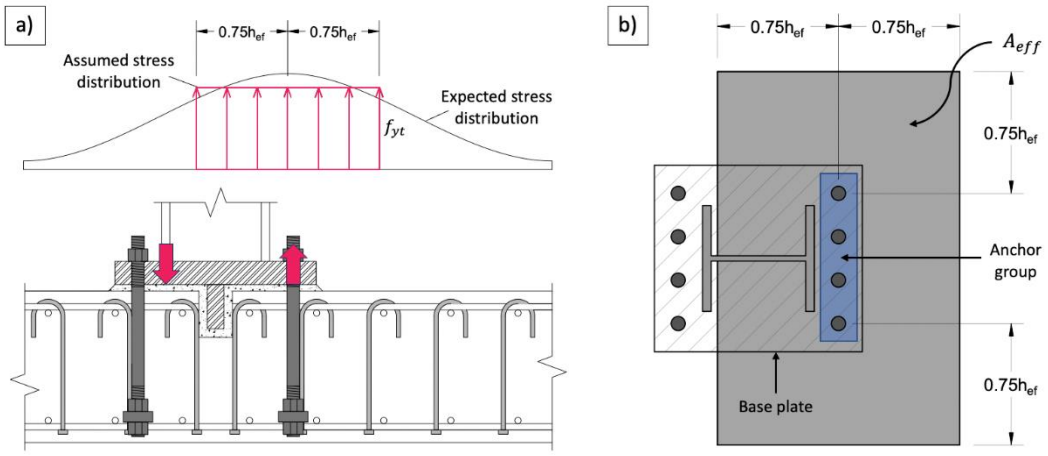

Figure 6. (a) Expected and assumed stress distributions in the shear reinforcement near the tension-loaded anchor group of a column-foundation connection, (b) effective area example

For the experimental data, the increase in anchor force due to the presence of shear reinforcement (N_s) can be calculated by taking the peak measured force and subtracting the strength of the corresponding unreinforced specimen ($P - P_0$). Section 0 described how the peak anchor force mainly depends on the reinforcing bars located near the anchors within about $0.75h_{ef}$. Figure 7 plots the increase in peak anchor force versus the area of shear reinforcement within the effective area assumed to extend $0.75h_{ef}$ from the anchors in both orthogonal directions (see example in Figure 6(b)). Twenty-four FE models with different shear reinforcing ratios and slab thicknesses from Worsfold and Moehle (2022b) [4] are included as well as four data points from physical tests from Worsfold and Moehle (2022a) [1]. Relatively small amounts of reinforcement result in notable strength gain. As the area of shear reinforcement increases, the strength reaches a plateau, suggesting an upper limit to the benefit of shear reinforcement. FE models with relatively high shear reinforcement exhibit damage patterns suggesting joint shear failure.

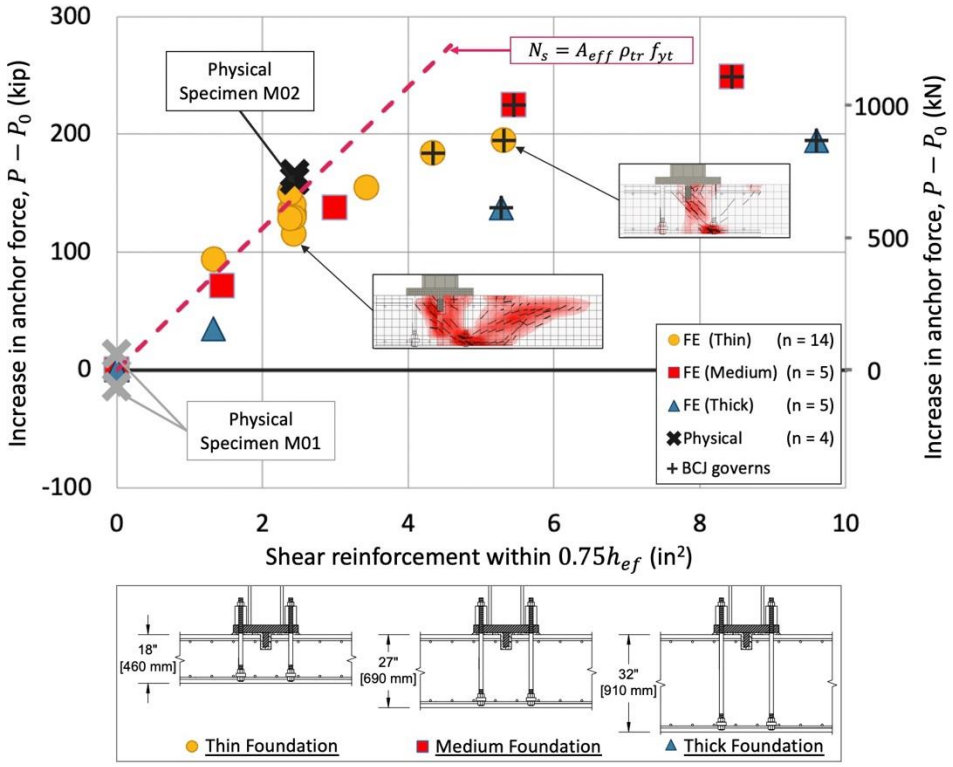

Figure 7. Increase in anchor force relative to the unreinforced case ($P - P_0$) versus area of shear reinforcement within $0.75h_{ef}$; select crack patterns are shown; black crosses overlay specimens governed by beam-column joint (BCJ) strength

Figure 8 plots the strength ratio (N_{test}/N_n) for the data points in Figure 7. Note that most data points come from calibrated FE models [4]. Figure 8(a) assumes the nominal anchor group capacity (N_n) equal to the nominal concrete breakout strength per ACI 318-19 (5% fractile) assuming uncracked concrete (N_c), which can be calculated with Equation (17) using $\Psi_{c,N} = 1.25$. For the data points representing the condition without shear reinforcement, the average strength ratio is about 1.75. Conservatism increases as shear reinforcement is added such that some data points exceed a strength ratio of 3.0. Models with thicker foundations and proportionally deeper anchors (see drawing in Figure 7) tend towards lower strength ratios. The ACI breakout strength equations are calibrated to a 5% fractile value which is not consistent with other nominal strength models calibrated to mean values. To convert the 5% fractile to a mean value, one may assume measured strengths follow a normal distribution with a coefficient of variation of 0.15 [16].

$$\frac{1}{1 + z_{0.05} * CV} = \frac{1}{1 + (-1.645) * 0.15} = 1.33 \tag{20}$$

Figure 8(b) shows how conservatism is reduced by considering the mean concrete strength. Conservatism increases with increasing shear reinforcing ratio.

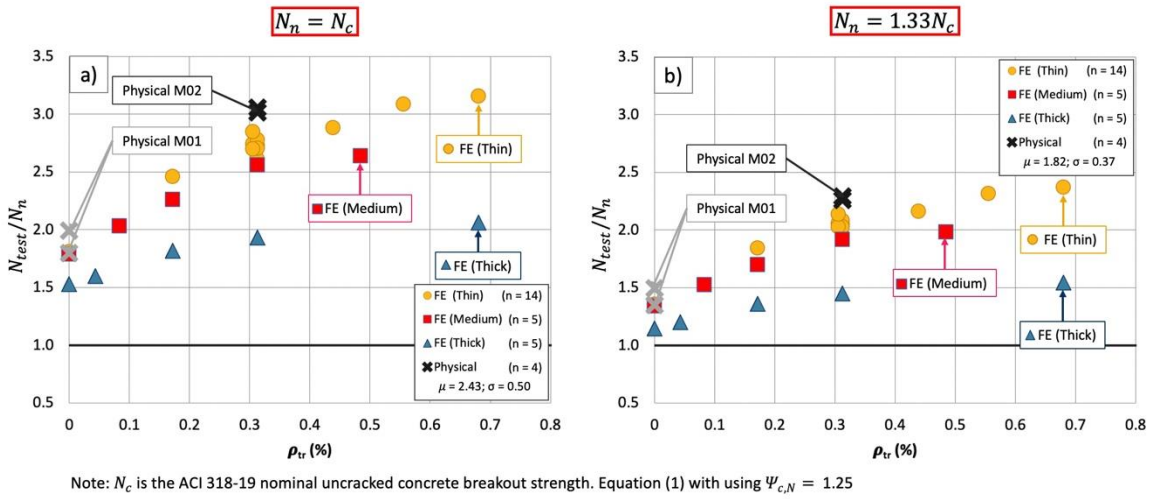

Note: N_c is the ACI 318-19 nominal uncracked concrete breakout strength. Equation (1) with using $\Psi_{c,N} = 1.25$

Figure 8. Strength ratio versus shear reinforcing ratio where the nominal strength (N_n) is taken as (a) the 5% fractile strength and (b) the mean strength

The nominal strength of the shear-reinforced concrete breakout failure mode $(N_{n,SRB})$ can be calculated by adding the mean concrete and reinforcement terms:

$$N_{n,SRB} = 1.33N_c + N_s \tag{21}$$

For the same data points as Figure 8, the strength ratio (N_{test}/N_n) using Equation (21) is shown in Figure 9(a). The downward trend indicates that for higher ρ_{tr}, this equation overestimates the strength. Many FE models with higher ρ_{tr} did not exhibit a breakout cone but rather a damage pattern indicative of joint shear failure. Figure 9(b) plots the strength ratio where the nominal strength is calculated as the minimum of that obtained with Equation (21) and the anchor group force present at nominal beam-column joint (BCJ) failure (N_{BCJ}). The BJC strength is calculated per ACI 318-19 Section 18.8.4.3 assuming a joint strength coefficient of 15 [1.2 SI] (assuming discontinuous column, continuous beam, and confinement by transverse beams). In general, the nominal BCJ strengths may not represent mean predictors. The strength calculations from Chapter 18 may be below the mean to account for nonlinear behavior. In Figure 9(b), data points where beam-column joint strength governs are overlaid with a black cross. This approach produces a relatively uniform strength ratio distribution across the range of tested ρ_{tr} with an average value of 1.19, suggesting this approach adequately describes the transition from concrete breakout failure

to joint shear failure. The FE crack patterns transition from a clean breakout failure to a clean joint shear failure, with intermediate models showing a combination of both failure modes.

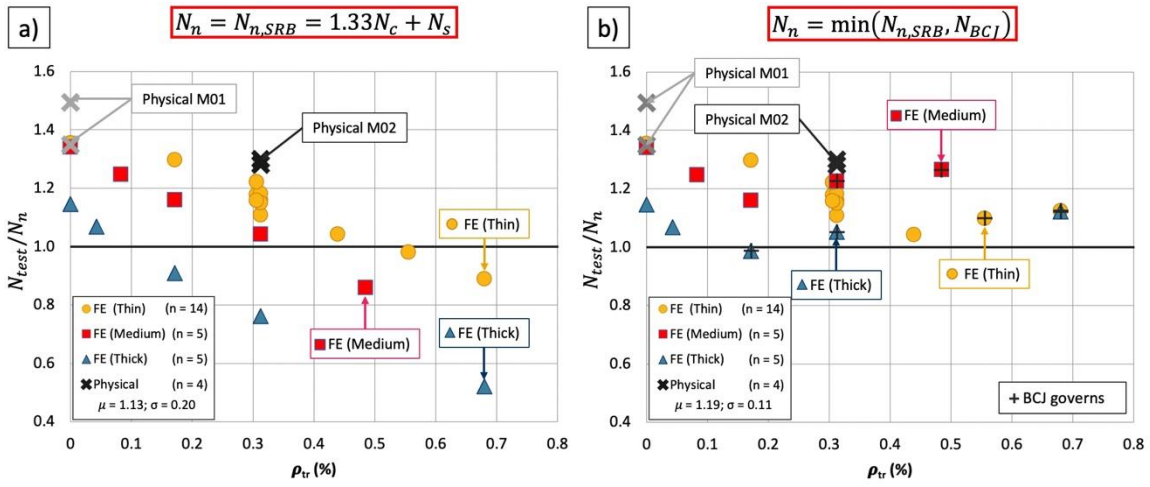

Figure 9. Strength ratio versus shear reinforcing ratio where the nominal anchor strength (N_n) is calculated as per (a) Equation (21) or (b) the minimum of Equation (21) and BCJ strength (N_{BCJ})

Including the Eurocode modification factor that considers the beneficial effect of the base plate compressive force for a connection transferring moment, Equation (21) becomes:

$$N_{n,SRB\Psi_M} = 1.33\Psi_M N_c + N_s \tag{22}$$

Figure 10(a) plots the strength ratio (N_{test}/N_n) for Equation (22). Including the Ψ_M factor increases the breakout strength of all data points, especially for those with thicker foundations ($\Psi_M = 1.08$ for "thin" slabs, $\Psi_M = 1.46$ for "medium" slabs, and $\Psi_M = 1.63$ for "thick" slabs). Figure 10(b) shows that increasing the breakout capacity causes a larger proportion of data points to be governed by BCJ strength. When considering BCJ strength, including Ψ_M reduces the average strength ratio from 1.19 to 1.12.

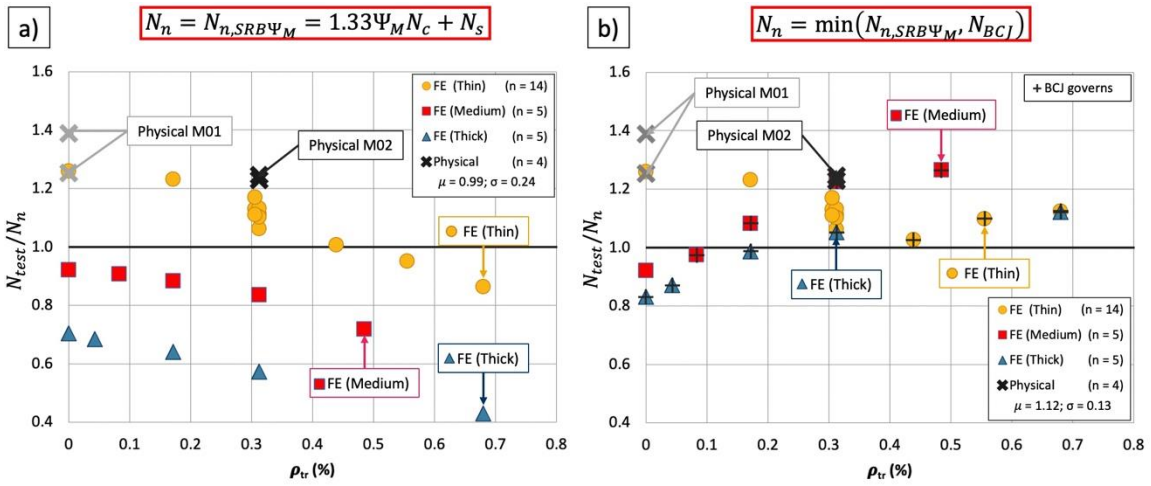

Figure 10. Strength ratio versus shear reinforcing ratio where the nominal anchor strength (N_n) is calculated as per (a) Equation (22) or (b) the minimum of Equation (22) and BCJ strength (N_{BCJ})

SECONDARY BREAKOUT FAILURE CONE

When shear reinforcement is placed around an anchor group, physical tests [1] and simulations [4] have revealed the potential for a secondary failure cone outside the reinforced region, as seen in Figure 4. If all other variables remain constant, the strength of the secondary cone (N_n^S) can be calculated from the strength of the primary cone (N_c) as:

$$N_n^S = 1.33 N_c \frac{A_{Nc}^S}{A_{Nc}^P} \tag{23}$$

where A_{Nc}^P and A_{Nc}^S are the projected failure areas for the primary and secondary cones, respectively. Generally, it is preferable that the reinforced region be large enough such that the secondary cone does not govern, as it is likely to be more brittle than the shear-reinforced primary cone. In specimen M02, the secondary failure cone governed for the east anchor group located in the smaller shear-reinforced region (see Figure 4). The primary cone exhibited a larger displacement capacity than the secondary cone. Using Equation (23), the secondary breakout cone strength would be expected to be 1.71 times that of the primary cone, which matches the measured value of 1.72. The calculated strength of the breakout cone beyond the shear reinforcement for the larger reinforced region is about 3.14 times the primary cone strength and was not observed in specimen M02.

DISCUSSION

Concrete breakout failure may limit the moment capacity of column-foundation connections with cast-in-place anchors. Physical tests and simulations have shown that distributed shear reinforcement in the potential breakout cone region can strengthen the connection and increase the displacement capacity. Figure 11 shows three failure modes that should be considered in design: 1) shear-reinforced breakout ($N_{n,SRB}$), 2) joint shear failure (N_{BJC}), and 3) secondary breakout failure outside the shear-reinforced region (N_n^S).

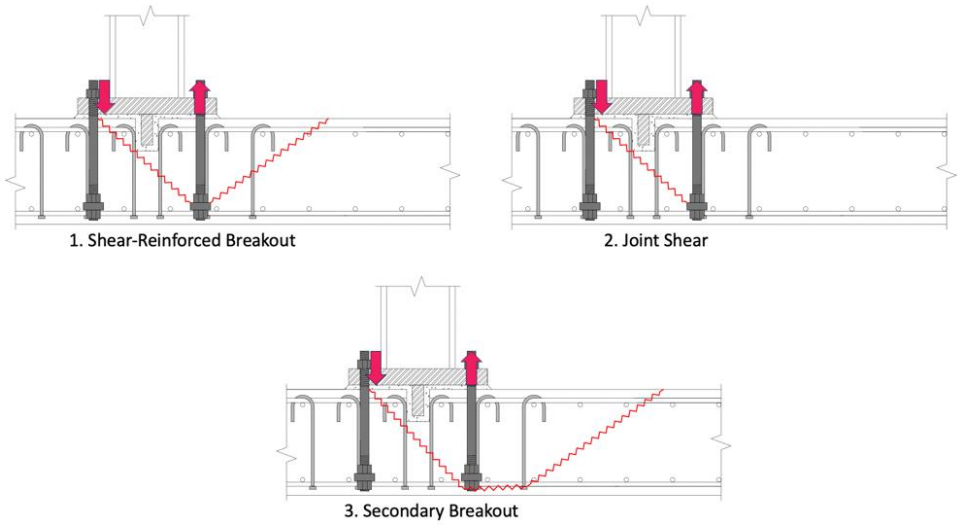

Figure 11. Possible concrete failure modes for shear-reinforced column-foundation connections

The nominal shear-reinforced breakout strength ($N_{n,SRB}$) can be calculated with Equations (19) and (21). Designers will be familiar with the form of this equation as it is analogous to current one-way shear provisions. The additive force terms allow for independent calibration of the concrete and reinforcement terms as opposed to a multiplicative model. The proposed reinforcement term (N_s) is based on a physical model assuming the yielding of shear reinforcement in an effective area (A_{eff}) around the anchor group (see Figure 6). Making N_s dependent on the effective area (instead of only on the reinforcing ratio ρ_{tr}) considers that deeper anchors will have larger failure cones and will be able to engage a larger number of reinforcing bars. As shown in Figure 5, physical tests and FE results suggest extending the shear-reinforced region to at least $0.75h_{ef}$ from the anchors to maximize the anchor force for a given reinforcing ratio. Figure 7 compares the proposed N_s equation with FE results and physical tests. In practice, the shear-reinforced region should extend beyond the effective area because the bars outside this region contribute to the connection strength and displacement capacity.

A secondary breakout cone outside the shear-reinforced region may govern. It is preferable that the reinforced region be large enough such that the secondary cone does not govern since it is likely more brittle than the shear-reinforced primary cone. The strength of the secondary cone may be calculated with Equation (23). If all other variables remain constant, this method only requires calculating projected cone areas. For typical connections, extending the shear reinforced region at least $1.5h_{ef}$ from the anchors may be adequate.

The data points in Figure 9 with black crosses are governed by beam-column joint (BCJ) strength and, as breakout failure did not govern, are overpredicted by Equation (21). This observation suggests that, in design, BCJ strength must be checked for column-foundation connections transferring moment. The relatively uniform strength ratio across the range of tested ρ_{tr} suggests this approach adequately describes the transition from breakout failure to joint shear failure. The average strength ratio is 1.19, with a standard deviation of 0.11 (see Figure 9(b)). Including the Eurocode flexural compressive force factor (Ψ_M) reduces the average strength ratio from 1.19 to 1.12 while the standard deviation increases from 0.11 to 0.13.

Previous researchers have observed that a steep breakout cone that does not engage shear reinforcement may control if the bar spacing is large [11]. Steep breakout cones were not observed in the current study, where the maximum spacing was about $0.5h_{ef}$. This spacing ensures that multiple bars will cross the assumed 1:1.5 plane of the primary failure cone. Limiting the maximum bar spacing in terms of h_{ef} limits the possible steep cone angles. Closely spaced, uniformly distributed bars may inhibit the formation of steep breakout cones if the spacing is sufficiently small, thereby simplifying design.

Shear reinforcement in specimen M02 yielded even though the length on each side of the failure cone was less than the code-specified development length, as would be required for ACI 318 anchor reinforcement. This shear reinforcement engaged the longitudinal bars with a standard hook at one end and a head at the other. This suggests that shear reinforcement used to strengthen concrete breakout failures may be effective if it engages longitudinal reinforcement at both ends. This approach would be analogous to the current code treatment of stirrup anchorage in ACI 318-19 25.7.1.2 and 25.7.1.3, which does not require explicit development or bond calculations. Alternatively, more detailed approaches may be used for partially developed bars [9] [21].

Previous approaches to calculating breakout strength combining the contributions from the concrete and the reinforcement require precisely arranged reinforcement configurations around the anchors [9] [10] [11] [19] [20] [21]. This approach may be sensitive to construction errors and require careful inspection. The proposed methodology envelops the potential breakout cone within a grid of uniformly distributed reinforcement which may simplify design and construction.

SUMMARY AND CONCLUSIONS

This paper reports on a study of steel-column-to-foundation connections in which the column transfers moment to the foundation. Relevant literature and applicable building code provisions are reviewed. Previous physical tests are reviewed with an emphasis on identifying the potential for concrete breakout failure as well as a method for strengthening the foundation against breakout failure. Finite element models, previously calibrated to physical tests, are used to extrapolate the results of the physical tests to better understand a range of typical conditions that should be considered in design. The results are used to develop a proposal for strengthening foundations against breakout failure by providing a grid of uniformly distributed shear reinforcement that envelopes the potential breakout cone in the foundation.

Based on the study, the following conclusions are made:

1. Breakout failure can limit the strength of a column-foundation connection and should be considered.
2. Uniformly distributed shear reinforcement encompassing the potential breakout cone can increase both the strength and displacement capacity of a column-foundation connection.
3. A design method is proposed by which breakout strength can be calculated as the sum of the concrete and distributed reinforcement contributions. Reinforcement detailing necessary for implementation of the design method is discussed concerning spacing, extent, and development.
4. Breakout failure outside the shear-reinforced region can limit the connection strength if the reinforced region is too small. This secondary breakout should be considered in design.
5. Joint shear strength can limit the moment transfer strength of a connection strengthened with distributed shear reinforcement. Joint failure, therefore, provides an upper limit on the amount of breakout shear reinforcement that is effective.

The authors recommend that ACI 318 consider provisions that would allow designers to account for the beneficial effect of distributed shear reinforcement on the concrete breakout failure mode.

ACKNOWLEDGMENTS

The authors express their gratitude to the ACI Foundation Concrete Research Council, the American Institute of Steel Construction (AISC), and the Hilti Corporation for financing this and other ongoing research projects at UC Berkeley relating to concrete anchorage. This study was greatly improved through discussions with the following individuals: Rafael Sabelli (director of seismic design at Walter P. Moore), James Malley (senior principal of Degenkolb Engineers), John Silva (senior director of codes and standards for Hilti North America), and Roberto Piccinin (VP for code development and research for Hilti).

NOTATION

A_{eff} = effective area for calculation of N_s. The rectangular area extends $0.75h_{ef}$ from the anchor group in both orthogonal directions.

A_{Nc} = projected failure area of a single anchor or an anchor group in question

A_{Nco} = projected concrete failure area of a single anchor if not affected by edges ($9h_{ef}^2$)

A_{Nc}^P = projected concrete failure area for the primary cone

A_{Nc}^S = projected concrete failure area for the secondary cone

CV = coefficient of variation

d_{max} = maximum aggregate size

f_{yt} = nominal yield stress of transverse reinforcement

G_f = fracture energy

h_{ef} = effective depth

N_{BCJ} = anchor group force at nominal beam-column joint failure

N_b = the 5% fractile basic concrete breakout strength of a single anchor

N_c = nominal concrete breakout strength as per ACI 318 (5% fractile) assuming uncracked concrete

N_{cbg} = nominal concrete breakout strength in tension of a group of anchors per ACI 318

N_n = nominal anchor strength

$N_{n,SRB}$ = nominal shear-reinforced breakout strength

$N_{n,SRB\Psi_M}$ = nominal shear-reinforced breakout strength modified by flexural compression factor

N_n^S = nominal secondary concrete breakout cone strength

N_s = reinforcement strength term

N_{test} = peak anchor force in physical test or FE simulation

P = peak measured anchor force

P_0 = peak measured anchor force of unreinforced case

w_c = crack width at which normal stress is zero

z = distance between the tensile and compressive resultants of a column

$z_{0.05}$ = standard normal distribution value for the 5% fractile

ρ_{tr} = shear reinforcing ratio

$\Psi_{ec,N}$ = breakout eccentricity factor

$\Psi_{ed,N}$ = breakout edge effect factor

$\Psi_{c,N}$ = breakout cracking factor

$\Psi_{cp,N}$ = splitting modification for post-installed anchors

Ψ_{M} = breakout flexural compression factor

REFERENCES

[1] Worsfold, B., Moehle, J., and Silva, J., 2022, Moment Transfer at Column-Foundation Connections: Physical Tests, ACI-Structural Journal, V. 119, No. 5, September 2022

[2] Worsfold, B. and Moehle, J., 2019, Laboratory Tests of Column-Foundation Moment Transfer Connections with Headed Anchors, Structural Engineering, Mechanics, and Materials (SEMM) Report, University of California, Berkeley, UCB/SEMM-2019/01, 171 pp.

[3] Worsfold, B. and Moehle, J., 2022a, Laboratory Tests of Column-Foundation Moment Transfer Connections with Shear Reinforcement, Structural Engineering, Mechanics, and Materials (SEMM) Report, University of California, Berkeley, UCB/SEMM-2022/01, 243 pp.

[4] Worsfold, B. and Moehle, J., accepted for publication 2022b, Moment Transfer at Column-to-Footing Connections: Analytical Studies, ACI Structural Journal

[5] Eligehausen, R., Mallée, R., and Silva, J. F., 2006, Anchorage in Concrete Construction, Berlin: Ernst and Sohn.

[6] Mahrenholtz, C., Akguzel, U., Eligehausen, R., and Pampanin, S., 2014, New Design Methodology for Seismic Column-to-Foundation Anchorage Connections, ACI Structural Journal, V. 111, No. 5, Sep.-Oct., 1179-1189 pp.

[7] Nilforoush, R., Nilsson, M., and Elfgren, L. 2018, "Experimental Evaluation of Influence of Member Thickness, Anchor-Head Size, and Orthogonal Surface Reinforcement on the Tensile Capacity of Headed Anchors in Uncracked Concrete," ASCE Journal of Structural Engineering, January 2018, p. 14 DOI: 10.1061/(ASCE)ST.1943-541X.0001976

[8] Papadopoulos, V., Murcia-Delso, J., and Benson Shing, P., 2018, Development of Headed Bars in Slab-Column Joints of Reinforced Concrete Slab Bridges. ACI-Structural Journal, V. 115, No. 5, September 2018, p. 1393-1406.

[9] Sharma, A., Eligehausen, R., and Asmus, J., 2017, Comprehensive analytical model for anchorages with supplementary reinforcement, Proceedings 3rd International Symposium on Connections between Steel and Concrete (ConSC 2017) September 27-29, Stuttgart, p. 253-265

[10] Sharma, A., Eligehausen, R., Asmus, J., 2017, Comprehensive experimental investigations on anchorages with supplementary reinforcement, Proceedings 3rd International Symposium on Connections between Steel and Concrete (ConSC 2017) September 27-29, Stuttgart, p. 242-252

[11] Berger, W., 2015, Load-displacement behavior and design of anchorages with headed studs with and without supplementary reinforcement under tension load, Ph.D. Thesis, Institute of Construction Materials, University of Stuttgart (German).

[12] ACI 318-19, 2019, Building Code Requirements for Structural Concrete (ACI 318-19) and

Commentary (ACI 318R-19), American Concrete Institute, Farmington Hills, MI, 624 pp.

[13] European Committee for Standardization, 2018, EN 1992-4:2018, Design of concrete structures. Design of fastenings for use in concrete, Brussels, European Committee for Standardization.

[14] Caltrans, 2016, Memo to Design MTD (MTD) 20-7, Seismic Design of Slab Bridges, California Department of Transportation, Sacramento, CA.

[15] Herzog, M., 2015, Beitrag zur Vereinheitlichung der Bemessung im Stahlbetonbau und in der Befestigungstechnik (Contribution to the standardization of design in reinforced concrete construction and fastening technology), Stuttgart, Germany: Institut für Werkstoffe im Bauwesen der Universität Stuttgart, 457 pp.

[16] Fuchs, W.; Eligehausen, R.; and Breen, J., 1995, Concrete Capacity Design (CCD) Approach for Fastening to Concrete, ACI Structural Journal, V. 92, No. 1, Jan.-Feb., pp. 73-94.

[17] Mahadik, V., Sharma, A., and Hofmann, J., 2021, Cast-in and Post-Installed Rebar Anchorage Systems in RC Column Foundation Joints: Experimental Investigations, Engineering Structures 238

[18] Hamad, B., Hammoud, R., and Kunz, J., 2006, Evaluation of Bond Strength of Bonded-In or Post-Installed Reinforcement, ACI Structural Journal, V. 103, No. 2, March-April, pp. 207-218.

[19] Bujňák, J., Mecár, J., and Bahleda, F., 2018, Tensile Resistance of an Anchor Plate with Supplementary Reinforcement, Structural Concrete

[20] Ferreira, M., Filho, MP., Lima, N., and Oliveira, M., 2019, Influence of the Flexural and Shear Reinforcement in the Concrete Cone Resistance of Headed Bars, Engineering Structures

[21] Kuhlmann U, Ozbolt A, Hofmann J, Eligehausen R, Berger W, Wald F, et al. New Market Chances for Steel Structures by Innovative Fastening Solutions Between Steel and Concrete (INFASO). Luxembourg; 2012.

CHAPTER 5 - SHEAR-REINFORCED CONCRETE BREAKOUT FAILURE IN AXIALLY LOADED ANCHOR GROUPS[5]

by Benjamin Worsfold, Dara Karać, and Jack Moehle

ABSTRACT

Steel columns are commonly attached to concrete foundations with groups of cast-in-place headed anchors. Recent physical tests and simulations have shown that the strength of these connections can be limited by concrete breakout failure. Four full-scale physical specimens of axially loaded columns attached to a foundation slab were tested, varying the shear reinforcement configuration in the slab. All specimens were governed by concrete breakout failure. The tests suggest that adequately placed distributed shear reinforcement can increase connection strength and displacement capacity. Steep cone failures were observed to limit the beneficial effect of shear reinforcement. Calibrated finite element models were used to investigate critical parameters such as the extent of the shear-reinforced region and bar spacing. A design approach is proposed to calculate connection strength by adding the strength of the concrete and the distributed shear reinforcement. Design detailing is discussed.

Keywords: reinforced concrete; anchoring to concrete; concrete breakout; foundations; shear reinforcement.

INTRODUCTION

The force flow between columns and foundations, as well as associated failure modes, are important considerations for structural design. Under lateral loading due to earthquake or wind effects, columns can experience high tensile forces that must be transferred to the foundation slab. Breakout failure can occur if the tensile force exceeds the local capacity of the foundation slab. The provisions in ACI 318-19 for anchoring to concrete can be useful for addressing concrete breakout failure at column-to-foundation-slab connections. Those provisions, however, ignore the beneficial effect of reinforcement that can be provided near the connection, potentially underestimating the connection breakout strength.

Physical testing and numerical simulations were used to understand potential failure modes and

[5] Planned to be submitted for consideration to be published in the *ACI Structural Journal*.

strengths of breakout failure cones reinforced with distributed shear reinforcement. Four nominally identical steel-column-to-concrete-foundation connections were constructed and tested in the laboratory. The steel column was loaded quasi-statically and monotonically in tension until failure. All specimens failed in a concrete breakout mode. Variations in slab shear reinforcement detailing were introduced to explore their effect on strength and displacement capacity of connections governed by breakout failure. Finite element models were calibrated with the experimental test data and used to investigate critical parameters such as the extent of the shear-reinforced region around the connection, shear reinforcement ratios, and shear reinforcement end anchorages.

The results from physical testing and numerical simulations are compared with results from a design approach proposed by the authors. Reinforcement detailing recommendations are made.

LITERATURE REVIEW

Mahrenholtz et al. (2014) performed physical tests in which monotonic and cyclic loading was applied to 16 full-scale reinforced concrete column-foundation connection specimens. They proposed breakout strength modification factors that consider the strength increase due to column compressive bending stresses and strength drop due to cyclic loading.

Worsfold et al. (2022) investigated the effect of shear reinforcement on anchors with two full-scale tests of interior steel-column-to-concrete-foundation connections with cast-in-place headed anchors. Breakout failure governed for both specimens even though ACI 318-19 commentary suggests the anchorage lengths were large enough to preclude breakout being greater than 2/3 the effective depth of the member. Adding a distributed grid of shear reinforcement in the breakout cone region was observed to increase the breakout strength and displacement capacity.

Sharma et al. (2017) describes a series of physical tests of 2 x 2 anchor groups welded to a common plate under tensile or shear loads where additional reinforcement was included. Relatively small amounts of reinforcement were shown to increase anchor strength and displacement capacity. These tests were used to develop a design model that adds the strength contributions of both concrete and steel (Sharma et al., 2018). This model includes strength limits considering the yielding of supplementary reinforcement, bond failure, strut crushing, and pryout failure.

Papadopoulos et al. (2018) investigated headed reinforcing bars in elevated column-slab connections for bridges through physical testing and finite element simulations. They demonstrated that shear reinforcement in the form of J-bars inside the joint and stirrups outside the joint prevented breakout failure. Additional shear reinforcing bars beyond the first row outside the joint seemed to have no effect. The results led to detailing recommendations adopted by Caltrans in MTD 20-7 (Caltrans, 2016).

RESEARCH SIGNIFICANCE

Full-scale laboratory tests of column-foundation connections with cast-in-place headed anchors focusing on the concrete failure modes are scarce, even though this construction detail is common. Potential failure modes are not well understood. This research provides benchmark physical data. The ACI 318-19 building code does not allow engineers to add the strength contribution of reinforcement to the concrete breakout strength. A previously proposed design approach is evaluated for shear-reinforced breakout strength.

CURRENT ACI PROVISIONS

The ACI 318-19 provisions for calculating concrete breakout capacity originated from the Concrete Capacity Design (CCD) method proposed by Fuchs (1995) based on physical test data. Breakout cones are characterized by cracks initiating at the anchor bearing surfaces and propagating towards the concrete surface at an angle of about 1.5:1 from the horizontal. The breakout capacity for a group of anchors located away from free edges and subjected to concentric tension is given by:

$$N_{cbg} = \frac{A_{Nc}}{A_{Nco}} \ \psi_{ec,N}\, \psi_{ed,N}\, \psi_{c,N}\, \psi_{cp,N}\, N_b \tag{24}$$

where A_{Nc} / A_{Nco} = projected concrete failure area for the anchor group divided by the failure area for a single anchor, $\Psi_{ec,N}$ = breakout eccentricity factor, $\Psi_{ed,N}$ = breakout edge effect factor, $\Psi_{c,N}$ = concrete cracking factor, $\Psi_{cp,N}$ = splitting modification for post-installed anchors, and N_b = the 5% fractile basic concrete breakout strength of a single anchor:

$$N_b = k_c \lambda_a \sqrt{f_c'}\, h_{ef}^{1.5} \tag{25}$$

where k_c = 24 for cast-in anchors and 17 for post-installed anchors, λ_a = lightweight concrete modification factor, and h_{ef} = anchor effective depth measured to the bearing surface of the anchor.

ACI 318-19 acknowledges two methods by which anchors can benefit from reinforcement. *Anchor reinforcement* consists of bars designed to transfer the full anchor force into the structural member, disregarding the concrete strength. The bars must be developed on both sides of the potential failure cone. Additionally, the code introduces the notion of *supplementary reinforcement*, which is arranged and placed similarly to *anchor reinforcement* but is not intended to carry the full anchor force. In this case, the strength of the reinforcement is disregarded, requiring the concrete to carry the complete anchor force with a slight increment to the strength reduction factor. Neither the *anchor reinforcement* nor

the *supplementary reinforcement* concepts permit designers to combine the strength contributions from the concrete and reinforcement.

TEST SPECIMEN DESIGN

Four nominally identical column-foundation connection specimens with varying shear reinforcement configurations were tested. Fig. 37 shows plan and elevation drawings of specimen A02 in the test setup, which is representative of the other specimens. **Error! Reference source not found.** summarizes the differences among specimens. Specimen A01 had no shear reinforcement, serving as the control. Specimens A02 and A03 maintained the same shear reinforcement spacing while varying the bar size (#4 @ 7.5 in. [Ø13@190 mm] and #5 @ 7.5 in. [Ø16@190 mm], respectively). Specimens A02 and A04 maintained the same shear reinforcement bar size while varying the spacing (#4 @ 7.5 in. [Ø13@190 mm] and #4 @ 6 in. [Ø13@152 mm], respectively). Specimens A03 and A04 maintained a constant shear reinforcement ratio while varying the bar size and bar spacing (#5 @ 7.5 in. [Ø16@190 mm] and #4 @ 6 in. [Ø13@152 mm], respectively).

The foundation slabs measured 90 x 90 x 18 in. [2286 x 2286 x 457 mm] with a centrally located steel column stub accommodating four anchors in a 2-by-2 square configuration. The anchor bolts (F1554 G105) [724 MPa] were 1-1/8 in. [28.6 mm] in diameter and were placed with an effective depth of h_{ef} = 10 in. [254 mm]. The anchor head consisted of two heavy hex nuts clamping a steel bearing plate measuring 2.75 x 2.75 x 0.75 in. [70 x 70 x 19 mm]. Shear reinforcement consisted of so-called “candy cane” or J bars with standard 180° hooks at one end and Lenton Terminator heads at the other meeting ASTM A970 requirements. The hooked ends engaged the intersections of the longitudinal reinforcement while the headed ends were tied to avoid bearing on the longitudinal reinforcement – the positioning of the heads was intended to represent a condition less favorable to performance than would have been achieved with the heads bearing against the longitudinal reinforcement. Top and bottom longitudinal reinforcement consisted of #5 bars, Grade 60 [Ø 16, 420MPa] spaced at 7-1/2 in. [190 mm] in both orthogonal directions. Longitudinal reinforcement in specimen A04 was spaced more closely at 6 in. [152 mm] to accommodate the closer shear reinforcing bars.

The target concrete compressive strength was 4000 psi [27.6 MP] with a nominal maximum aggregate size of ¾ in. [19 mm]. Specimens A01 and A02 were cast from one concrete batch, while A03 and A04 were cast from another. **Error! Reference source not found.** summarizes test day measured concrete properties. All reinforcement was ASTM A706 Grade 60 (see **Error! Reference source not found.** for measured reinforcement properties).

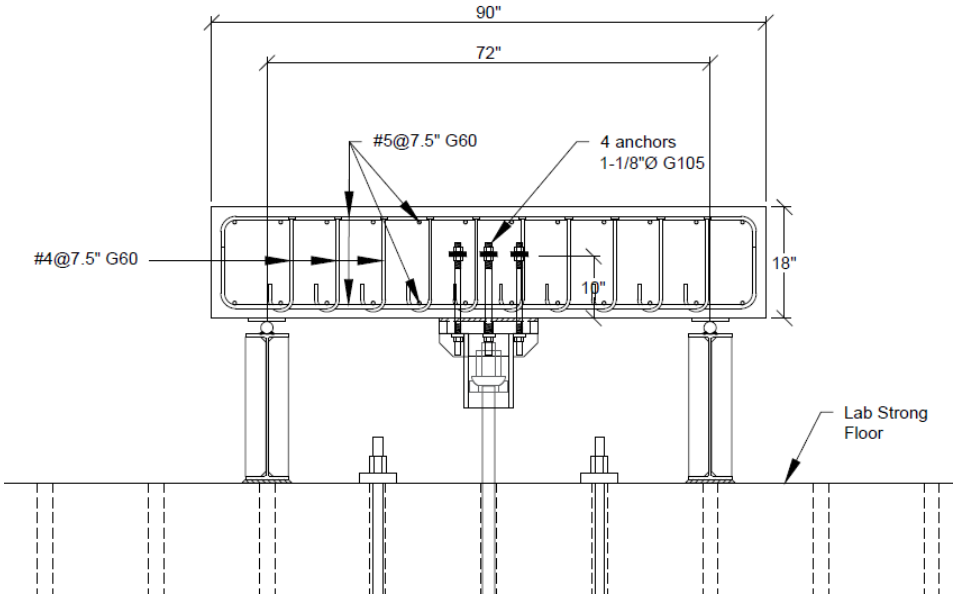

Elevation

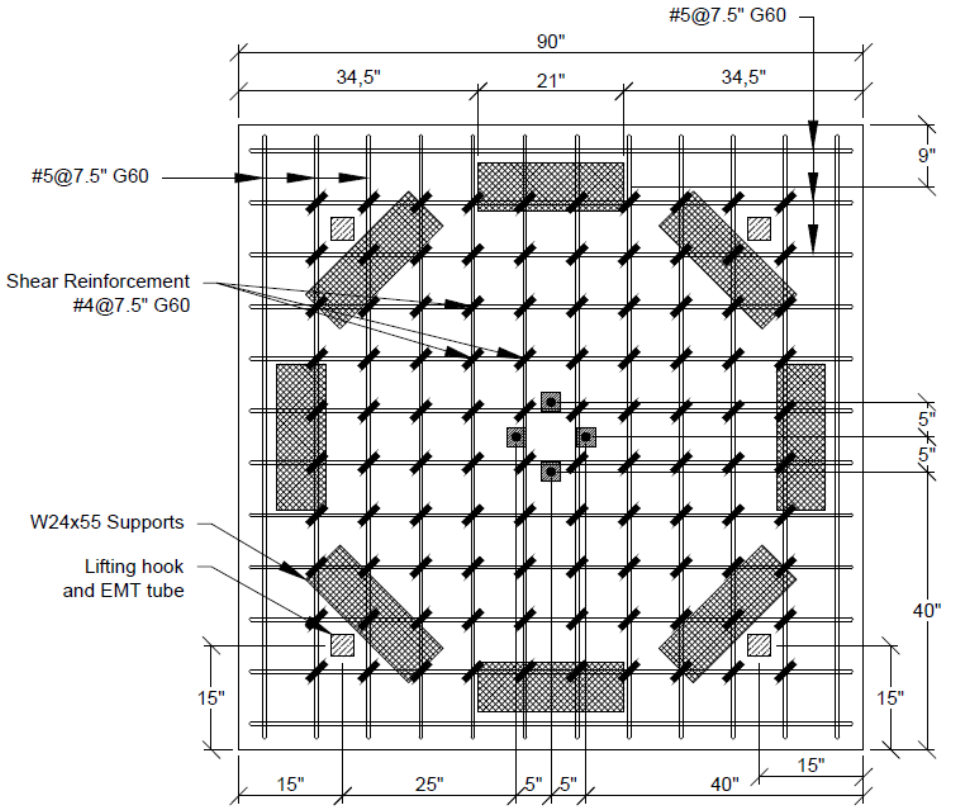

Plan

Fig. 37 – Drawings for specimen A02

Table 6–Specimen design and peak anchor group force

Specimen	A01	A02	A03	A04
Shear reinf. grid	NA	#4 @ 7.5 in. [Ø13@190 mm]	#5 @ 7.5 in. [Ø16@190 mm]	#4 @ 6 in. [Ø13@152 mm]
ρ_{tr} (%)	0	0.36	0.55	0.56
Longitudinal reinf. mesh top and bottom	#5 @ 7.5 in. [Ø16@190 mm]	#5 @ 7.5 in. [Ø16@190 mm]	#5 @ 7.5 in. [Ø16@190 mm]	#5 @ 6 in. [Ø16@152 mm]
Peak anchor group force, P_{test} (kip) [kN]	111 [494]	235 [1050]	226 [1010]	265 [1180]

Table 7–Test-day measured concrete material properties from 6 x 12 in. cylinders [150 x 300 mm]

Property	Standard	A01	A02	A03	A04
f'_c psi [MPa]	ASTM C39	3940 [27.2]	4000 [27.6]	3380 [23.3]	3380 [23.3]
f_t psi [MPa]	ASTM C496	415 [2.86]	381 [2.63]	342 [2.35]	352 [2.43]

Table 8–Measured reinforcement material properties

Bar	Yield stress ksi [MPa]	Ultimate stress ksi [MPa]
#4 G60 A706 (shear)	68.8 [474]	98.0 [676]
#5 G60 A706 (shear)	64.1 [442]	98.1 [676]
#5 G60 A706 (long.)	66.7 [460]	93.6 [645]

The base plate assembly was designed to remain elastic while transferring the loading to the anchors. The steel column stub consisted of an 8 x 8 in. [203 x 203 mm] box column welded to a 16 x 16 x 2 in. [406 x 406 x 50 mm] steel plate with stiffeners. The base plate was grouted to the concrete slab. The slab was supported on eight wide-flange steel sections arranged in an octagonal pattern (see Fig. 37). These supports were placed 36 in. [914 mm] from the specimen center to not interfere with the breakout cone. The steel sections included web stiffeners to avoid local buckling. A plain round steel bar was placed between the slabs and the steel supports to provide moment release. A semi-spherical bearing was provided at the connection of the loading rod to the column stub to avoid moment transfer. **Error! Reference source not found.** shows a photo of the test setup. Refer to Karać and Moehle (2022) for further details.

Fig. 38– Specimen A01 in test setup

INSTRUMENTATION AND LOADING PROTOCOL

Fig. 39 shows the instrumentation for specimen A02, which is representative of all other specimens. A load cell pack was placed below the column stub to measure the total axial force. Two wire pots measured the vertical displacement of the base plate (WP1 and WP2). Five linear potentiometers were used to measure the slab vertical deformations: two measured the cone displacement along the slab bottom surface (N1 and N2), one measured midspan displacement of the flexural compression face of the slab opposite the column base plate (N3), and two measured the vertical displacement of the top surface of the slab opposite the pin supports (N4 and N5). A horizontal linear potentiometer was placed at slab mid-depth on each lateral face to measure movement perpendicular to each face (N6-N9). Strain gauges were placed at mid-height along a line of shear reinforcing bars for each shear-reinforced specimen to observe the distribution of bar strains.

All specimens were loaded monotonically to achieve a load rate of about 15 kips/min [67 kN/min] in the initial elastic range. This displacement rate was maintained through the peak load until the force dropped to approximately one-third of the maximum load and the failure mode was visible.

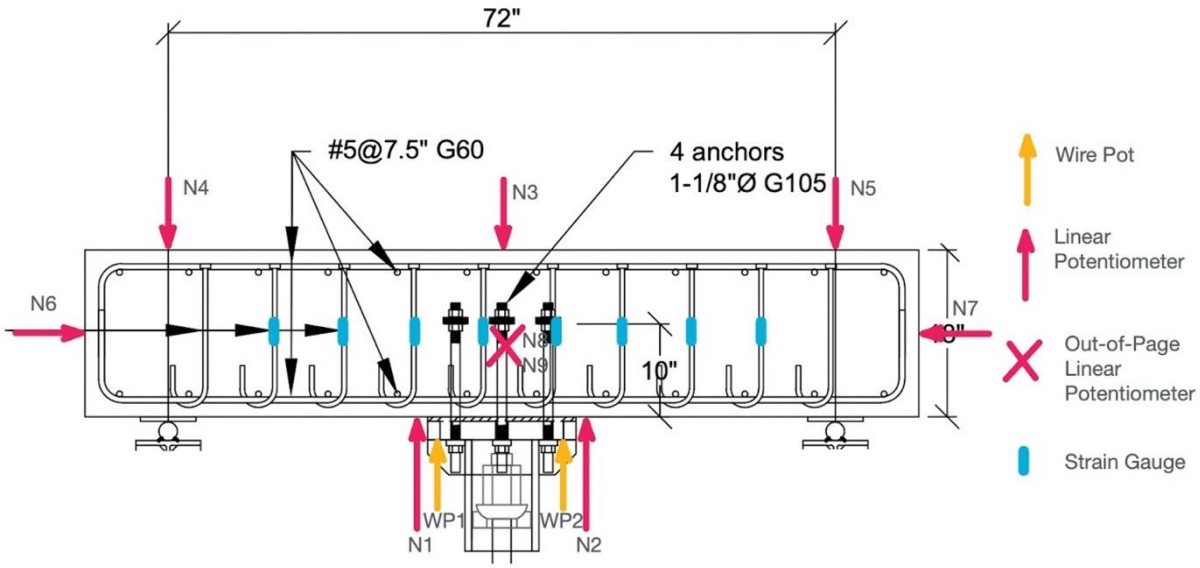

Fig. 39– Specimen A02 instrumentation

TEST SPECIMEN RESULTS

Error! Reference source not found. plots the measured anchor group force vs. the displacement of the breakout cone for all specimens. The anchor group force is normalized proportional the square root of f'_c (see **Error! Reference source not found.** for non-normalized values). The cone displacement is calculated as the average slab displacement minus the average support displacement $(N1 + N2)/2 - (N4 + N5)/2$. All test specimens experienced an initial drop in stiffness around 100 kip [445 kN] after which flexural cracks emanating radially from the anchor group became apparent. Control specimen A01 with no shear reinforcement did not experience any additional strength gain beyond this point and failed in a brittle manner. The shear-reinforced specimens continued to gain strength, reaching peak strengths of more than double that of the unreinforced specimen. Overall, larger shear reinforcement ratios corresponded with larger peak strengths. When comparing specimens A02 and A03, increasing the shear reinforcing bar size from #4 to #5 [⌀13 mm to 16 mm] resulted in a 55% increase in the shear reinforcement ratio. However, this change led to only a 5% increase in overall strength. Steep concrete cone failure governed. Specimen A03 and A04 were designed with the same reinforcement ratio, but with different bar sizes and spacings. In specimen A04, the smaller and more tightly spaced bars resulted in a 17% increase in peak strength and about a 40% increase in post-peak stiffness when compared with specimen A03. When comparing specimens A02 and A04, decreasing the bar spacing from 7.5 to 6 in.

[190 to 152 mm], increases the shear reinforcement ratio by roughly 56%, resulting in a 23% increase in peak strength. However, if the spacing between the shear reinforcing bars is large, steep concrete cone failure may govern, limiting the benefit of additional shear reinforcement.

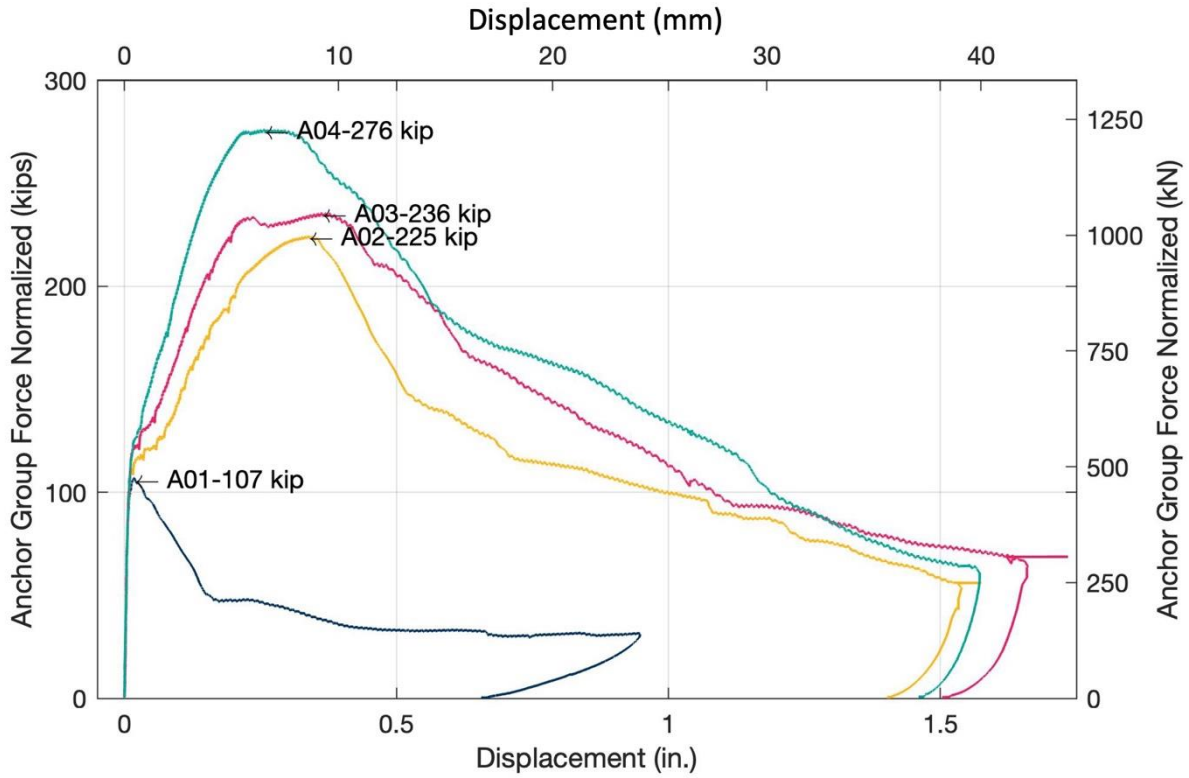

Fig. 40 – Force - displacement relationships (Force normalized to average f'_c = 3680 psi [25.3 MPa])

Error! Reference source not found. shows a cross section of each test specimen after saw cutting a vertical plane slightly offset from the centerlines to not intersect the anchor rods. Drawings of the anchors and reinforcement are overlayed on the images. Control specimen A01 with no shear reinforcement displayed a single breakout cone with a slope near 1:1.5 (vertical:horizontal). However, the three shear-reinforced specimens display multiple nested breakout cones. Nested cones extend from the anchor head to the top ends of the shear reinforcement. In specimen A04, which resulted in the highest peak strength, additional breakout cones are observed around each anchor individually thereby avoiding the shear reinforcing bars (Cone 1). Specimen A04 also displays a breakout cone originating from the bottom of the inner shear reinforcing bars (Cone 3). This suggests that even though the shear reinforcement strengthens the original breakout failure, the shear reinforcement itself can trigger new breakout failures in potentially unreinforced regions.

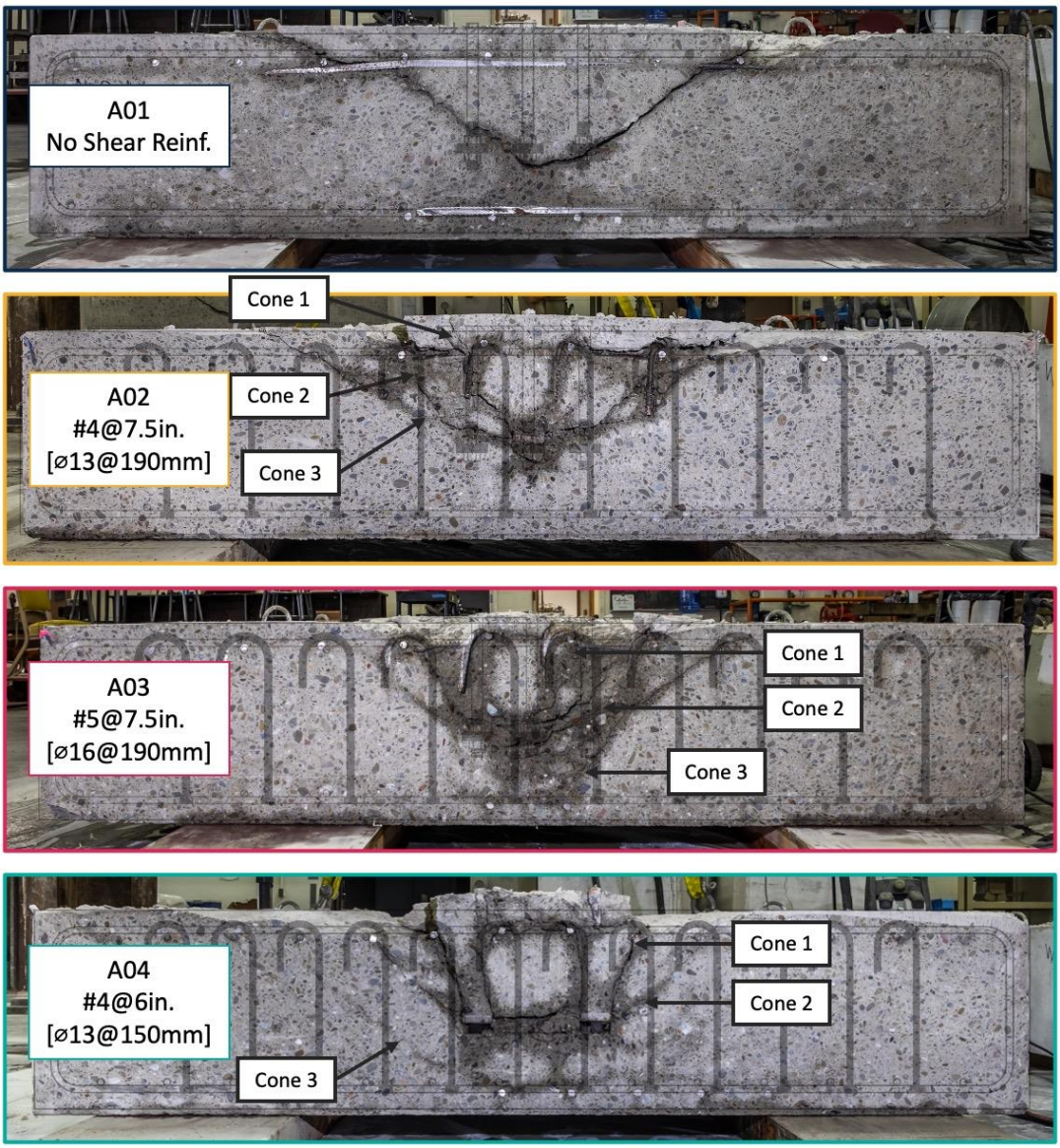

Fig. 41 – Cross sections showing post-failure crack patterns

Error! Reference source not found. plots the measured strain of each shear reinforcing bar at failure vs. the distance from that bar to the anchor group. In general, as the distance to the reinforcing bar increases, the strain decreases. Only reinforcing bars within about $0.75h_{ef}$ from the anchor group exceeded the nominal yield strain of 2000 $\mu\varepsilon$ for G60 bars.

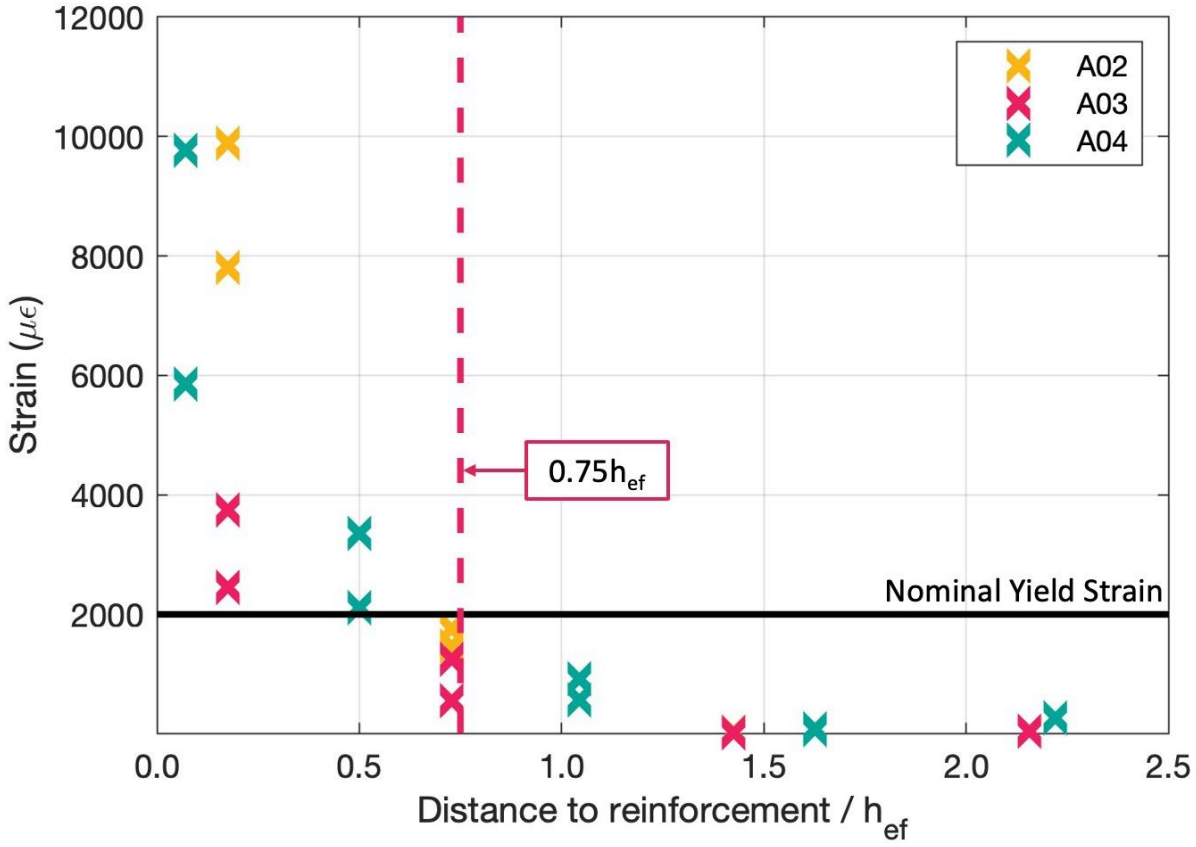

Fig. 42 – Strain in each shear reinforcing bar at failure versus distance to outer perimeter of the anchor group

FINITE ELEMENT MODEL CALIBRATION

The physical test data described above were used to calibrate finite element (FE) models providing reasonable representations of the observed failure modes, crack patterns, stiffness, cracking strength, and peak strength. The FE software ATENA (V5.7.0) was used as it has previously provided reasonable results (Worsfold and Moehle, 2023a). The concrete material model is based on the smeared crack and crack band method for both tension and compression with the combined fracture-plastic model proposed by Červenka and Pappanikolaou (2008). Table 9 summarizes the modeling parameters for the calibrated models. To reduce analysis run time, quarter-space models were built to take advantage of specimen symmetry. The anchors were modeled as 3D solid-elastic steel elements fixed to the concrete only along the anchor head bearing surface. The concrete was meshed with 8-node hexahedra elements and a 2x2 integration scheme. A 2in [50mm] mesh size produced a reasonable representation of the breakout cone,

accommodating five elements along the anchor embedment length. The minimum crack band width was set to 1.5 times the maximum aggregate size to reduce the sensitivity to mesh size as recommended by Červenka et al. (2018). A concrete shrinkage value of 400e-6 was assumed. All reinforcement was modeled at 1D truss elements fixed to the concrete elements except for the top surface reinforcement which was modeled as 1D fiber beam elements to simulate dowl action and flexural stiffness. A rotated crack value of 0.4 was used to permit stress redistribution as the breakout cones propagated from the anchor heads to the concrete surface. The fracture energy (G_f) was calculated from FIB Model Code 1990 recommendations, which considers aggregate size.

Table 9–Finite element parameters for calibrated models

Modeling Parameter	**Notes**
Anchor	3D solid-elastic steel fixed to the concrete at the bearing surface (no other contacts)
Transverse Reinforcement	1D truss elements fixed to concrete
Longitudinal Reinforcement	1D beam elements fixed to concrete
Mesh size	d_{max} < mesh size < h_{ef} / 5
Rotated crack	0.40
Fracture Energy (G_f)	FIB Model Code 1990
Elements	8-node hexahedra
Integration scheme	2 x 2
Minimum crack band	1.5 d_{max}
Concrete Shrinkage	400 $\mu\varepsilon$
Concrete Modulus of Elasticity (E)	$57{,}000\sqrt{f_c'}$ (psi) $4700\sqrt{f_c'}$ (MPa)

Error! Reference source not found. plots the FE models calibrated to the physical test data. Each FE peak anchor group force is within 10% of the corresponding experimental value, which is within the expected dispersion of physical breakout tests (covariance of 0.15 measured by Fuchs et al., 1995). The pre-cracking FE stiffnesses match the experimental data. Initial cracking of some FE models occurred at larger forces than the physical specimens, potentially due to inaccuracies in assumed material properties and assumed shrinkage. The sudden drop observed in the FE models after initial cracking is likely due to the assumption of material homogeneity, which results in cracks opening suddenly. Between initial cracking and the peak force, the models for the reinforced specimens (A02, A03, and A04) are stiffer than the experimental data, potentially due to inaccuracies in the assumed reinforcement modeling and the fact that bar slip is not modeled. The models for specimens A02 and A03 show excessive post-

peak displacement capacity which may result due to differences in the post peak loading protocol.

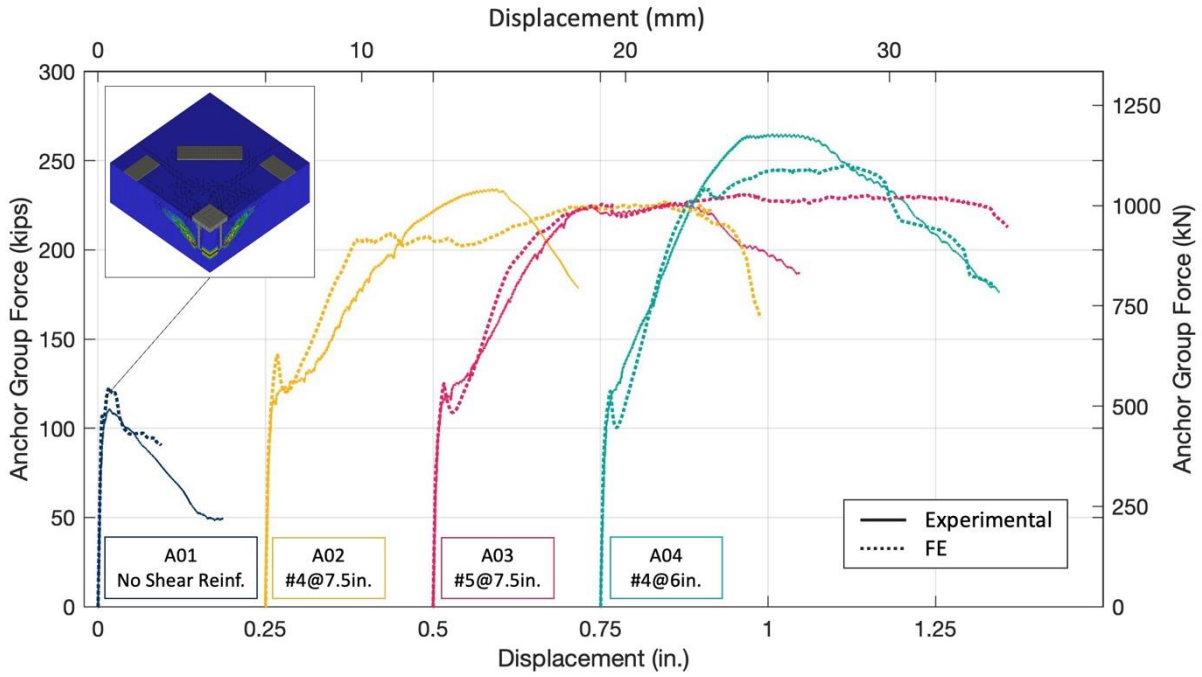

Fig. 43 – Finite element models calibrated to test data

FINITE ELEMENT PARAMETRIC STUDIES

FE parametric studies were performed to investigate the effects of shear reinforcement detailing on breakout failure. The calibrated models were simplified by substituting the 1D fiber beam surface reinforcement for 1D truss elements. This simplification mainly affects the post-peak behavior due to the lack of dowel action and flexural stiffness of the surface reinforcement which is of secondary importance in this study.

Size of Shear-Reinforced Region

In the physical specimens, the shear reinforcement extended throughout the whole slab. The strains in the shear reinforcing bars decreased the farther the bars were from the anchor group. Various FE models were run, taking models for specimens A02, A03, and A04 and reducing the size of the shear-reinforced region while maintaining the same shear reinforcement ratio (ρ_{tr}). **Error! Reference source not found.** plots the peak anchor force for each model (P_{test}) relative to the strength of the corresponding unreinforced model (P_0) versus the distance from the anchor group outer perimeter to the farthest shear reinforcing bar. For all

three specimens, no strength decrease is observed until reinforcement within about $0.75h_{ef}$ from the anchors is removed.

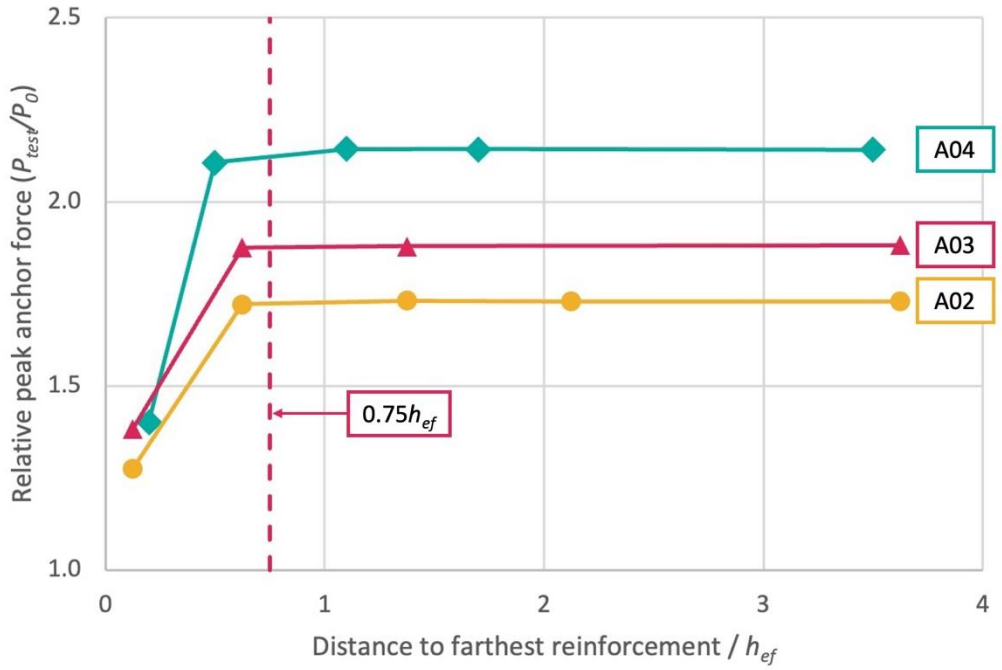

Fig. 44 – Relative peak anchor force versus distance from the anchor group outer perimeter to the farthest shear reinforcing bar for multiple finite element models.

Shear Reinforcement Terminations

In the physical tests, the shear reinforcement terminated in standard 180° hooks at one end and heads at the other. The calibrated FE models described above idealize transverse reinforcement as fixed to the concrete along the full length with no bond model. To investigate the effect of this assumption, the force–displacement curves for FE models of specimen A03 are plotted in **Error! Reference source not found.** where the shear reinforcement is idealized as 1) fixed to the concrete along the length, 2) a bond-slip model is added with only one end fixed to the concrete and the other free to slip, and 3) a bond-slip model is added with both ends free to slip. Removing bar terminations resulted in decrease in peak forces and displacement capacities. The bars fixed to the concrete along the entire length yielded, while the bars with one or two free ends only developed about 80% of the nominal yield stress. These observations suggest that, for short bars, inadequate bar terminations may limit the reinforcement contribution to breakout strength. However, even though the bars do not yield, strength gain is observed beyond the initial

cracking stage instead of a suddden breakout failure which might be expected in unreinforced connections.

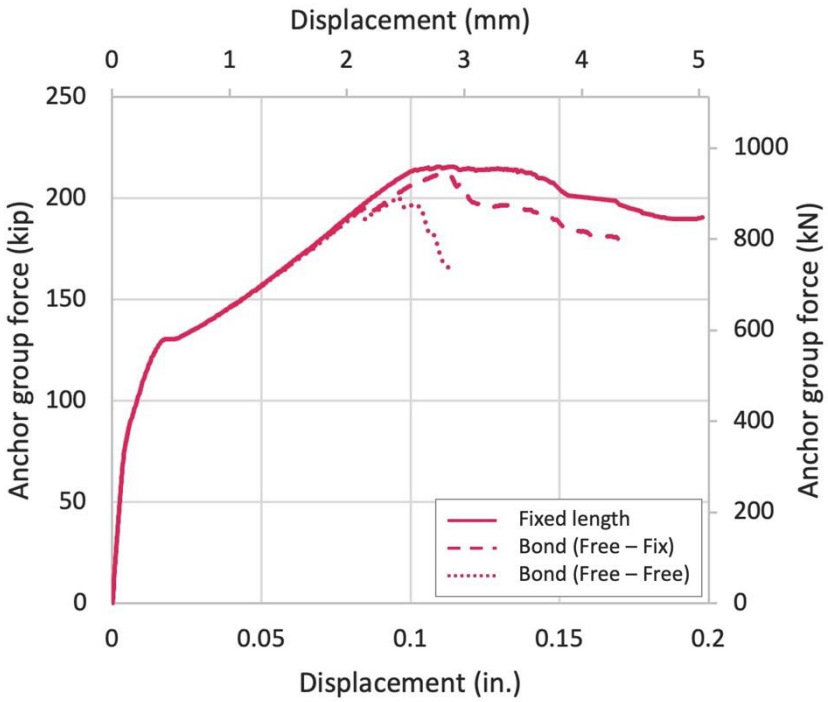

Fig. 45 – Force versus displacement curves for FE models of specimen A03 with different reinforcement end anchorages

Amount of Shear Reinforcement

This parametric study investigates whether there is an upper limit to the strength increase that can be expected from additional shear reinforcement. Models for specimens A02 and A04 were modified by varying the size of the shear reinforcing bars while maintaining the bar spacing constant. **Error! Reference source not found.** plots the strain in each shear reinforcing bar at failure versus the distance from the bar to the outer perimeter of the anchor group. As bar sizes increase, the strains at failure decrease and fewer bars yield. Additionally, the model for specimen A02 was modified varying the bar size and the bar spacing in such a way as to maintain the shear reinforcement ratio (ρ_{tr}) constant (see **Error! Reference source not found.**).

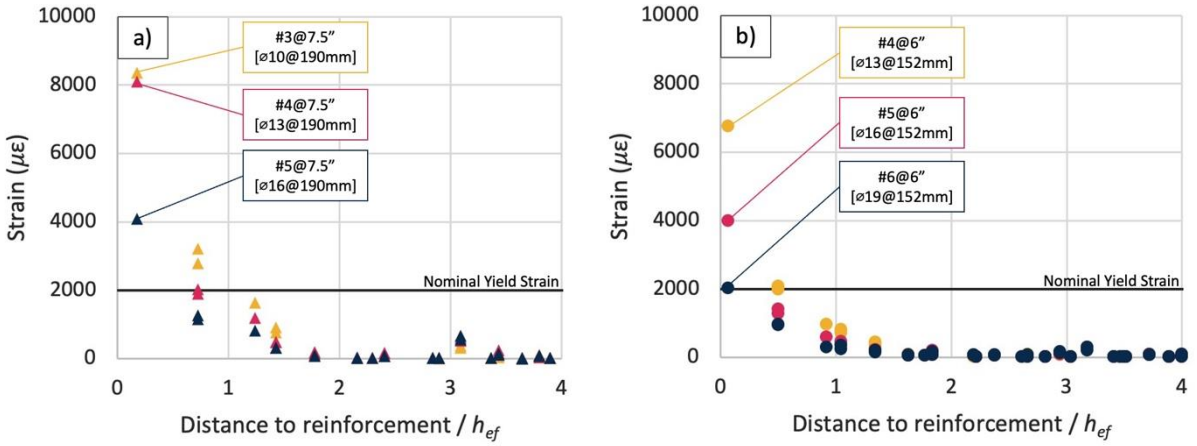

Fig. 46 – Strain in each shear reinforcing bar at failure versus distance to anchor group for FE models varying the size of the shear reinforcing bar for bar spacing of (a) 7.5 in. [190 mm] (Specimen A02) and (b) 6 in. [152 mm] (Specimen A04)

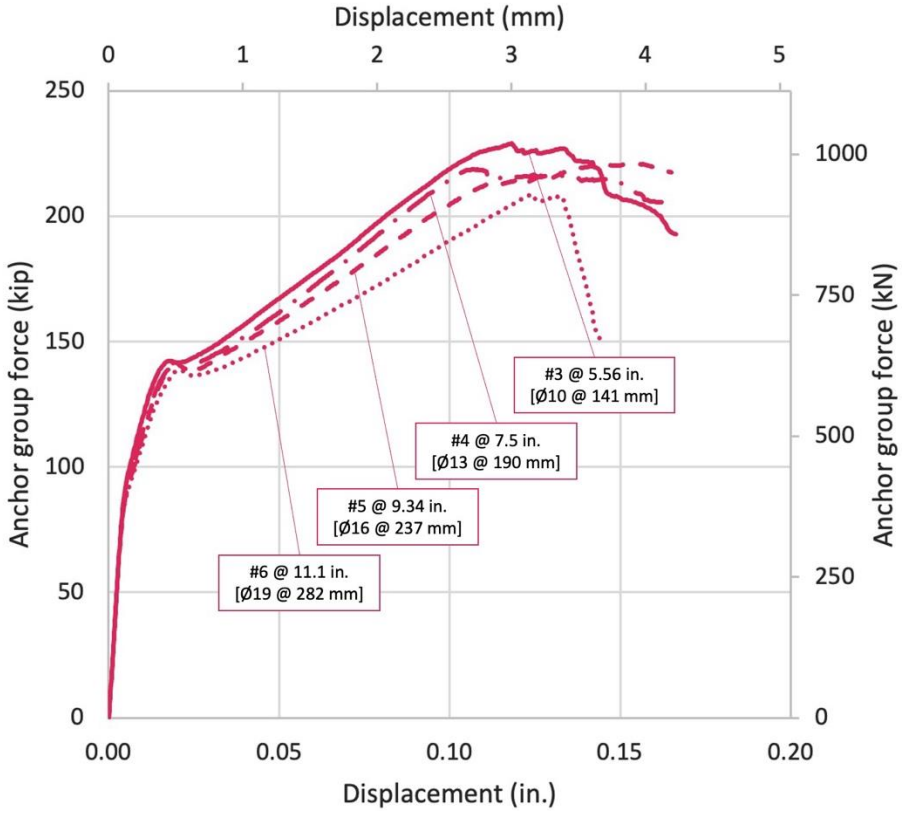

Fig. 47 – Force versus displacement curves for FE models varying the shear bar sizes and spacings while maintaining constant ρ_{tr} =0.36%

As the bar size and the spacing between bars increased, the strains in the shear reinforcement dropped, the peak force dropped, and reduced displacement capacity was observed. The model with the largest bars (#6 [Ø16]) showed no reinforcement yielding at failure. These results suggest that as the amount of shear reinforcement increases, concrete failure may govern before yielding of the transverse reinforcement. For a given reinforcement ratio, closely spaced bars resulted in higher strengths as the failure cone between adjacent reinforcing bars was forced to be steeper.

DISCUSSION

Shear-Reinforced Concrete Breakout Design

Based on physical tests and FE simulations, Worsfold and Moehle (2023b) proposed a design approach for shear-reinforced concrete breakout failure of moment-transfer column-foundation connections. This methodology can be extended to axially loaded connections. According to the approach, the nominal shear-reinforced breakout strength ($N_{n,SRB}$) is calculated by summing the contributions of concrete (N_c) and shear reinforcement (N_s):

$$N_{n,SRB} = N_c + N_s \tag{26}$$

$$N_c = 1.33 N_{cbg} \tag{27}$$

$$N_s = \mathrm{A_{eff}} * \rho_{tr} * f_{yt} \tag{28}$$

where N_{cbg} is the 5% fractile ACI 318-19 breakout strength, Eq. (24), A_{eff} is the anchor group effective area, ρ_{tr} is the shear reinforcement ratio, and f_{yt} is the nominal yield stress. The effective area is the region around the anchor group where the shear reinforcement is assumed to yield. The shear reinforcement strain measurements for the physical tests (see **Error! Reference source not found.**) suggest that the effective area extends outward about $0.75h_{ef}$ from the anchor group outer perimeter which is consistent with previous tests for moment-loaded connections. The mean concrete breakout strength (N_c) can be calculated by multiplying the 5% fractile ACI 318-19 breakout strength (N_{cbg}) by a modification factor, assuming measured strengths follow a normal distribution with a coefficient of variation of 0.15 (Fuchs, 1995):

$$\frac{1}{1 + z_{0.05} * CV} = \frac{1}{1 + (-1.645) * 0.15} = 1.33 \tag{29}$$

In addition to the test specimens reported above, data from other shear-reinforced concrete breakout failures exists in the literature. Having calculated the nominal strengths for these data with the approach above, **Error! Reference source not found.** plots the measured experimental increase in peak

anchor force relative to the unreinforced specimens ($N_{s,exp} = P_{test} - P_0$) versus the calculated force increase (N_s) from Equation (28). The data generally follow the 1=1 dashed line suggesting good agreement.

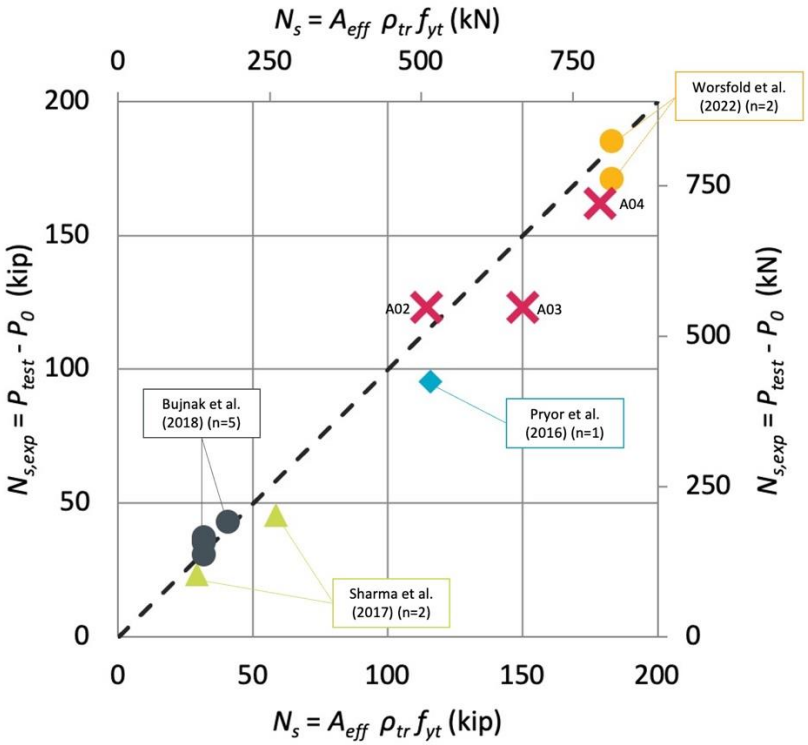

Fig. 48 – Experimental ($N_{s,exp}$) versus calculated (N_s) increase in peak anchor force due to additional reinforcement for physical data from various researchers

Error! Reference source not found. plots the test-to-predicted ratios for test data from various researchers using a) ACI 318-19 concrete breakout strength (N_{cbg}) and b) the proposed shear-reinforced breakout strength ($N_{n,SRB}$) from Equation (26). The ACI 318-19 breakout equation is calibrated to a 5% fractile value and ignores the beneficial effect of distributed reinforcement, resulting in an average test-to-predicted ratio of 2.93 with high points exceeding 4.5 and a standard deviation of 1.04. The proposed design equation considers a mean concrete breakout strength and the effect of distributed reinforcement, resulting in a lower average test-to-predicted ratio of 1.13 and a lower standard deviation of 0.27. The data points do not show a strong upward or downward trend across the range of tested reinforcement ratios.

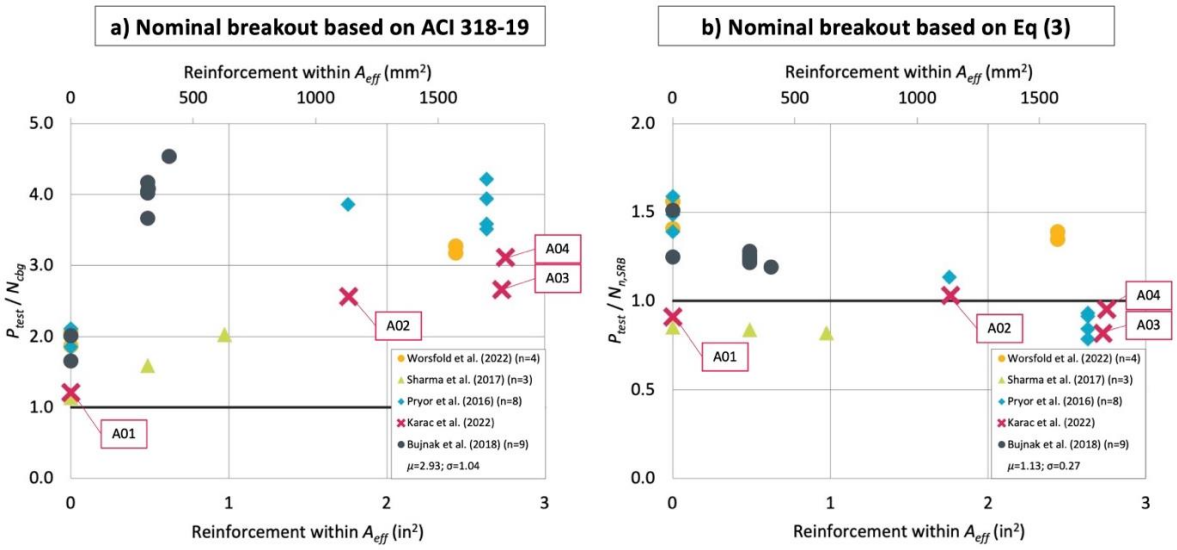

Fig. 49 – Test-to-predicted ratios of shear-reinforced breakout physical test data from various researchers

Reinforcement Detailing

The ACI 318 Chapter 17 breakout cone is a nominal cone that is used to calculate a design strength. Engineers sometimes take it as the literal physical cone that needs to be reinforced, leading, in turn, to concentrated shear reinforcement within the nominal cone and none outside. This view ignores the more complex crack patterns observed involving nested steep failure cones, secondary failure cones extending beyond the reinforced region, and breakout triggered the reinforcing bars themselves. A grid of closely spaced small diameter reinforcing bars can be designed to address these failure modes.

The proposed design approach assumes that the shear reinforcement within the effective area around an anchor group will yield. Using ACI 318-19 *anchor reinforcement* provisions (17.5.2.1) would require that bars be developed on both sides of the nominal cone failure plane. Even though only the first ring of bars around each anchor group was developed in this way, the strain in many other bars approached or exceeded the yield strain (**Error! Reference source not found.**). These bars contributed to the connection strength by restraining breakout cones other than the nominal cone. The headed end was tied such that it did not engage the longitudinal reinforcement representing a less favorable anchorage condition. The FE results (**Error! Reference source not found.**) suggest that if one end of the shear reinforcement is free, the bars are less likely to yield. These results suggest that reinforcement should be anchored at both ends to be effective. Engaging longitudinal reinforcement likely improves anchorage.

Previous physical tests (Worsfold et al., 2022) suggest that a secondary breakout cone outside the shear-reinforced region may govern if the reinforced region is small. Worsfold and Moehle (2023b) provide an expression that can be used to calculate the strength of the secondary cone. Alternatively, a simpler approach is to extend the shear-reinforced region to fully encompass the original breakout cone so the strength of the secondary one is unlikely to govern. Extending shear reinforcement a specified distance beyond a critical section serves a similar purpose to ACI detailing requirements for punching shear reinforcement.

The proposed design method assumes that the bar spacing of the distributed shear reinforcement is small enough such that steep concrete cone failures bypassing the shear reinforcement will not occur before bar yielding. Specimens A03 and A04 had the same shear reinforcement ratio ($\rho_{tr} \approx 0.55\%$), but the strength of specimen A03 with wider spacing was about 17% lower than A04 with smaller spacing. FE results (**Error! Reference source not found.**) suggest that for a given shear reinforcement ratio (ρ_{tr}), larger bars with larger spacing produce lower peak strengths and lower bar strains at failure. The FE model with bar spacing larger than $1.0h_{ef}$ failed without yielding the shear reinforcement at a peak force corresponding to only about 82% of that expected from Equation (28). The model with a bar spacing of about $0.5h_{ef}$ was able to strain harden and achieve the strength increase expected from Equation (28). A maximum bar spacing of $0.5h_{ef}$ is recommended to encourage bar yielding and discourage steep concrete cone failures.

Specimen A04 displays a breakout cone originating from the headed ends of the inner shear reinforcing bars (Cone 3). Even though this failure cone did not govern, it demonstrates that under specific conditions, shear reinforcement itself can trigger new breakout failure cones. These new cones may extend beyond the reinforced region due to the increased effective depth of the shear reinforcement, potentially resulting in brittle failures. Breakout failure of *anchor reinforcement* should be considered in design.

Steep Cone Failure as Upper Strength Limit

Previously described FE models suggest that at high shear reinforcement ratios, concrete failure may limit the beneficial effect of shear reinforcement. The cross sections of the physical specimens (see **Error! Reference source not found.**) show nested cone failures extending from the anchor heads to each row of shear reinforcement. The smallest (inner) cones do not engage the shear reinforcement, while each consecutively larger cone engages additional reinforcement. It cannot be generalized that steeper or shallower cones will govern as this depends on each connection geometry. All else being equal, the

strength of an unreinforced steep cone is generally higher than that of a shallow cone. However, steeper cones engage fewer reinforcing bars.

Based on physical tests and simulation, Berger (2015) proposed a modification factor to calculate the strength increase of steep cones:

$$\Psi_s = 2.75 - 1.17\frac{x}{h_{ef}} \geq 1 \tag{30}$$

where x is the distance from the anchor centerline to the intersection of the assumed steep cone with the concrete surface. This equation is here expanded to consider cone restrictions in the two perpendicular directions and presented in terms of the projected failure areas:

$$\Psi_{c,steep} = 2.75 - 1.75\frac{A'}{A_{Nc}} \geq 1 \tag{31}$$

where A' is the projected failure area of the assumed steep cone and A_{Nc} is the projected failure area of the unrestricted cone. The following modification factor is proposed to reduce the contribution of shear reinforcement for steep cones:

$$\Psi_{s,steep} = 2\frac{A'}{A_{Nc}} - 1 \geq 0 \tag{32}$$

Once the steep cone area (A') is less than half the unrestricted cone area (A_{Nc}), the contribution of shear reinforcement drops to zero. The strength of a steep failure cone in a region of distributed shear reinforcement can be calculated as follows:

$$N_{n,steep} = \Psi_{c,steep}N_c + \Psi_{s,steep}N_s \tag{33}$$

This equation may serve as an upper limit to Equation (26). For a given connection, the strength of each nested cone is calculated, and the minimum strength governs.

Additional FE models were created to investigate upper strength limits by taking models calibrated to the physical specimens and varying the size and spacing of the shear reinforcing bars. **Error! Reference source not found.** plots the test-to-predicted strength ratios versus the area of shear reinforcement within the effective area. If no upper limit is imposed on Equation (26), the test-to-predicted strength ratios display a downward trend, reaching test-to-predicted strength ratio values below 0.6 (blue diamonds). Equation (26) can overpredict the connection strength because steep cone failures occur before bar yielding. Imposing the proposed steep cone strength upper limit ($N_{n,steep}$) from Equation (33), the downward trend is eliminated, resulting in an average strength-to-predicted ratio of 1.05 (red circles). If a simpler upper limit of $2.5N_c$ is imposed, the downward trend is also eliminated, resulting in an average strength-to-predicted ratio of 0.89 (yellow triangles).

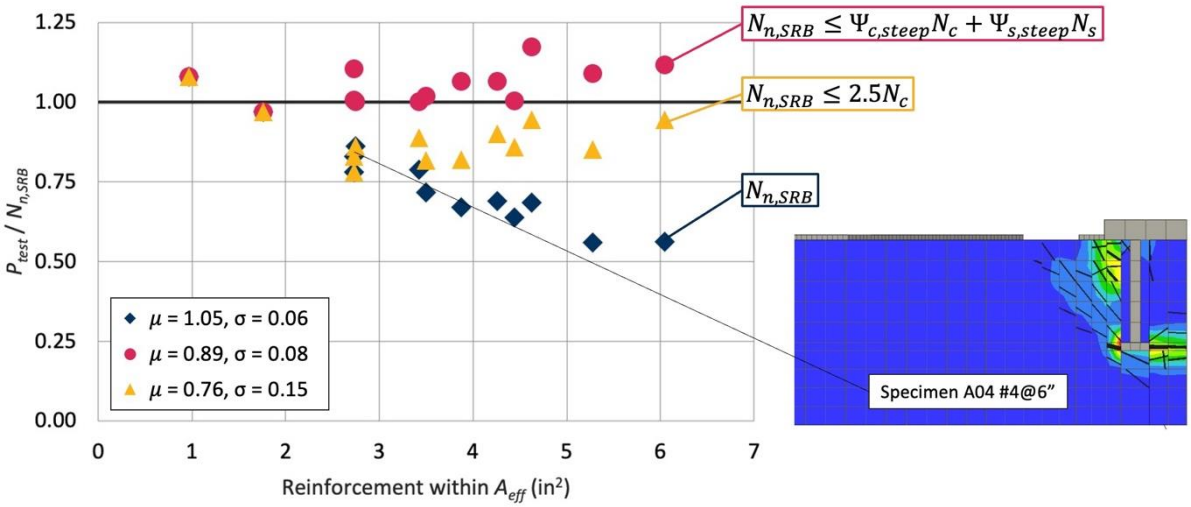

Fig. 50 – Test-to-predicted ratios for thirteen FE models considering three different upper strength limits

CONCLUSIONS

Four full-scale steel-column-to-concrete-foundation connections with cast-in-place anchors were subjected to monotonic axial tensile forces until failure. The main variables investigated were the size and spacing of the distributed shear reinforcing bars in the foundation. The control specimen had no shear reinforcement. All specimens experienced concrete breakout failures. Principal observations include:

1. Concrete breakout failure can govern axially loaded column-foundation connections with cast-in-place headed anchors.
2. The addition of a uniformly distributed grid of shear reinforcement around the anchor groups more than doubled the connection strength and the displacements at failure increased by about one order of magnitude when compared with the control specimen.
3. Considering physical specimens from this study and other authors, higher shear reinforcement ratios correlate with higher peak strengths.
4. The test specimens with distributed shear reinforcement developed failure modes consisting of multiple nested breakout cones. Some observed cones had slopes steeper than the 1:1.5 nominal cone assumed in ACI 318. The steeper cones were able to bypass some of the additional reinforcing bars limiting the beneficial effect of the additional bars.
5. Under specific conditions, the shear reinforcement placed to strengthen a breakout failure can itself trigger new, larger breakout failure cones in potentially unreinforced regions. The breakout failure

of anchor reinforcement should be considered in design even though it is not discussed in ACI 318-19.

6. The 1:1.5 nominal breakout cone used in ACI 318 Chapter 17 is simply a design tool, and should not be taken as the literal physical cone that needs to be reinforced. That approach may lead to concentrated shear reinforcement within the nominal cone and none outside ignoring secondary failure modes.
7. Shear reinforcing bars yielded even though they were not developed on both sides of the standard 1:1.5 failure cone as would be required by ACI 318-19 anchor reinforcement provisions. The multiple nested failure cones engaged bars that the anchor reinforcement provisions would not have deemed effective.
8. FE results suggest that additional shear reinforcing bars beyond about 0.75hef from the outer perimeter of the anchor group seem to have little effect on the peak strength.
9. FE results suggest that steep concrete cone failure can occur before yielding the adjacent shear reinforcing bars, limiting the reinforcement strength contribution. Given the same shear reinforcement ratio (ρtr), more closely spaced bars result in higher peak strengths as the failure cones are forced to be steeper.
10. A strength equation for shear-reinforced breakout failure for connections governed by moment transfer (Eq. 3) was extended to axially loaded connections. Including physical test results from other researchers, this approach reduced the average strength-to-predicted ratio from 2.93 (obtained using the current ACI 318-19 breakout equation) to 1.13.
11. An upper limit on the strength gain from additional shear reinforcement is proposed to consider the possibility of steep cone failures before bar yielding which may occur in highly reinforced connections (Eq. 10).

Concrete breakout failure can govern axially loaded column-foundation connections. An appropriately detailed grid of distributed shear reinforcement can increase connection peak strength and displacement capacity. The proposed design approach may be a simple yet effective approach to strengthening connections susceptible to breakout failure. The strengthened connection may improve the overall behavior of a structure by removing brittle failure modes that may have previously been overlooked. The authors recommend that ACI 318 consider provisions allowing designers to account for the beneficial effect of distributed reinforcement on the concrete breakout failure mode.

NOTATION:

A' = projected failure area of the assumed steep cone

A_{eff} = anchor group effective area

A_{Nc} = projected failure area of a single anchor or an anchor group in question

A_{Nco} = projected concrete failure area of a single anchor if not affected by edges ($9h_{ef}^2$)

d_{max} = maximum aggregate size

E = concrete modulus of elasticity

f'_c = concrete compressive strength (psi)

f_t = concrete tensile strength

f_{yt} = nominal yield stress of shear reinforcement

G_f = concrete fracture energy

h_{ef} = anchor effective embedment depth (in)

k_c = coefficient for basic concrete breakout strength in tension

N_b = basic concrete breakout strength of a single anchor in tension in cracked concrete ACI 318

N_c = mean concrete breakout strength ($N_c = 1.33N_{cbg}$)

N_{cbg} = nominal concrete breakout strength in tension of a group of anchors ACI 318

$N_{n,SRB}$ = nominal shear-reinforced breakout strength

$N_{n,steep}$ = nominal strength of shear-reinforced steep cone failure

N_s = nominal strength contribution of distributed shear reinforcement to breakout strength

$N_{s,exp}$ = experimental increase in peak anchor force relative to the unreinforced specimens

P_{test} = measured peak anchor group force

P_0 = measured peak anchor group force for the corresponding unreinforced case

x = distance from the anchor centerline to the intersection of the assumed steep cone with the concrete surface (Berger, 2015)

$z_{0.05}$ = statistical z-value for 0.05

λ_a = lightweight concrete modification factor

ρ_{tr} = shear reinforcement ratio

$\Psi_{ec,N}$ = modification factor for anchor groups loaded eccentrically in tension

$\Psi_{ed,N}$ = modification factor for edge effects of anchors in tension

$\Psi_{c,N}$ = modification factor for anchors in uncracked concrete under service loads

$\Psi_{cp,N}$ = modification factor for concrete splitting with post-installed anchors

$\Psi_{c,steep}$ = concrete term modification factor for steep cones

Ψ_s = modification factor for steep cones (Berger, 2015)

$\Psi_{s,steep}$ = steel term modification factor for steep cone failure

REFERENCES

ACI Committee 318, 2019, Building Code Requirements for Structural Concrete (ACI 318-19) and Commentary ACI (ACI 318R-19), American Concrete Institute, Farmington Hills, MI, 624 pp.

Caltrans, 2016, Memo to Design MTD (MTD) 20-7, Seismic Design of Slab Bridges, California Department of Transportation, Sacramento, CA.

Berger, W., 2015, Load-displacement behavior and design of anchorages with headed studs with and without supplementary reinforcement under tension load, Ph.D. Thesis, Institute of Construction Materials, University of Stuttgart (German).

Bujňák, J., Mecár, J., and Bahleda, F., 2018, Tensile Resistance of an Anchor Plate with Supplementary Reinforcement, Structural Concrete

Červenka, J., Červenka, V., Lasernab, S., 2018, On crack band model in finite element analysis of concrete fracture in engineering practice, Engineering Fracture Mechanics

Červenka, J. and Papanikolaou, V., 2008, Three-dimensional combined fracture-plastic material model for concrete. Int. J. Plast. 2008; 24:2192–220. 2008.01.004.

FIB Bulletin 213/214: Model Code 90, Lausanne, Switzerland, 1993, ISBN 978-0-7277-1696-5, p. 460

Fuchs, W., Eligehausen, R., and Breen, J., 1995, Concrete Capacity Design (CCD) Approach for Fastening to Concrete, ACI Structural Journal, V. 92, No. 1, Jan.-Feb., pp. 73-94.

Karać, D., 2022, Shear Reinforced Concrete Breakout Failure, Structural Engineering, Mechanics, and Materials MS Thesis, University of California, Berkeley

Mahrenholtz, C., Akguzel, U., Eligehausen, R., and Pampanin, S., 2014, New Design Methodology for Seismic Column-to-Foundation Anchorage Connections, *ACI Structural Journal*, V. 111, No. 5, Sep.-Oct., 1179-1189 pp.

Papadopoulos, V., Murcia-Delso, J., and Benson Shing, P., 2018, Development of Headed Bars in Slab-Column Joints of Reinforced Concrete Slab Bridges. ACI-Structural Journal, V. 115, No. 5, September 2018, p. 1393-1406.

Pryor, S., Montague, E., Fischer, S., Ding, F., and Mochizuki, G., 2016, Detailing for Increased Capacity of Tension-Only Steel Anchor Rods Embedded in Elevated Concrete Slabs, 2016 SEAOC Convention

Sharma, A., Eligehausen, R., Asmus, J., 2017, Comprehensive experimental investigations on anchorages with supplementary reinforcement, Proceedings 3rd International Symposium on Connections between Steel and Concrete (ConSC 2017) September 27-29, Stuttgart, p. 242-252

Sharma A, Eligehausen R, Asmus J, Bujnak J, Schmid K., 2018, Analytical model for anchorages with supplementary reinforcement under tension or shear forces. High Tech Concrete: Where Technology and Engineering Meet—Proceedings of the 2017 fib symposium, Maastricht, the Netherlands; 2017. p. 974–982.

Vecchio, F. and Collins, M., 1986, The modified compression field theory for reinforced concrete elements subjected to shear, Journal of the American Concrete Institute, Vol. 83, No. 2, pp. 219-231.

Worsfold, B. and Moehle, J., 2023a, Moment transfer at column-to-footing connections: analytical studies. ACI Struct J 2023;120(2).

Worsfold, B and Moehle, J., 2023b, Shear-reinforced concrete breakout design methodology for moment transfer at column-foundation connections, Engineering Structures, Volume 283, 2023

Worsfold, B., Moehle, J., and Silva, J., 2022, Moment transfer at column-foundation connections: physical tests, ACI-Struct J 2022;119(5).